



**Michigan
Technological
University**

Michigan Technological University
Digital Commons @ Michigan Tech

Dissertations, Master's Theses and Master's Reports

2016

PROBABILITY-BASED HURRICANE RESILIENCE EVALUATION AND RETROFITTING FOR RESIDENTIAL COMMUNITY

Yadong Dong
Michigan Technological University, yadongd@mtu.edu

Copyright 2016 Yadong Dong

Recommended Citation

Dong, Yadong, "PROBABILITY-BASED HURRICANE RESILIENCE EVALUATION AND RETROFITTING FOR RESIDENTIAL COMMUNITY", Open Access Dissertation, Michigan Technological University, 2016.
<https://doi.org/10.37099/mtu.dc.etr/236>

Follow this and additional works at: <https://digitalcommons.mtu.edu/etr>



Part of the [Civil Engineering Commons](#), [Risk Analysis Commons](#), and the [Structural Engineering Commons](#)

PROBABILITY-BASED HURRICANE RESILIENCE EVALUATION AND
RETROFITTING FOR RESIDENTIAL COMMUNITY

By

Yadong Dong

A DISSERTATION

Submitted in partial fulfillment of the requirements for the degree of

DOCTOR OF PHILOSOPHY

In Civil Engineering

MICHIGAN TECHNOLOGICAL UNIVERSITY

2016

© 2016 Yadong Dong

This dissertation has been approved in partial fulfillment of the requirements for the Degree of DOCTOR OF PHILOSOPHY in Civil Engineering.

Department of Civil and Environmental Engineering

Dissertation Advisor: *Dr. Yue Li*

Committee Member: *Dr. William M. Bulleit*

Committee Member: *Dr. Raymond A. Swartz*

Committee Member: *Dr. Qiuying Sha*

Department Chair: *Dr. David Hand*

*This dissertation is dedicated to my wife, Andrea Jean Bowen, and my parents,
Zhixiong Dong and Hong Liu, and my grandparents, Linsheng Dong and Shihua
He.*

Table of Contents

List of Tables	vi
List of Figures	viii
Preface	xi
Acknowledgements	xii
Abstract	xiii
1. Introduction	1
1.1 Background and Motivations	1
1.2 Objectives	5
1.3 Organization and Outlines	5
2. Reliability of Roof Panels in Coastal Areas Considering Effects of Climate Change and Embedded Corrosion of Metal Fasteners	7
2.1 Introduction	7
2.2 Hurricane Wind Models and Impact from Climate Change.....	9
2.3 Time-Dependent Roof Panel Uplift Resistance	12
2.4 Fragility model of CCA-treated roof panels.....	22
2.5 Reliability Analysis of CCA-Treated Wood Roof Panels.....	27
2.6 Retrofitting Strategies.....	31
2.7 Conclusions	36
3. Hurricanes Risk-Based Assessment of Wood Residential Construction Subjected to Hurricane Events Considering Indirect and Environmental Loss	37
3.1 Introduction	37
3.2 Hurricane Simulation	38
3.3 Basic Failure Modes and Limit State Function	49
3.4 Fragility Analysis	55

3.5 Risk-Based Loss Estimation.....	58
3.6 Conclusions	70
4. A Framework for Hurricane Resilience of Residential Community.....	71
4.1 Introduction	71
4.2 Community Resilience and De-aggregation.....	75
4.3 Formulation of resilience for individual residential buildings	79
4.4 Discussions of individual and community resilience	91
4.5 Conclusions	93
5. Evaluation of Hurricane Resilience of Residential Community Considering a Changing Climate, Social Disruption Cost, and Environmental Impact	94
5.1 Introduction	94
5.2 Hurricane Simulation	96
5.3 De-aggregation of Community Resilience	100
5.4 Formulation of Resilience for Individual Residential Buildings.....	101
5.5 Illustrative Case Study.....	108
5.6 Conclusions	113
6. Summary, Conclusions, and Future Work.....	115
6.1 Summary and Conclusions	115
6.2 Future Work	118
7. References	119
Appendix A: Permission to Publish Chapter 2	131
Appendix B: Permission to Publish Chapter 3.....	132

List of Tables

Table 2.1 Wind load statistics.....	11
Table 2.2 Projected 50-year return period gust wind speed (m/s) in Miami (Bjarnadottir et al. 2011; Liu and Pang 2013; Mudd et al. 2014)	12
Table 2.3 Comparison and calibration of roof panel capacity calculated by tributary area method and experiments	16
Table 2.4 Time-dependent roof panel capacities for steel fasteners with zinc-coating	22
Table 2.5 Lognormal fragility parameters for roof panel with slope 6:12.....	27
Table 2.6 The percentage increase in the annual probability of failure of CCA-treated roof panel (6d @6/12 in., slope 6:12, distance between construction and coast less than 1 km) for different climate change scenarios	31
Table 3.1 Wind load statistics.....	45
Table 3.2 Comparison of wind speeds corresponding to different return periods.....	47
Table 3.3 Climate change scenarios.....	48
Table 3.4 Damage state definition	57
Table 3.5 Damage state/ injury/ fatality relationship.....	64
Table 3.6 Life-time indirect loss considering various climate change scenarios	65
Table 3.7 η_j values related to the cost of $CO_2 - e$ emissions for wood buildings.....	67
Table 4.1 Random variables	82
Table 4.2 Damage state definition.	83
Table 4.3 Damage state/ injury/ fatality relationship.....	85
Table 5.1 Wind load statistics.....	98
Table 5.2 Climate change scenarios.....	99
Table 5.3 Hurricane wind speed (m/s) at 27.3°N, 80.3°W for various climate scenarios.	99

Table 5.4 List of damage state definition.....	102
Table 5.5 Damage state/ injury/ fatality/social disruptions relationship.....	104
Table 5.6 η_j values related to the cost of $CO_2 - e$ emissions for wood buildings.....	107
Table 5.7 Resistance statistics.....	109

List of Figures

Figure 2.1 Roof panel zones for wind pressure (Gable roofs 6:12 ($7^\circ < \theta \leq 27^\circ$)).....	11
Figure 2.2 Roof panel fastening schedule.....	15
Figure 2.3 Two types of corrosion on fasteners.....	17
Figure 2.4 Roof panel capacity for CCA-treated roof panel with 6d nails @6/12 in.	21
Figure 2.5 Fragility analysis of new CCA-treated roof panel (Exposure B)	23
Figure 2.6 Fragility analysis of time-dependent CCA-treated roof panel (6d nails @6/12 in.).....	25
Figure 2.7 Probability of failure of CCA-treated roof panel (Zinc, 6d nail @6/6 in., slope 6:12) for 50-year return period wind speeds under climate change scenario LMA+RCP8.5 (distance between construction and coast less than 1 km).....	26
Figure 2.8 Annual probability of failure under selected climate change scenarios (distance between construction and coast less than 1 km)	30
Figure 2.9 Illustration for three different configurations of ccSPF retrofitting strategies of wood roof panel	33
Figure 2.10 Fragility curves after applying retrofitting strategies in 2020 (distance between construction and coast greater than 1 km)	34
Figure 2.11 Annual probability of failure for roof panel (6d@6/12in.) after applying retrofitting strategies in 2020 under climate change scenario LMA+RCP8.5 (distance between construction and coast greater than 1 km).....	35
Figure 3.1 Hurricane simulation model flowchart.....	44
Figure 3.2 Validation of Hurricane Simulation	46
Figure 3.3 Hurricane wind speed at 27.3°N, 80.3°W for various climate scenarios.....	49
Figure 3.4 Roof panel capacity for CCA-treated roof panels (6d nails with 152.4/304.8 mm).....	53

Figure 3.5 Fragility analysis of time-dependent CCA-treated roof panels (6d nails with 152.4/304.8 mm).....	56
Figure 3.6 Fragility of four damage modes in wind	57
Figure 3.7 Fragility of damage states in wind.....	58
Figure 3.8 Annual probability of failure for four damage modes under climate change scenario 5 (+10% change in intensity, +10% change in frequency).....	59
Figure 3.9 Annual probability of failure for window under climate change scenarios	60
Figure 3.10 Annual probability of failure for various damage states subjected to climate change scenario 5 (+10% change in intensity, +10% change in frequency)	62
Figure 3.11 Life-time direct loss under various damage states subjected to climate change scenario 5 (+10% change in intensity, +10% change in frequency).....	63
Figure 3.12 Direct/indirect/environmental losses comparison under scenario 1 (baseline), 5 (+10% change in intensity, +10% change in frequency), 6 (+20% change in intensity, +15% change in frequency) and 7 (-20% change in intensity, +15% change in frequency)	68
Figure 3.13 The percentage increase in monetary loss of residential buildings compared to scenario 1 (baseline) subjected to hurricane events for different climate change scenarios for year 2020	69
Figure 3.14 The percentage increase in monetary loss of residential buildings compared to scenario 1 (baseline) subjected to hurricane events for different climate change scenarios for year 2050	69
Figure 4.1 Flowchart of the framework	74
Figure 4.2 Probability of failure for individual building versus system reliability of the housing stock	78
Figure 4.3 Flowchart of formulation for individual building resilience	80
Figure 4.4 Hurricane fragility with four different damage states	83

Figure 4.5 Monetary losses including direct and indirect losses	86
Figure 4.6 Sensitivity analysis for monetary losses direct and indirect losses	87
Figure 4.7 Sensitivity analysis of actual recovery time	90
Figure 4.8 Quantification of resilience for individual residential buildings	91
Figure 5.1 Emissions for common materials	105
Figure 5.2 Hurricane fragility with four different damage states	110
Figure 5.3 Monetary losses including environmental and non-environmental losses	111
Figure 5.4 Loss Comparison under climate change scenario 6 (+20% chance in intensity, +15% change in frequency) under 100-yr return period hurricane event.....	112
Figure 5.5 Individual resilience for climate change scenarios under 100-yr return period hurricane event.....	113

Preface

A version of Chapter 2 has been published as *Reliability of Roof Panels in Coastal Areas Considering Effects of Climate Change and Embedded Corrosion of Metal Fasteners* in *ASCE-AMCE J. Risk Uncertainty Eng. Sys., Part A: Civ. Eng* (10.1061/AJRUA6.0000851, 04015016 Norville and Minor). The author developed a framework of hurricane risk assessment of coastal wood construction considering effects of climate change on altering patterns of hurricane hazard and embedded corrosion of metal fasteners (metal fastener refers to nail in this paper). Dr. Yue Li reviewed the paper and offered valuable suggestions.

A version of Chapter 3 has been published as *Hurricanes Risk-Based Assessment of Wood Residential Construction Subjected to Hurricane Events Considering Indirect and Environmental Loss* in *Journal of Sustainable and Resilient System* (10.1080/23789689.2016.1179051). The author evaluated the loss of the wood residential construction subjected to hurricane winds including direct, indirect loss and environmental impact. Dr. Yue Li reviewed the paper and offered valuable suggestions.

A version of Chapter 4 has been submitted to *ASCE-AMCE J. Risk Uncertainty Eng. Sys., Part A: Civ. Eng* with the title: *A Framework for Hurricane Resilience of Residential Community*. The author proposed a framework to evaluate if a residential community could achieve its resilience goal by de-aggregating the community resilience goal to individual building resilience goal and quantifying the individual building resilience. Dr. Yue Li reviewed the paper and offered valuable suggestions.

A version of Chapter 5 has been submitted to *ASCE Journal of Architectural Engineering* with the title: *Evaluation of Hurricane Resilience of Residential Community Considering a Changing Climate, Social Disruption Cost, and Environmental Impact*. The author developed a comprehensive framework to evaluate hurricane resilience of residential community considering the potential effects of a changing climate, social disruption cost, and environmental loss. Dr. Yue Li reviewed the paper and offered valuable suggestions.

Acknowledgements

First of all, I would like to express my sincerest gratitude to my advisor, Dr. Yue Li for his constant guidance and encouragement, without which this work would have been impossible. In the past four years, he showed tremendous support and patience and never gave up on me when I was in my low-tide period. I also would like to thank my committee members, Dr, William M. Bulleit, Dr. Raymond A. Swatz, and Dr. Qiuying Sha for their valuable assistance and guidance throughout my doctoral study.

I would like to thank my friends and colleagues, Abdullahi M. Salman, Ji Zhang, Ruilong Han, Ruiqiang Song, Enhua Bai and many others for their support and help. Those good time we spent together have become unforgettable memories which I will cherish for a life time.

I would like to thank the financial support given from Department of Civil & Environmental Engineering. Without their support, this study will be a lot harder to finish.

I would like to send the most special thanks to my parents, Zhixiong Dong and Hong Liu. Words failed to express how lucky I felt to be their son. Their endless support and love have been and continue to be a driving force of my life. I also would like to thank my grandparents, Linsheng Dong and Shihua He. I am who I am today because of them.

Lastly, I would like to thank my wife, Andrea J. Bowen. She has been extremely supportive of me throughout my doctoral study and has made countless sacrifices in all manners. She has been a perfect wife anyone can ever ask and I have been so thankful she is in my life.

Abstract

Wood residential construction is vulnerable to hurricanes, as evident in recent hurricane events. Many studies indicated that the changing climate may very likely alter hurricane patterns, which could lead to more severe hurricane damage to the wood residential construction that accounts for 90% of the residence in the USA. On the other hand, deterioration of material increases the chance of structural failure by reducing the structural capacity (e.g., corrosion of fasteners in roof panel could significantly reduce the withdrawal capacity of the roofing structure during hurricane events).

Currently, most hurricane damage estimations only focus on direct loss (e.g., structural loss). Under this context, hurricane damage to wood residential construction could be underestimated. Other than just evaluating direct monetary loss, this research evaluates indirect, social disruption, and environmental losses of wood residential construction subjected to hurricane events considering a changing climate.

This dissertation proposes a framework to evaluate hurricane resilience of residential community, which has been recognized a more comprehensive risk-based measure for risk assessment. The advantages of applying hurricane resilience framework include: 1) the incorporation of community recovery time modelling from hurricane events, 2) the ability to integrate all the key input from traditional risk assessment framework into a simple probabilistic expression, 3) a more accurate criterion to be used in the planning stage for designer and decision maker. The proposed framework consists of hurricane fragility analysis, reliability analysis, loss evaluation (i.e., direct, indirect, social disruption, and environmental losses), recovery time model, and potential impacts on hurricane hazard patterns from a changing climate. Sources of uncertainties in the framework include: 1) structural capacity uncertainty (e.g., changes in roof-panel-resistance-side due to effects of corrosion on metal fasteners), 2) load uncertainty (e.g., hurricane wind characteristics, hurricane simulations), 3) uncertainty in loss estimation, 4) recovery time modeling uncertainty, and 5) uncertainty from climate change.

1. Introduction

1.1 Background and Motivations

Wood residential construction is among the structures that are susceptible to natural hazards (e.g., hurricane, earthquake and flooding). Light-frame wood construction is the most widely built structure in the United States (U.S.). 90% of residential buildings are light-frame wood construction (NAHB. 1999). The insured coastal property values in Florida contributed to the rise in insurance claims due to the increase of hurricane damage by 55% from the year 1988 to 1993, with totals increasing from \$566 billion to \$872 billion (Stewart et al. 2003). It is estimated that the damage caused by Atlantic hurricanes in 2004 to 2005 was more than \$150 billion (Pielke Jr et al. 2008). Clark (2008) stated that Hurricane Katrina (2005) caused 1,833 death and countless injuries with an accordingly \$43.6 billion in insurance losses. In addition, hurricanes have large environmental impact because each time a damaged structure is rehabilitated after a hurricane event, new materials are consumed and greenhouse gases emissions produced (Arroyo et al. 2015).

It had been reported that the changing climate is the contributor to the rising sea temperature (SST) in recent decades (IPCC 2007). Hurricane frequency and intensity have increased to a certain extent in the Atlantic Ocean in recent years (Goldenberg et al. 2001; Msadek et al. 2015). The latest ASCE 7-16 added 3000-year return period for design wind map for risk category IV structures and increased the corresponding wind speeds in southeast area in consideration of the possibly aggravating hurricane activity in the future (<http://kupce.ku.edu/sites/kupce.ku.edu/files/docs/cpep/structural/speaker-presentations-2016/soules.pdf>). There are studies that have shown that the increased hurricane frequency and intensity are very likely affected by the rising SST (Elsner et al. 2008; Emanuel 2005; IPCC 2007; Mann et al. 2007). Accordingly, the increase of both will inevitably aggravate the degree of damage to coastal buildings (Banholzer et al. 2014).

The effect of corrosion on structural performance should not be ignored since corrosion increases the vulnerability of structural systems during hurricanes (Salman and Li 2016). For example, the effects of corrosion can render the reduction of strength in wood roof panels which will make the roof structure more vulnerable to intensified hurricane hazards (Leicester 2001; Nguyen et al. 2011; Nguyen et al. 2013).

Roof panel has been identified as one of the most vulnerable component for hurricanes (Sparks 1991). In most cases, the structural envelop breach that starts from the damage of roof panel will cause the correspondingly progressive damage (e.g., rainwater intrusion) (Manning and Nichols 1991). Therefore, a cost-effective mitigation strategy needs to be proposed and evaluated. The previous studies have investigated some mitigation strategies. For example, Datin et al. (2011) explored the employment of closed-cell Spray Polyurethane Foam (ccSPF) to reinforce the roof panel. Unnikrishnan and Barbato (2016) proposed to use 8d nail size instead of 6d for roof to rafter connection.

In the last few decades, significant research was devoted to developing risk assessment frameworks for residential buildings subject to hurricane hazard. Leicester et al. (1979) developed fragility curves based on hurricane damage survey after cyclone Tracy in 1974. Stubbs and Perry (1996) conducted component fragility analysis based on different component vulnerability models. Huang et al. (2001) built a hurricane loss evaluation framework for single house units using insurance data from Hurricanes Hugo and Andrew. Pinelli et al. (2004) developed a risk assessment model of residential construction using basic damage modes for individual structural and non-structural components. Li and Ellingwood (2006) proposed a framework to evaluate reliability of wood residential construction by convolving structural fragility and wind distribution function. van de Lindt et al. (2007) developed a performance-based approach that included the fragilities for different performance objectives applied to wood construction. Bjarnadottir et al. (2011) improved the risk assessment framework by integrating the potential impact of climate change on hurricane wind speed. Barbato et al. (2013) proposed a probabilistic

performance-based hurricane engineering (PBHE) framework for the risk assessment and loss analysis of structural systems subjected to hurricane hazards.

The up-to-date studies regarding climate change and corrosion risk analysis mainly focused on reinforced concrete (RC) and steel structures. The main driver to increased RC corrosion is carbon dioxide (CO_2) concentration, temperature, and relative humidity (Hunkeler 2005). Corrosion of steel reinforcement occurs when carbonation of the concrete cover, or chloride concentration at the level of the steel reinforcement exceeds a critical level; in both conditions, expansive corrosion generates tensile stresses on the concrete which causes cover cracking and eventually spalling and loss of structural capacity (Stewart et al. 2012). Wang et al. (2012) proposed the corrosion damage state as when crack widths exceed 1.0 mm and conducted probabilistic analysis of concrete corrosion considering the worst emission scenario A1F1 proposed by IPCC in Australia. Stewart and Deng (2015) assessed the direct costs of corrosion on RC structures and effectiveness of adaptation strategies considering climate change. Peng and Stewart (2016) adopted the damage state above and conducted time-dependent risk analysis for RC structures in China. Nguyen et al. (2013) investigated the potential impact of climate change on the atmospheric corrosion rate of exposed steel structures.

It needs to be noted that hurricane risk assessment shares a great uncertainty, in particular under the potential impact of climate change (Stainforth et al. 2005). Two types of uncertainty (i.e., aleatoric uncertainty and epistemic uncertainty) can be identified in the risk assessment process. Aleatoric uncertainty can be identified and quantified, however, it cannot be reduced because of the unpredictable and random nature of the physical system. On the other hand, epistemic uncertainty is the results of lack of knowledge of the system and can be quantified by conducting sensitivity analysis. Epistemic uncertainty can be reduced by a better understanding and comprehensive study of the system. In this study, the aleatoric uncertainties are found in the random variables (e.g., hurricane intensity and frequency in hurricane simulation model, wind load parameters) due to their inherent randomness. The epistemic uncertainty includes where assumptions are made (e.g., the

vulnerability function, corrosion rate, ultimate capacity of roof panel, assumed discount rate, recovery time function etc.).

Based on the review of existing risk assessment framework, the following observation can be made: 1) previous studies have not considered the combining effects of climate change and corrosion on wood structures in the risk analysis; 2) while most previous studies conducted loss analysis, the loss estimation was only limited to structural or structural related damage under hurricane events; 3) previous research has not considered the potential impact of climate change on wind speed by identifying two parameters (i.e., frequency and intensity) in hurricane simulation; 4) previous studies have not considered the community recovery time in the risk assessment framework.

Due to the limitations of the existing risk assessment frameworks, a more accurate and comprehensive risk assessment needs to be studied. Hurricane resilience, which has been identified as a more effective metric for the risk assessment of residential community, refers to the ability of communities to withstand the impacts of hurricane events and to recover from such disasters in effective and efficient manners. The proposed community resilience framework consists of hurricane fragility analysis, reliability analysis, loss evaluation (i.e., direct, indirect, social disruption, and environmental losses), recovery time model, and potential impacts on hurricane hazard patterns from a changing climate.

The evaluation of community resilience can be achieved by de-aggregating community resilience to individual resilience and quantification of individual resilience (Wang and Ellingwood 2015). Tokgoz and Gheorghe (2013) quantified hurricane resilience for individual residential building. Other than hurricane, resilience has also been used in assessing risks regarding other natural hazard such as earthquakes (Bonstrom and Corotis 2014; Bruneau et al. 2003; Bruneau and Reinhorn 2007; Cimellaro et al. 2010; Wang and Ellingwood 2015).

The motivation of this study comes from: (1) It was unknown how a changing climate and effect of corrosion affect the performance of the roof structures; (2) the traditional cost analysis does not include indirect, environmental, social disruption costs; and (3) it is needed to establish and improve hurricane resilience assessment framework in order to more accurately measure hurricane risks to residential construction.

1.2 Objectives

The objectives of this dissertation are

1. Evaluate the reliability of wood roof panels with zinc-coated fasteners subjected to hurricane events considering the combined effects of changing climate and embedded corrosion and extend the traditional risk assessment of untreated wood construction to treated wood construction.
2. Proposed and evaluate various retrofitting strategies to reduce the hurricane damage to the roofing structure.
3. Assess hurricane damage to wood residential construction in monetary losses including direct, indirect, social disruption, and environmental impact.
4. Conduct hurricane simulations including both stationary and non-stationary scenarios in the process of risk analysis.
5. Propose a probability-based comprehensive framework to assess hurricane resilience of residential community.

1.3 Organization and Outlines

Each of the chapters from Chapter 2~5 are from a single paper that has either been published by a journal, or submitted to a journal. Chapters 2~5 are summarized as follows.

Chapter 2 proposes a framework of hurricane risk assessment of coastal wood construction considering effects of climate change on altering patterns of hurricane hazard and embedded corrosion of metal fasteners in hurricane risk assessment. Uncertainty in load-side (hurricane wind speed) and changes in roof panel resistant-side (the effects of embedded corrosion on the diameter of metal fasteners) are considered. The effectiveness of various retrofitting strategies is assessed.

Chapter 3 evaluates the loss of the wood residential construction subjected to hurricane winds including direct, indirect loss and environmental impact. Hurricane simulation model is used to predict the future wind speed accounting for the key parameters of climate change such as intensity and frequency. Four structural damage modes and the effect of corrosion are considered in the structural fragility analysis.

Chapter 4 proposes a framework to evaluate if a residential community could achieve its resilience goal by de-aggregating the community resilience goal to individual building resilience goal and quantifying the individual building resilience. The de-aggregating of community resilience for hurricanes will be investigated. The presented results also can be used for decision makers to achieve the goals of community resilience through initial design and hurricane mitigation.

Chapter 5 aims to improve the framework aforementioned in Chapter 4, and investigates the sensitivity of the hurricane resilience of communities by including three key components, a changing climate, social disruption cost, and environmental cost. Hurricane simulation models in the framework include both stationary and non-stationary wind scenarios.

2. Reliability of Roof Panels in Coastal Areas Considering Effects of Climate Change and Embedded Corrosion of Metal Fasteners¹

2.1 Introduction

In recent decades, it has been recognized that the effects of climate change could alter patterns of hurricane hazards, which would aggravate the degree of damage to coastal buildings (Banholzer et al. 2014). Many researchers have reported increasing hurricane intensity activities over the last 30 years (Emanuel 2005; IPCC 2007; Mudd et al. 2014). It was estimated that the effects of climate change will increase hurricane-induced losses in the United States by up to 75% by 2080 (Donat et al. 2011). On the other hand, the effects of corrosion can render the reduction of strength in wood roof panels which will make the roof structure more vulnerable to intensified hurricane hazards (Leicester 2001; Nguyen et al. 2011; Nguyen et al. 2013).

The coastal wood structure performances under hurricane wind loads were investigated in the past; and the building envelope is the most vulnerable part of residential construction to hurricane-induced damage (Bjarnadottir et al. 2011; Ellingwood et al. 2004; Li and Ellingwood 2005; Li and Ellingwood 2006). Manning and Nichols (1991) found that damage or failure of the roof structural system might cause walls to lose lateral support and lead to building failure. It was estimated that approximately 60 % of the total damage from hurricane Hugo occurred to residential buildings, the majority of which is due to the roof panels' failure (Sparks 1991). Baskaran and Dutt (1997) indicated that nearly 95% of monetary losses from hurricanes Iniki (1992) and Andrew (1992) were a result of the failure of roof panel systems. Keith and Rose (1994) observed that almost 24% of residential wood constructions in South Florida lost one or more roof-sheathing panels and proposed that failures of the roof result from inadequate resistant of fasteners to wind uplift.

¹ A version of this chapter was previously published in *ASCE-AMCE J. Risk Uncertainty Eng. Sys., Part A: Civ. Eng.*, and is re-used herein with permission from Elsevier. The permission is presented in Appendix A.

In this chapter, the building performance limit state is defined as the breach of the building envelope through the failure of roof panels.

Climate change is defined as a long-term atmospheric phenomenon that includes significant change in the state of the climate (IPCC 2007; Wang et al. 2012). IPCC (Intergovernmental panel on climate change) (2007) has identified five climate changes of particular importance to coastal constructions, which are rising sea levels, increases in hurricane intensity, intense precipitation events, arctic temperature, and very hot days. Scientists specifically indicate the possibility of significant alteration of severe hurricane wind intensity and frequency worldwide, which falls in the period of existing buildings and infrastructure (CSIRO 2014). Wang et al. (2013) suggested that ± 10 m/s changes in extreme wind gust speeds in a 500-year return period are likely to happen when subjected to ± 20 % intensity change and ± 50 % occurrence frequency change of hurricanes. Knutson et al. (2010) predicted a global warming with an increase of + 2 % to + 11 % in the mean maximum annual wind speed in 21st century. Mudd et al. (2014) showed a maximum increase of approximately 20 % in the mean maximum wind speed for the 700-year event in U.S. east coast areas. Furthermore, the intensified hurricane events will cause more severe damage to coastal building considering that the current design codes exclude the potential impact of changing climate.

There has been growing recognition of the need for a more explicit consideration of material degradation effects (Bjarnadottir et al. 2011). This study is among the first to take the effects of embedded corrosion into account in the risk assessment of wood roof panels. The embedded corrosion is defined as corrosion on shanks of the fasteners that are tightly embedded in wood, where the corrosive agents are the wood acidity, preservatives and moisture (Nguyen et al. 2011; Nguyen et al. 2013). Nguyen et al. (2008) adopted a power law function in CCA (Chromated copper arsenate)-treated wood to describe the progress of corrosion with time. The function demonstrates that the corrosion progresses successively for steel fasteners with zinc coatings in that the corrosion progress is unlikely to be diminished by the corrosion product due to the chemical agent of CCA-treated wood

(Nguyen et al. 2013). Nguyen et al. (2011) assumed that the zinc-coating is only viewed for protection and does not increase the fastener strength. Based on that, the fastener strength can be determined by the remaining thickness of the fastener cross-section.

This chapter proposed a framework of hurricane risk assessment of coastal wood construction considering effects of climate change on altering patterns of hurricane hazard and embedded corrosion of metal fasteners (metal fastener refers to nail in this chapter) in hurricane risk assessment. Uncertainty in load-side (hurricane wind speed) and changes in roof panel resistant-side (the effects of embedded corrosion on the diameter of metal fasteners) are considered. The effectiveness of various retrofitting strategies is assessed. Some of the improvements in this chapter over previously studies include: 1) considering roof panel withdrawal capacity degradation due to embedded corrosion of fasteners; 2) determining hurricane-induced load with IPCC designated climate change scenarios; 3) extending hurricane risk analysis of untreated wood to treated wood (CCA) construction; 4) investigating retrofitting strategy to be applied in the wood roof panels.

2.2 Hurricane Wind Models and Impact from Climate Change

A wide range of hurricane wind models have been developed. Generally, there are three categories: general circulation models (GCMs), Monte Carlo simulation, and peaks-over-threshold methods. GCMs are built on a solid theoretical foundation but are not frequently used due to their overwhelming computing demand (Lorenz 1967; Wang et al. 2013; Weart 2008). The advantages of peaks-over-threshold methods include that they do not need the climate data every year, but the projected results tend to be quite conservative; the most popular distribution for the method is generalized Pareto distribution (GPD) (Walsh 2004; Wang et al. 2013). Vickery and Twisdale (1995) employed Monte Carlo simulation techniques to estimate extreme wind speeds based on sufficient existing data; the model is used as the basis for wind speed contours along the coastlines of the US, which demonstrates very good agreement with recorded mean and gust time histories for most locations affected by severe hurricanes.

IPCC (2007) indicated that increase in wind speeds is very likely to happen due to the rise in sea surface temperature (SST) and a 1 °C increase in SST converts to a nearly 5% increase in hurricane speed. For the projected worst-case scenario (i.e., Representative Concentration Pathway 8.5) in the IPCC Fifth Assessment Report (AR5), the bound of range is an increase from 2.6 to 4.8 °C in SST (Stocker et al. 2013). Liu and Pang (2013) indicated that the wind speed may increase by more than 24% by the end of the 21st century in hurricane-prone areas. It needs to be noticed that the wind pressure acting on a building envelope is related to the wind speed, and the wind pressure $W(t)$ acting on structure is determined by ASCE (2010),

$$W(t) = q_h(t)[GC_p - GC_{pi}] \quad (2.1)$$

in which $q_h(t)$ = velocity pressure evaluated at mean roof height at t year, G = gust factor, C_p = external pressure coefficient, and C_{pi} = internal pressure coefficient. GC_p is the external pressure coefficient, which is area-dependent on the zone of the building envelope considered as shown in Fig. 2.1. Interior pressure coefficient (GC_{pi}) for both fully enclosed and partially enclosed residential constructions are considered. It needs to be noted that the greatest wind pressures on a roof occur in the regions of flow separation at the ridge, eave and corners (Zone 2 and 3) and the roof panels are model as components and cladding (C&C) (ASCE 2010). This is the basis for the winds pressures in *ASCE Standard 7*. The velocity pressure is calculated as

$$q_h(t) = 0.613K_hK_{zt}K_dV^2 \text{ (N/m}^2\text{)} \quad (2.2)$$

in which K_h = exposure factor, K_{zt} =topographic factor (taken equal to unity in this chapter), K_d = directional factor, $V(t)$ = 3s wind speed at the height of 10 m (33 ft) in an open-country exposure at t year. Table 2.1 summarizes the wind load statistics for a typical low-rise residential structure. The dimensions are 8.5 m by 12.2 m (28 ft by 40 ft), and the

mean roof height is 3.8 m (12.5 ft). The external pressure coefficients (GC_p) are dependent on various gable roof slopes.

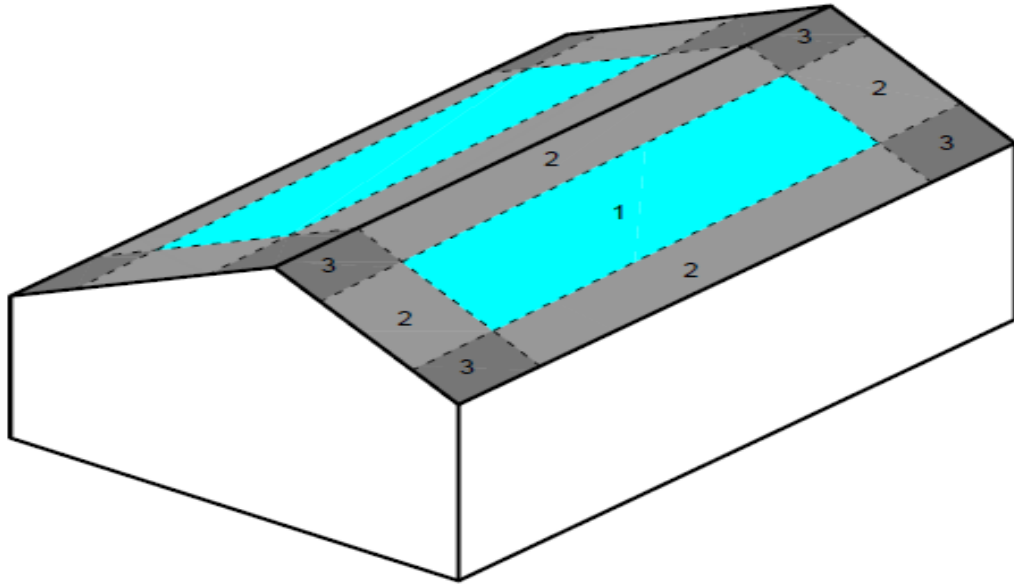


Figure 2.1 Roof panel zones for wind pressure (Gable roofs 6:12 ($7^\circ < \theta \leq 27^\circ$))

Table 2.1 Wind load statistics

	Mean	COV	CDF	Source
K_h (Exposure B)	0.57	0.12	Normal	
GC_p (C&C) Zone 3 (slope 1:12, $\theta < 7^\circ$)	2.02	0.22	Normal	(Li and Ellingwood 2006)
GC_p (C&C) Zone 3 (slope 6:12, $7^\circ < \theta \leq 27^\circ$)	2.32	0.22	Normal	
GC_p (C&C) Zone 3 (slope 12:12, $27^\circ < \theta \leq 45^\circ$)	1.12	0.22	Normal	
GC_{pi} (Enclosed)	0.15	0.05	Normal	
GC_{pi} (Partial enclosed)	0.45	0.09	Normal	
K_d	0.89	0.14	Normal	

C&C: Component and cladding

Liu and Pang (2013) examined the changes in wind speeds over time for different climate scenarios and plotted against the projection years for 50-year mean recurrence interval (MRI) wind speeds. It is found that the climate change scenarios (OMA (oscillating moving average) +RCP (Representative Concentration Pathway) 8.5) and (LMA (Linear Moving

Average) +RCP8.5) have the highest wind speeds by the end of the century and highest rates of increases in wind speeds over time (Liu and Pang 2013).

In this chapter, five climate change scenarios from IPCC will be considered, which are: 1) OMA+RCP8.5, 2) OMA+RCP4.5, 3) OMA+RCP2.6, 4) CON+RCP8.5, 5) LMA+RCP8.5. Oscillating Moving Average (OMA) and Linear Moving Average (LMA) are annual storm frequency models while Constant (CON) is a baseline model which assumes the annual storm frequency to remain stationary over time with a constant mean and standard deviation. The IPCC Representative Concentration Pathway (RCP) is Sea Surface Temperature model (SST) and includes: 1) a climate change retrofitting scenario leading to a very low forcing level of 2.6 w/m^2 (RCP2.6), 2) a medium stabilization scenario (RCP4.5), and 3) a high scenario (RCP8.5). The projected 50-year return period wind speeds are shown in Table 2.2. Liu’s model is integrated in the framework to get the annual probability of failure because the non-stationary hurricane wind speed due to climate change is considered.

Table 2.2 Projected 50-year return period gust wind speed (m/s) in Miami (Bjarnadottir et al. 2011; Liu and Pang 2013; Mudd et al. 2014)

Year	LMA+RCP	OMA+RCP	OMA+RCP	OMA+RCP	CON+RCP
	8.5	8.5	4.5	2.6	8.5
2020	60	60	59	59	55
2030	62	61	61	60	59
2040	64	63	62	61	62
2050	69	68	65	64	66

2.3 Time-Dependent Roof Panel Uplift Resistance

A typical roof sheathing arrangement for a one-story light-frame wood residential house illustrated in Fig. 1 is considered for this chapter. For the interest of practice, gable roof without roof overhang is selected with various slopes including 1:12, 6:12, and 12:12. Recently it is reported that the membrane roofs (continuous roofing system), which is used on flat or closely flat roofing system to prevent leaks and water intrusion, are becoming

increasingly popular in residential application in the United States (Carter 2007). Hence a representative low slope of 1:12 is selected in the example. A 6:12 slope is chosen from the conventional roof pitch from 4:12 to 9:12, which is the dominating roofing system currently in South Florida and a 12:12 slope from steep-slope roofing system (Schmid 2013).

The roof panel is 1.2 m by 2.4 m (4 ft by 8 ft) with two nailing patterns: nominal nail diameters are 2.9 mm and 3.3 mm (0.113 in. and 0.131 in.) for “6d” and “8d” nails, respectively. The building codes suggest that the steel fasteners are hot-dip galvanized to American Society for Testing and Materials (ASTM) A153, Class D, which is averagely 0.3 kg/m^2 (1 oz/ft^2). The coating thickness regarding to density required to equal 0.3 kg of zinc per square meter of surface is $43 \mu\text{m}$ (1.7 mils). American Galvanizers Association (AGA) stipulated that the coating thickness for all shapes and sizes of nail ranges from 35.6 to $99.1 \mu\text{m}$ (1.4 to 3.9 mils) (AGA 2012). Based on above information, the thickness of zinc coating is set to be $43 \mu\text{m}$ (1.7 mils) in the chapter.

Panels are nailed at a spacing of 150 mm (6 in.) at the edges of the perimeter and 300 mm (12 in.) in the panel interior and the sheathing thickness is 15.9 mm (15/32 in) (Li and Ellingwood 2006). The framing members, such as trusses or rafters, consist of 50.8 mm by 101.6 mm (2 in. by 4 in.) Spruce-Pine-Fir (SPF) lumbers and are spaced 0.6 m (24 in.) on center with a specific gravity of 0.36.

2.3.1 Panel Uplift Resistance Using Tributary Area Method

The roof panel withdrawal capacity can be determined based on the intended fastener and rafter framing spacing. He and Hong (2012) employed a finite element method to show that tributary area method is valid in evaluating the roof panel withdrawal capacity with an underestimation of Resistance (R) by 10%. Sutt (2000) demonstrated that tributary area method is appropriate for determining roof panel withdrawal capacity from single fastener capacity. The fasteners with the largest tributary areas on the interior areas of the panel are

of the most concern to the designer as these large areas have more negative pressure. Figure 2.2 shows the roof panel fastening schedule for 6d nails (2.9 mm (0.113 in.)) with 152.4/304.8 mm (6/12 in.) for wind uplift and the largest tributary areas on the interior of the panel. In order to determine the design panel capacity for negative pressure, the fastener withdrawal resistance should be divided by the largest tributary area. Sutt (2008) considered the panel effect and the underperformance of the nails in single fastener withdrawal based on the test data and proposed the design panel capacity as shown below

$$P(t) = \left[\frac{R(t) * CF}{TA} \right] / SF \quad (2.3)$$

in which $P(t)$ is the design panel capacity at t year; CF is 1.7 in this chapter, which is correction factor of panel effect and delta between actual nail withdrawal and design for smooth shank nail; TA is tributary area; SF is a factor of safety of 2. The National Design Specification (NDS) (AFPA 2005) gives an empirical equation for the design nail withdrawal capacity per unit length for single smooth shank fastener driven into the side grain of wood that considers specific gravity of the wood and fastener diameter. The equation is given as:

$$R(t) = KG^{\frac{5}{2}}D(t)L \quad (2.4)$$

in which $R(t)$ is resistant force at t year; L is the depth of penetration of the nail in the member holding the nail point; G is the specific gravity of the wood based on oven-dry weight and volume at 12% moisture content; $D(t)$ is the reduced diameter of the nail at t year; K is an empirical constant that equals 1,380. The design capacity of nail can be approximately evaluated by the multiplication of $P(t)$ and 5 (the factor between the design capacity and the ultimate capacity for nail) (Sutt 2008). Due to lack of data, in this study the same factor is assumed between the design capacity and the ultimate capacity for roof panel. If there is more accurate roof panel ultimate capacity model available in the future, it can be easily incorporated in this study.

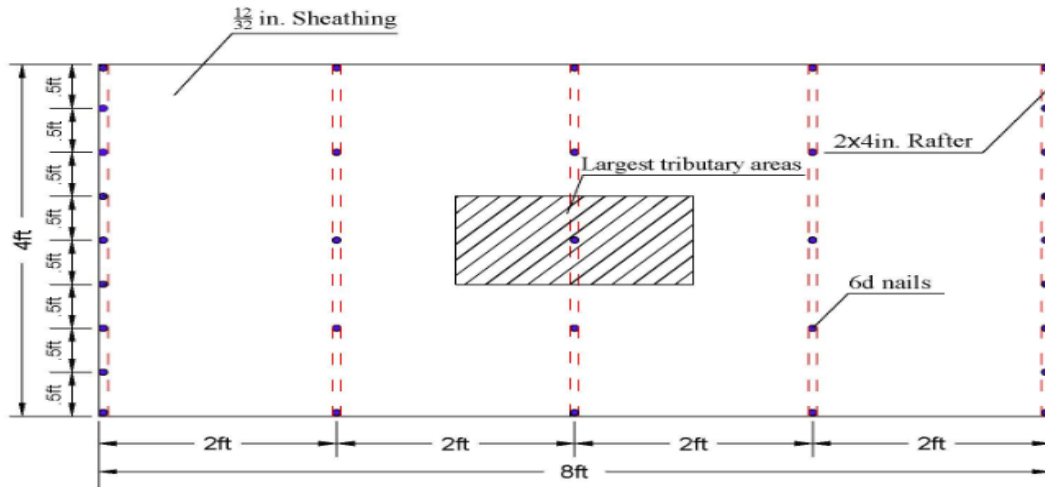


Figure 2.2 Roof panel fastening schedule

The roof panel resistant forces using tributary area method for each configuration are calculated as listed in Table 2.3. Also, the calculated results are calibrated in contrast to the experimental findings from Mizzell (1994) and Lee and Rosowsky (2005). From comparison, the calculated numbers are approximately consistent with the experimental results. The slight difference may be caused by the modelling and experiment errors, which could be the combined aleatory and epistemic uncertainties (Ang and Tang 2007). Furthermore, Datin et al. (2011) indicated that the determinations of wood uplift capacity scatter in the history due to the absence of generally accepted methodology and natural variability in wood strength and type of nails. Hence, the results calculated by tributary area method are acceptable and valid considering the great variability in the prediction of uplift capacity. Based on the structural model, the maximum tributary area is 0.1 m^2 (1 ft^2) for nails with 152.4/152.4 mm (6/6 in.) and 0.2 m^2 (2 ft^2) for nails with 152.4/304.8 mm (6/12 in.). Due to lack of experimental data, here it is assumed that nail lengths for all nails are the same.

Table 2.3 Comparison and calibration of roof panel capacity calculated by tributary area method and experiments

Type (inch)	Panel design capacity(<i>psf</i>)	Panel ultimate capacity (<i>psf</i>)	Calibration for panel ultimate capacity (<i>psf</i>)	CDF	COV	Source
	Tributary area method		Experiment			
6d@6/6	15.8	78.9	-	Normal	0.1	(Lee and Rosowsky 2005; Mizzell 1994)
8d@6/6	24.3	121.4	107	Normal	0.2	
6d@6/12	7.9	39.5	26	Normal	0.1	
8d@6/12	12.1	60.7	60	Normal	0.2	

2.3.1.1 Mean Embedded Corrosion Depth

Generally, there are two types of corrosion of fasteners in wood construction: embedded corrosion and atmospheric corrosion. Embedded corrosion is generated by corrosive agents that are within the surrounding wood, including wood acidity and timber moisture content (Nguyen et al. 2011). Therefore, only parts inside the wood, such as the shank of nails, screws are affected. On the other hand, atmospheric corrosion is produced due to corrosive agents that are within the surrounding air, such as airborne salinity and airborne pollution agents. Thus, the parts exposed to the air, such as the heads of nails and screws, are affected (Nguyen et al. 2011). Figure 2.3 illustrates the two different types of corrosions. In this chapter, only embedded corrosion is considered because only withdrawal failure mode is considered and the effect of climate change to timber moisture content can be neglected.

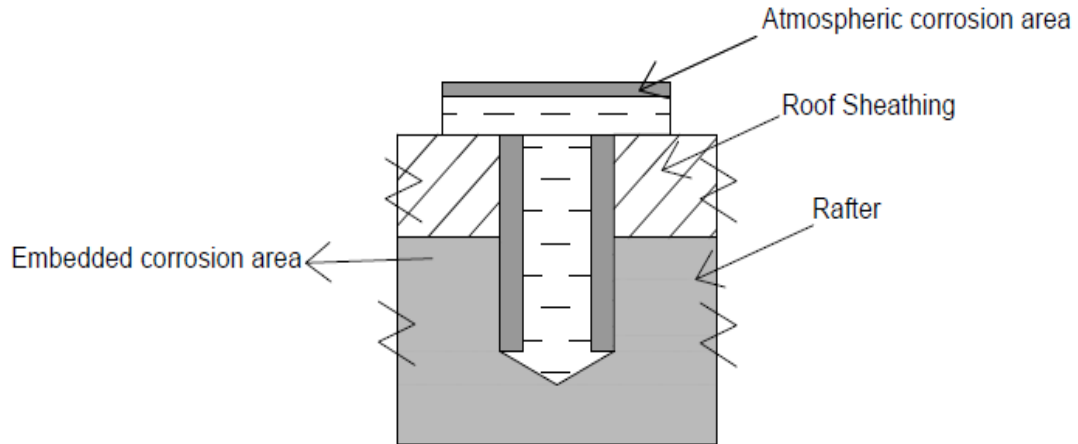


Figure 2.3 Two types of corrosion on fasteners

The effects of embedded corrosion on CCA-treated wood roof panel withdrawal capacities are investigated. It has been pointed out that the effects of embedded corrosion would have a significant influence on untreated wood only if the equilibrium moisture content (EMC) is not less than 15% (Nguyen et al. 2011). Through a careful investigation toward the equilibrium moisture content (EMC) of wood in the United States hurricane-prone coastal area (Bergman 2010; Simpson 1999), it was found the EMCs of untreated wood are generally lower than 15%. Hence, the embedded corrosion for untreated wood is not considered due to the interest of geography, though it does affect the performance of zinc-coated nail in hardwood (e.g., some Oriented Strand Board (OSB) is made with layers of hardwood). However, hardwood is commonly used in floor or subfloor instead of roof sheathing (AWC 2013). On the other hand, it is observed that the EMCs over most hurricane-prone areas are higher than 12%, for example, the EMCs is 13.46% in Miami-Dade County. Therefore, the embedded corrosion is expected to largely affect the roof panel withdrawal capacity by degrading fastener withdrawal capacity in CCA-treated wood.

Since the 1970s, CCA has been the most commonly used chemical preservative added to wood structures, such as roof panels, utility poles, and marine docks etc., to protect the wood from biological deterioration in the United States, and it has been reported that CCA-

treated roof panels comprised over 90 percent of the market before 2001 (Rowell 2012). Another reason for this material gaining so much popularity is that CCA has very good permeability than other materials (Shibata et al. 2007). However, the presence of arsenic in the presentative and the awareness of that this presentative chemical can be released over time from CCA-treated structures through contact with rainfall, new CCA-treated wood was no longer manufactured for residential uses in the United States as of January 1, 2004 (Shibata et al. 2007).

Although CCA-treated wood has been phased-out for residential applications, many in-service CCA-treated roof panels currently exist in the United States due to the standard service life of 50 years. It has been reported that the cost of treated wood with alternative pesticides is estimated to cost about 10 to 20 percent more than CCA-treated wood (Lebow et al. 2001; Shibata et al. 2007). In addition, availability of alternatively treated wood is greatly limited compared to CCA material. Furthermore, the United States Environmental Protection Agency (EPA) has never been advocating remove the existing deck due to the difficulty in recycling and disposing such materials (Cooper et al. 1997). Hence, the CCA-treated roof panels would still exist in a foreseeable future and need to be investigated as for the impact of embedded corrosion to CCA-treated wood roof panel withdrawal capacity. Practically, assuming most wood residential construction with CCA-treated roof panels built at the year of 2000, then the service life could be up to the year of 2050. The time-dependent mean embedded corrosion depth $C_{emb}(t)$, over the period t years is calculated by a power-law function (Nguyen et al. 2008),

$$C_{emb}(t) = C_0 t^n \tag{2.5}$$

in which $C_0(\mu m)$ is the embedded corrosion depth for the first year; for metal embedded in copper chrome arsenate (CCA)-treated wood $n = 0.6$ for zinc-coating and $n = 1.0$ for steel. The embedded corrosion depth for the first year $C_0(\mu m)$ can be estimated by the following equations. For the case of CCA-treated wood,

$$C_0 = Af_{120}(BTM_{mean}) \quad (2.6)$$

where $A = 1.3$ for zinc-coating and $A = 2.1$ for steel. BTM_{mean} is annual mean value of the timber moisture content in service. f_{120} is the 120-day corrosion depth, and is a function of the moisture content of the wood. For CCA-treated wood, the 120-day corrosion depth function $f_{120}(M)$ and the annual mean moisture contents BTM_{mean} of timber in service are expressed below,

$$f_{120}(M) = \begin{cases} 0 & \text{if } M \leq 12; \\ 0.7(M - 12) & \text{if } M > 12; \end{cases} \quad (2.7)$$

$$BTM_{mean} = TM_{mean} + \Delta_{climate} + \Delta_{rain} \quad (2.8)$$

in which $\Delta_{climate}$ is the adjustment factors for the climate. The value is 2.5 when the distance between object and coast is not greater than 1.0 km and is 0.5 when the distance is greater than 1.0 km. Δ_{rain} is the rain factor (Nguyen et al. 2008). It describes three physical states of fasteners: sheltered, vertically surface exposed to rain and horizontal surface exposed to Rain. Especially for sheltered fastener, it means the fastener is completely protected and not exposed to rain at all. The mean seasonal moisture content of a piece of timber, TM_{mean} , is estimated below (Nguyen et al. 2008),

$$TM_{mean} = \exp(1.9 + 0.05SEMC_{mean}) \quad (2.9)$$

in which $SEMC_{mean}$ is the surface equilibrium moisture content of the timber.

2.3.1.2 Reduced CCA-Treated Wood Roof Panel Withdrawal Capacity by Embedded Corrosion

Using Eqns. (2.5)-(2.9), the projected corrosion rate can be evaluated. Then, the reduced diameter of fastener $D(t)$ at t year is,

$$D(t) = D - 2C_{emb}(t) \quad (2.10)$$

It needs to be noted that the rain factor in the model is geography-related and only given for Australia. The proper factor is carefully selected based on the counterpart similarity (e.g., Orlando is geographically alike to Melbourne, then the Melbourne rain factor is applicable to the case of Orlando). Based on the counterpart similarity, the rain factor for Miami-Dade County is classified in Zone C in Australia hazard zone map. The roof panel withdrawal capacity can be obtained by plugging the single nail capacity into Eq. (2.3). The roof panel withdrawal capacity with 6d nails with 152.4/304.8 mm is demonstrated in Fig. 2.4. The overall trend of time-dependent capacity is presented as negligently decreasing in the first stage, then dropping down significantly afterwards. The first stage means the zinc-coating still exists on the fastener surface, and afterwards is the point of all zinc-coating being exhausted. For roof panels under all conditions, before taking sharp downturns, roof panel withdrawal capacities decrease less than 5%. It can be observed that the performance of the roof panels could remain excellent and the capacities only reduce slightly under all circumstances before the zinc coatings are fully corroded.

With well sheltered fasteners, the roof panel withdrawal capacities do not illustrate protruding trend in reduction throughout the service life. However, for roof panels with horizontal-surface-exposed condition, the withdrawal capacity is degraded by 50% approximately in 30 years. Among those and for the condition that the coastal distance is less than 1 km, it drops down to zero in 50 years. With the same exposure condition, the roof panel withdrawal capacity only varies slightly with distance to coast. Hence, the fastener exposure condition is one of the most dominating factors affecting roof panel withdrawal capacity.

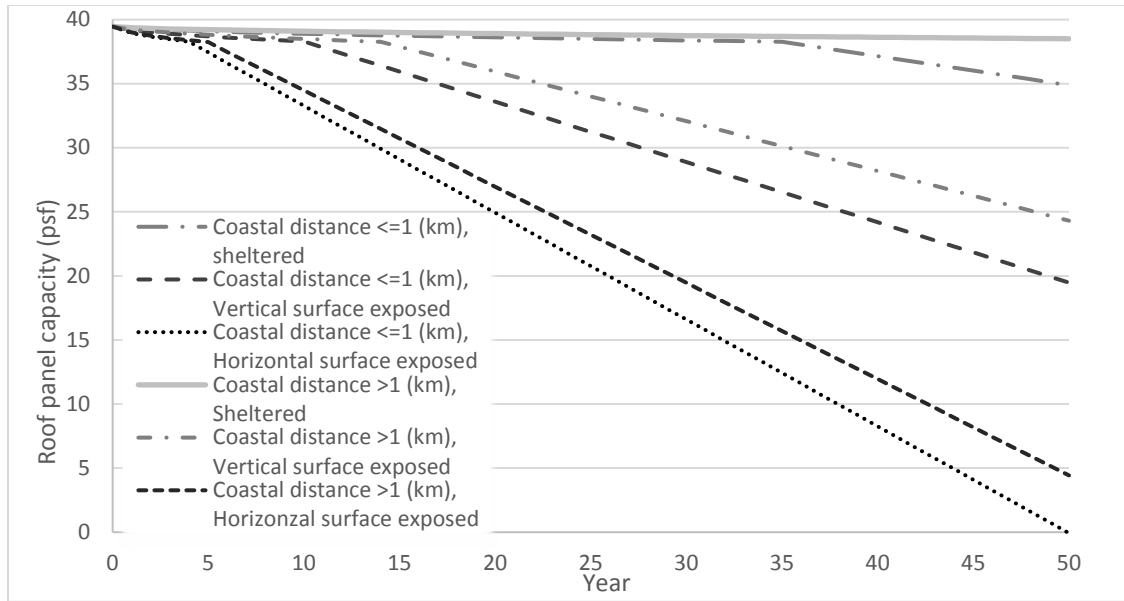


Figure 2.4 Roof panel capacity for CCA-treated roof panel with 6d nails @6/12 in.

In real world, usually it is very rare for nails to be completely sheltered (underestimating the risks) or horizontal surface exposed to rain (too conservative) in wood roof panels. The condition the horizontal surface of fasteners exposed the rain in panels is therefore selected in order to balance and minimize the errors in the following risk assessments.

Table 2.4 shows the time-dependent roof panel withdrawal capacities with residential constructions in various locations. It can be observed that nail size, nail schedule and distance between construction and coast affect roof panel withdrawal capacities in different degree with time elapsing. A more compact nail schedule (152.4/152.4 mm) gives more capacities and shows better reliability. For the base case (6d nails with 152.4/304.8 mm), the roof panel withdrawal capacity in 2020 is 1.6 kPa (33.6 psf) for distance greater than 1 km. By only improving the nail size up to 8d nails for the base case, the capacity increases by 47%; and by just changing the nail schedule to 152.4/152.4 mm, the capacity could be doubled. For the case (6d nails with 152.4/304.8 mm), the roof panel withdrawal capacity reduces rapidly after the zinc-coating is corroded completely. Hence, proper retrofitting strategies are in demand to improve the structural reliability and elongate the service life for the CCA-treated roof panels with steel fasteners with zinc coatings.

Table 2.4 Time-dependent roof panel capacities for steel fasteners with zinc-coating

Year	6d@6/6 in.		6d@6/12 in.		8d@6/6 in.		8d@6/12 in.	
	<= 1km	> 1km	<= 1km	> 1km	<= 1km	> 1km	<=1 km	>1km
	(psf)	(psf)	(psf)	(psf)	(psf)	(psf)	(psf)	(psf)
2001	78.3	78.4	39.2	39.2	120.6	120.7	60.3	60.4
2010	76.6	77.0	38.3	38.5	118.3	118.8	59.1	59.4
2020	67.2	71.9	33.6	35.9	105.8	112.0	52.9	56.0
2030	57.8	64.1	28.9	32.1	93.3	101.8	46.7	50.9
2040	48.4	56.4	24.2	28.2	80.8	91.5	40.4	45.7
2050	39.0	48.6	19.5	24.3	68.3	81.2	34.2	40.6

2.4 Fragility model of CCA-treated roof panels

In this chapter the building performance limit state is defined as the breach of the building envelope, and specifically the component limit state is roof panels uplift due to fastener failure (Li and Ellingwood 2006). The governing limit state for roof performance is expressed as,

$$R(t) - (W(t) - D) = 0 \quad (2.11)$$

in which $R(t)$ = structural resistance to wind uplift, and D and $W(t)$ are respectively, the dead and wind load effects, all terms expressed in dimensionally consistent units.

Note that the dead load counteracts wind uplift to the roof panels, and is beneficial in reducing the vulnerability of the roof structure, hence the roof dead load is included. The mean value of the dead load effect is based on the weight of roof: 77 Pa (1.6 psf) for roof panels, while its coefficient of variation is assumed to be 0.1(Li and Ellingwood 2006). The dead load can be modeled by a normal distribution (Li and Ellingwood 2006).

It is assumed that lognormal distribution is the best fit for fragility model and a Kolmogorov-Smirnov test was conducted to verify the assumption (Li and Ellingwood 2006).

$$F_R(y) = \Phi\left[\frac{\ln\left(\frac{y}{m_R}\right)}{\xi_R}\right] \quad (2.12)$$

where $\Phi(\cdot)$ is standard normal probability integral; m_R is median capacity; ξ_R is logarithmic standard deviation, which is the inherent variability in the capacity.

Monte Carlo simulation is used here to generate fragility curves. Figure 2.5 illustrates the fragility analysis of a new CCA-treated roof panels (without considering embedded corrosion). The status of the building enclosure integrity is enclosed. The graph shows that roof pitch has relatively large impact on the hurricane wind load acting on the roof panels and the overall roof reliability. The scenario of slope 12:12, 8d nails with 152.4/304.8 mm has the utmost safety margin that the probability of failure only goes to 0.55 at 89.4 m/s (200 mph).

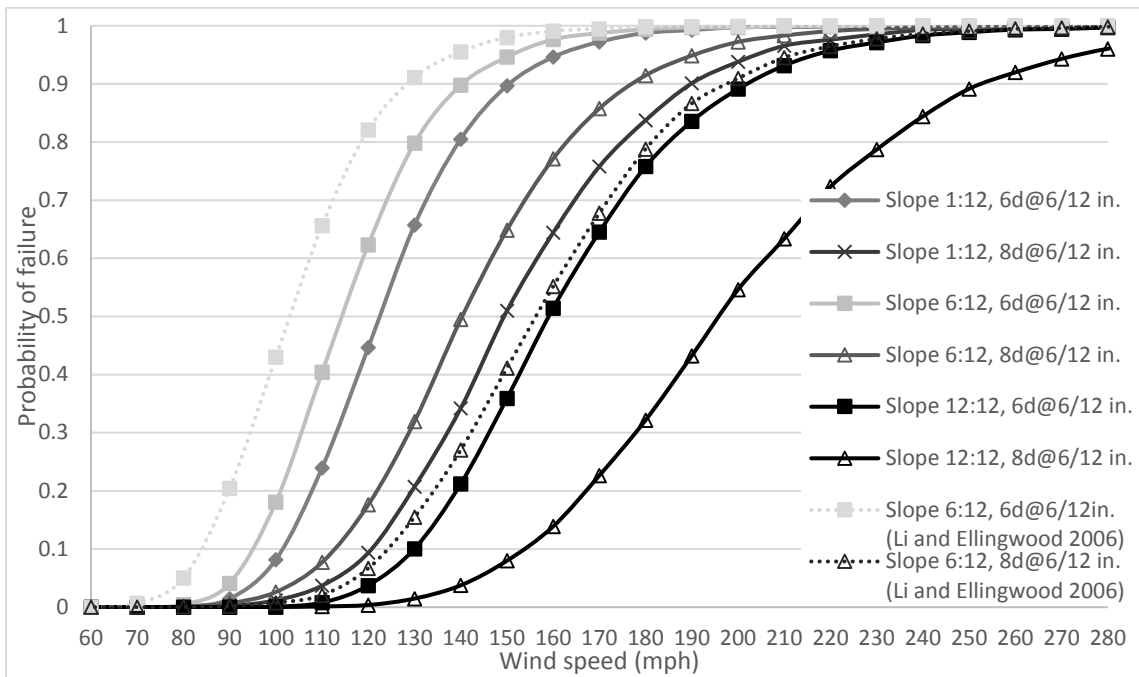


Figure 2.5 Fragility analysis of new CCA-treated roof panel (Exposure B)

For the purpose of calibration, two scenarios (slope 6:12, 6d nails with 152.4/304.8 mm & 8d nails with 152.4/152.4 mm) are compared with existing literature. According to Li and Ellingwood (2006), the probability of failure is nearly 0.43 when the wind speed is 44.7 m/s (100 mph) and is 0.66 at 49.1 m/s (110 mph) for 6d nails with 152.4/304.8 mm. For Fig. 5, the probability of failure is approximately 0.18 at 44.7 m/s (100 mph) and is up to 0.40 at 49.1 m/s (110 mph). The reasons for the difference include: 1) the external pressure coefficient is 1.81 for Li and Ellingwood (2006) which is based on ASCE 7-95 while the coefficient is 2.32 for this chapter which is based on ASCE 7-10; 2) different panel ultimate withdrawal capacities (see details in Table 2.3).

Figure 2.6 illustrates the time-dependent fragility analysis of CCA-treated roof panels under the case (6d nails with 152.4/304.8 mm) with coastal distance less than 1 km. The analysis includes time periods from 2000 through 2050 respectively for demonstrating the time-dependent embedded corrosion. The fragility curves of year 2000 and 2010 almost overlap while the fragilities show big difference after year 2010. For a given wind speed of 35.8 m/s (80 mph), the probability of failure is less than 0.1 from 2000 through 2030, but it increases to approximately 0.45 in 2040 and 0.75 in 2050. Similarly, when wind speed is 44.7 m/s (100 mph), the chance of failure is around 0.2 before 2010; however, it increases by 75% in 2020 and almost triples in 2030. It can be observed that after the zinc coatings being exhausted in 10 years, the embedded corrosion has increasingly impact on the reliability of roof panels with higher wind speeds.

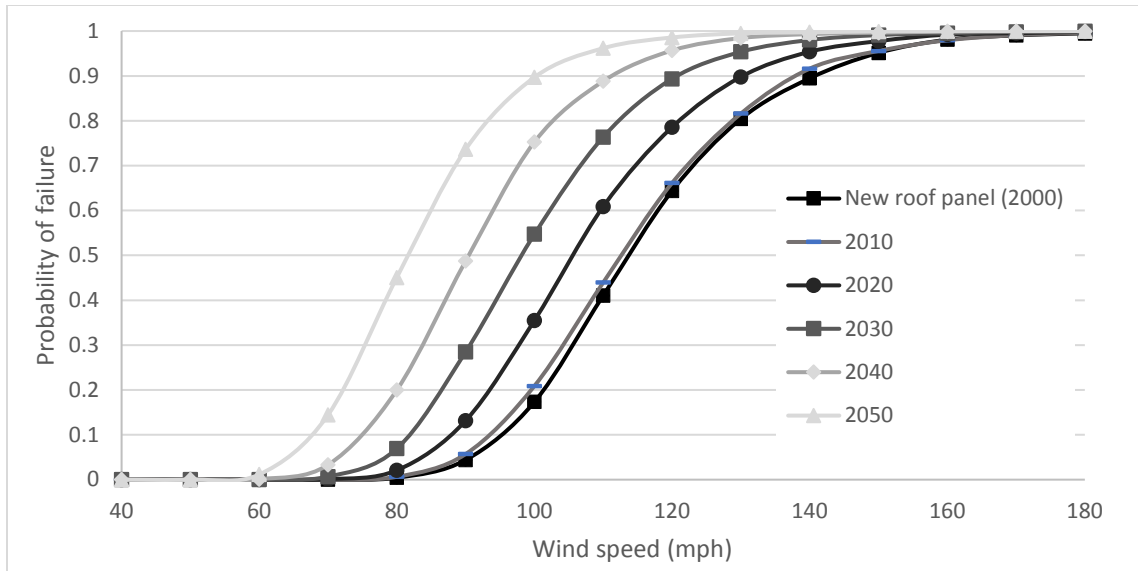


Figure 2.6 Fragility analysis of time-dependent CCA-treated roof panel (6d nails @6/12 in.)

Figure 2.7 shows the probability of failure of CCA-treated roof panels for the case (6d nails with 152.4/152.4 mm) with distance between construction and coast less than 1 km in 2020. Three climate change scenarios and corrosion status in Miami-Dade in a 50-year return period are presented and 10th, 30th, 50th, 70th and 90th percentile values account for uncertainty present in these estimations. For example, these values are 0.667, 0.540, 0.461, 0.374 and 0.270 for climate change scenario CON+RCP8.5 with corrosion. It can be observed that the roofing system is under significant damage risks under all selected climate scenarios in 2020.

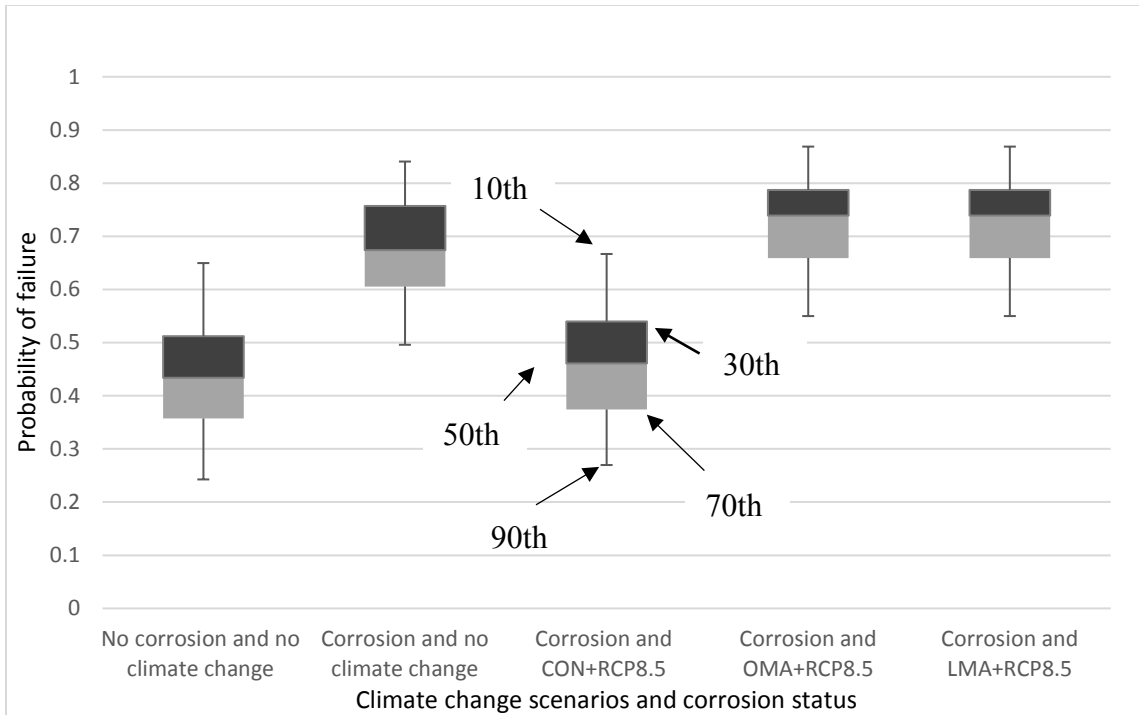


Figure 2.7 Probability of failure of CCA-treated roof panel (Zinc, 6d nail @6/6 in., slope 6:12) for 50-year return period wind speeds under climate change scenario LMA+RCP8.5 (distance between construction and coast less than 1 km)

Table 2.5 shows the time-dependent lognormal fragility parameters for roof panels with slope 6:12. The effects of distance between construction and coast, nail size, nail schedule, and building enclosure integrity to the roof panels are considered. From analysis, it can be concluded that the distance has relatively limited influence to the roof panel reliability. This result is in accordance with the roof panel withdrawal capacity analysis earlier. The same method can be applied to different slopes such as 1:12 and 12:12, and it should yield similar conclusions.

Table 2.5 Lognormal fragility parameters for roof panel with slope 6:12

Year	Building enclosure integrity	Nail size and schedule	Distance between construction and coast (<i>km</i>)			
			≤ 1		> 1	
			λ	ξ	λ	ξ
2020	Enclosed	6d@6/12 in.	4.659	0.1588	4.691	0.1551
		8d@6/12 in.	4.875	0.1789	4.903	0.1816
		6d@6/6 in.	4.995	0.1545	5.026	0.1615
		8d@6/6 in.	5.216	0.1774	5.243	0.1769
	Partially Enclosed	6d@6/12 in.	4.601	0.1741	4.632	0.1499
		8d@6/12 in.	4.817	0.1777	4.677	0.1547
		6d@6/6 in.	4.938	0.1492	4.972	0.1515
		8d@6/6 in.	5.156	0.1800	5.188	0.1702
	Enclosed	6d@6/12 in.	4.587	0.1572	4.634	0.1646
		8d@6/12 in.	4.812	0.1754	4.857	0.1750
		6d@6/6 in.	4.921	0.1606	4.974	0.1499
		8d@6/6 in.	5.153	0.1719	5.198	0.1695
2030	Partially Enclosed	6d@6/12 in.	4.533	0.1503	4.580	0.1577
		8d@6/12 in.	4.755	0.1783	4.795	0.1828
		6d@6/6 in.	4.864	0.1491	4.916	0.1562
		8d@6/6 in.	5.093	0.1786	5.137	0.1759
	Enclosed	6d@6/12 in.	4.502	0.1575	4.578	0.1534
		8d@6/12 in.	4.746	0.1703	4.801	0.1859
		6d@6/6 in.	4.837	0.1565	4.913	0.1524
		8d@6/6 in.	5.082	0.1761	5.141	0.1922
	Partially Enclosed	6d@6/12 in.	4.446	0.1558	4.518	0.1600
		8d@6/12 in.	4.688	0.1756	4.748	0.1739
		6d@6/6 in.	4.778	0.1585	4.853	0.1496
		8d@6/6 in.	5.027	0.1661	5.088	0.1776
2040	Enclosed	6d@6/12 in.	4.401	0.1560	4.506	0.1577
		8d@6/12 in.	4.667	0.1727	4.746	0.1860
		6d@6/6 in.	4.731	0.1547	4.838	0.1565
		8d@6/6 in.	5.001	0.1750	5.087	0.1756
	Partially Enclosed	6d@6/12 in.	4.344	0.1458	4.447	0.1557
		8d@6/12 in.	4.610	0.1680	4.693	0.1722
		6d@6/6 in.	4.673	0.1564	4.780	0.1536
		8d@6/6 in.	4.944	0.1695	5.030	0.1658

2.5 Reliability Analysis of CCA-Treated Wood Roof Panels

The annual probability of failure is determined by convolving the structural fragility curve and the projected hurricane wind speed curves (Li and Ellingwood 2006),

$$P_f(t) = \int_0^{\infty} F_R(v(t))f_V(v(t))dv \quad (2.13)$$

in which $F_R(v(t))$ is the structural fragility, defined as the conditional probability of failure of certain limit states given a certain wind speed and $f_V(v(t))$ is the probability density function for hurricane wind speed. The wind speed, $V(t)$, is a time-dependent variable at t year here.

Vickery et al. (2000) performed hurricane simulations and proposed the Weibull distribution is appropriate model for hurricane wind speed prediction in the United States. The PDF of the Weibull equation considering non-stationary wind speed due to climate change is given by Bjarnadottir et al. (2011):

$$f_v(v, t) = \frac{\alpha(t)}{u(t)} \left(\frac{v}{u(t)}\right)^{\alpha(t)-1} \exp\left[-\left(\frac{v}{u(t)}\right)^{\alpha(t)}\right] \quad (2.14)$$

where v is the 3-s gust wind speed, $\alpha(t)$ and $u(t)$ are time-dependent parameters of the Weibull distribution. The wind speed v , is related to the return period (T) of the hurricane by

$$v = u(t)\left[-\ln\left(\frac{1}{T}\right)\right]^{\frac{1}{\alpha(t)}} \quad (2.15)$$

Miami-Dade County is chosen to illustrate the potential impact of climate change. The wind speed maps developed from Vickery et al. (2000) indicate that the 50, 100, and 1000-year return period 3-sec gust wind speeds are 59, 67 and 81 m/s (132, 150 and 182 mph) respectively. The corresponding Weibull distribution parameters are $u = 27.58$, $\alpha = 1.79$. The above is set as baseline case. Stewart (2015) indicated that a time-dependent linear change of climate impact is still valid to 2070 and the effect of a non-linear time-dependent change in wind speed have a minor influence on damage risks. Hence, it is considered here that a time-dependent linear change in wind speed is legitimate for all climate change

scenarios for every 10 years. For example, the change in wind speed is linear from 2020 through 2030, and then from 2030 through 2040 and so on for 50-year return period wind speeds. The percentage change for 50-year return period wind speed is applied to the scenarios of 100- or 1000-year return period wind speeds. For instance, under emission scenario LMA+RCP8.5 the 1000-year return period wind speed at 2020 will be 82.4 m/s (184 mph). If the 50-year return period wind speed increases by 1.67% in a 50-year return period from 2020 through 2025, then the wind speed at 2025 is 83.8 m/s (188 mph) in a 1000-year return period. The corresponding Weibull parameters are $u(1) = 28.03$, $\alpha(1) = 1.79$; $u(5) = 28.48$, $\alpha(5) = 1.79$.

The projected hurricane wind speed above and fragility models developed previously are convolved to determine the limit state probability shown by Eq. (2.13). The annual probability of failure for CCA-treated roof panels are determined in Figure 2.8. Three climate change scenarios are selected to show the potential impact of climate change and embedded corrosion to CCA-treated roof panels configured with 6d nails with 152.4/304.8 mm. The annual probability of failure increases due to combined effects of climate change and embedded corrosion. By 2050, the damage risks are all tripled and particularly for emission scenarios LMA+RCP8.5, CON+RCP8.5 and OMA+RCP8.5 are quadrupled approximately.

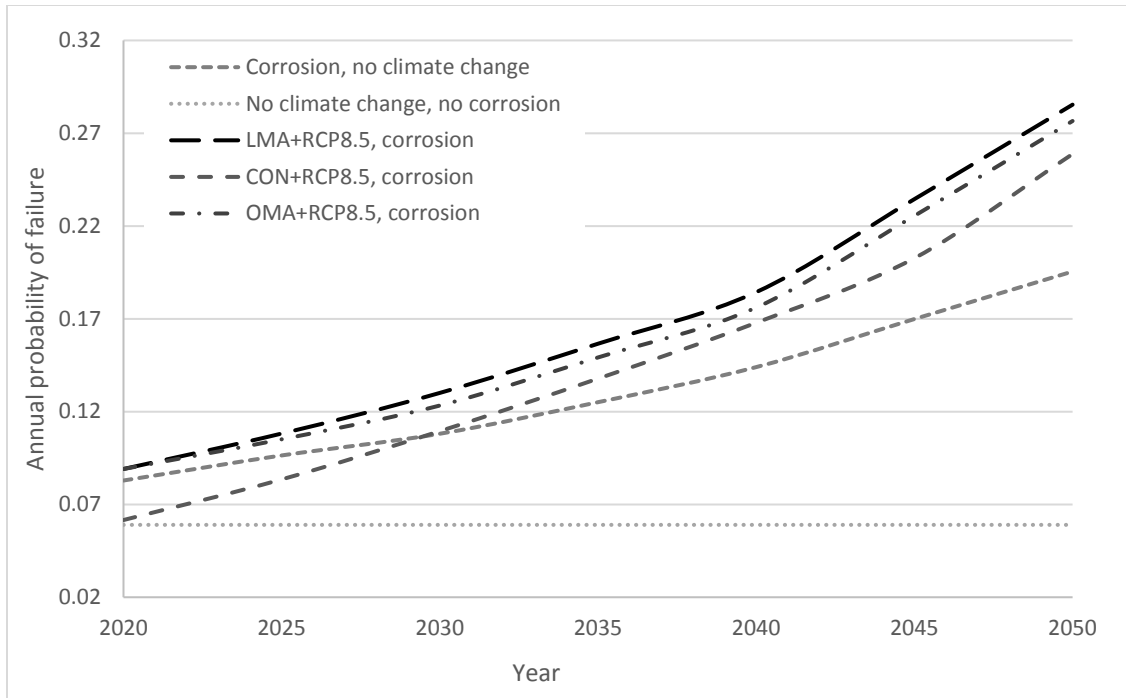


Figure 2.8 Annual probability of failure under selected climate change scenarios (distance between construction and coast less than 1 km)

The percentage increase in the annual probabilities of failure of CCA-treated roof panels (distance between construction and coast less than 1 km) for various climate change scenarios and corrosion status are demonstrated in Table 2.6. The case of year 2020, enclosed envelope and 6d nails with 152.4/304.8 mm is set as a target value for comparison. It can be observed that, within a typical 50 years' service life, two climate change scenarios, OMA+RCP8.5 and LMA+RCP8.5 respectively have the biggest impact on the reliability of roof panels. Building enclosure integrity is considered including two scenarios, enclosed and partially enclosed of the building envelop respectively. The probability of failure is relatively greater when the envelope of the building is partially enclosed. Furthermore, it can be observed that even without considering climate change, the effect of corrosion can still increase the failure probability significantly. Hence, effective retrofitting strategy needs to be studied accordingly.

Table 2.6 The percentage increase in the annual probability of failure of CCA-treated roof panel (6d @6/12 in., slope 6:12, distance between construction and coast less than 1 km) for different climate change scenarios

Year	Building enclosure integrity	Climate change scenarios						
		No C&C*	Ratio of climate change scenarios and no corrosion and no climate change scenario (%)					
			No climate change	1	2	3	4	5
2020	Enc.	0.059*	141	151	141	141	151	104
	Penc.	128	177	188	177	177	188	134
2030	Enc.	100	185	209	209	197	220	186
	Penc.	128	227	253	253	240	266	227
2040	Enc.	100	244	299	285	271	313	285
	Penc.	128	296	354	340	325	369	340
2050	Enc.	100	331	469	423	408	484	439
	Penc.	128	387	529	482	467	545	498

Enc.: Enclosure
Penc: Partially Enclosure
C&C*: Climate Change and Corrosion

2.6 Retrofitting Strategies

2.6.1 Hurricane Damage Risks and Retrofitting Strategies

Some studies have been done to evaluate the damage risks subject to hurricane as well as the accordingly retrofitting strategies. van de Lindt et al. (2007) identified that the water intrusion damage caused by a nearly loss of a roof panel for a Mississippi residential building is tantamount to the purchase price of the house five years ago. Li (2012) suggested that the highest priority should be assigned to study and development in mitigating the risks, protecting a building's roof and openings and proposed hurricane retrofitting measures including: 1) using 8d nails as a substitute for 6d nails, 2) replacing window panels with glass panels, 3) employing H2.5 connector for roof-to-wall connection.

It has been demonstrated that the structural adhesives are feasible and effective for retrofitting wood roof panels (Grayson 2014; Prevatt et al. 2014; Turner et al. 2009). Jones (1998) discovered that the adhesives can double the uplift capacity of the sheathing over the rafters by conducting suction tests on 1.2 m by 2.4 m (4 ft by 8 ft) roof sheathing panels in a pressure chamber loading the panels monotonically until failure. Recently, Prevatt (2007) proposed another retrofitting method called closed-cell sprayed applied polyurethane foam (ccSPF). The ccSPF insulation is primarily used in residential construction as thermal insulation in the roof and exterior walls of a building; however, ccSPF is also impermeable to water penetration, has relatively high tensile and compressive strength (around 137.9 kPa (20 psi)), and can develop a firm bond with wood (Prevatt (2007)). Currently, there are at least three adhesive products (i.e., Alpha FOAMSEAL Hurricane Adhesive, Insulstar Plus and ComfortFoam) and two ccSPF products approved as structural retrofits for wood roof-sheathing panels in Florida (Datin et al. 2011).

Datin et al. (2011) tested the failure pressures for roof panels by applying three different configurations of ccSPF retrofitting strategies as shown in Figure 2.9, and found out that the nail size and spacing have no effect on the uplift capacity once the ccSPF fillet or the full foam is applied, indicating that configuration A&B can be grouped together as fillet. Furthermore, the probability distributions for the failure pressures of fillet and full foam were assessed using the Anderson-Darling (AD) goodness-of-fit (GOF) test; they both follow lognormal distributions with $LN\sim(5.232,0.175)$ and $LN\sim(5.392,0.182)$ respectively (Datin et al. 2011).

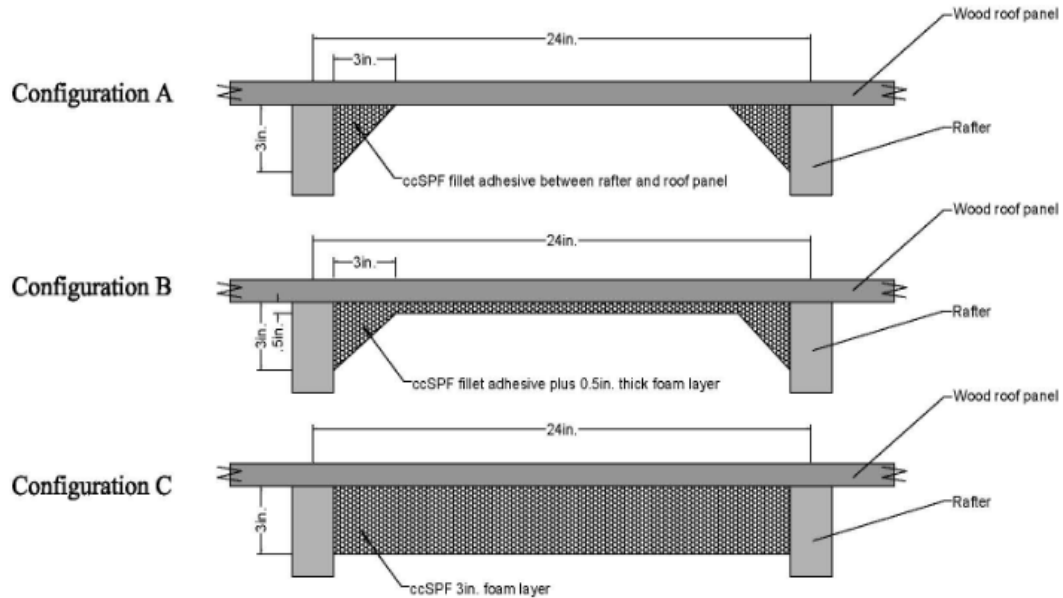


Figure 2.9 Illustration for three different configurations of ccSPF retrofitting strategies of wood roof panel

In this chapter, replacement of roof panels is not considered due to the difficulty of disposing the CCA-treated roof panels. Hence, only roof re-nailing is included, and actually it has been wide recognized as the easiest and most inexpensive method of reinforcing the roof sheathing attachment. APA (2000) mentioned that “during re-nailing the roof for high wind uplift regions, existing 6d nails should be ignored”. Based on this principle, the calculation of the resistant capacity for re-nailed roof panels will not include the remaining 6d nails. Five retrofitting strategies are selected including:

1. Roof panels that are attached to rafters with 8d nails instead of 6d nails;
2. Nail scheduling with 152.4/152.4 mm instead of 152.4/304.8 mm;
3. Roof panels with 8d nails with 152.4/152.4 mm;
4. Using ccSPF fillet;
5. Using ccSPF full foam layer.

Now consider a wood residential construction with a roof pitch of 6:12 in 2000 in Miami-Dade County and would like to see if it is necessary to retrofit in 2020. The original roofing

plan, which it is referred to “business-as-usual scenario”, was to use zinc-coating fastened CCA-treated wood roof panels with 6d nails with 152.4/304.8 mm. For the purpose of comparing the effectiveness of these proposed strategies with the business-as-usual scenario, and a 50-year service period is selected in order to explore the effectiveness of the selected retrofitting strategies.

Figure 2.10 shows the fragility curves after applying retrofitting strategies in 2020. As shown in Figure 10, all strategies are improving the performance of the roof panels with different extent. Strategy 1, which employs the bigger nail size, has the minimum impact while Strategy 5, which is to use ccSPF full foam layer, accounts for the greatest influence on the roof panel performances.

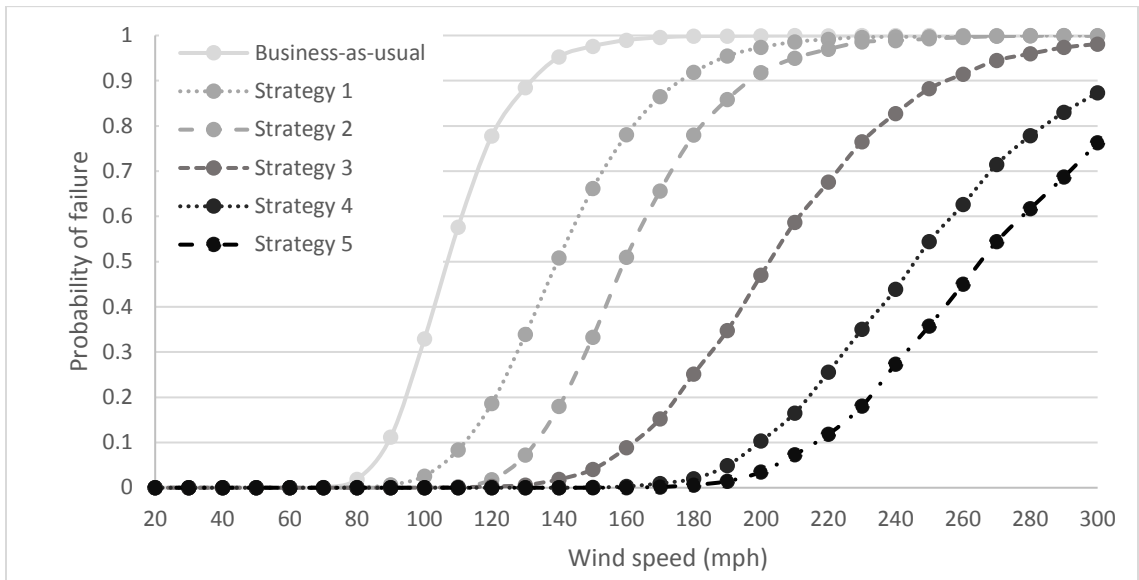


Figure 2.10 Fragility curves after applying retrofitting strategies in 2020 (distance between construction and coast greater than 1 km)

Figure 2.11 shows the annual probabilities of failure of the roof panels after applying the retrofitting strategies. By observing the scenario of business-as-usual, the roof panels have a great chance of failure, of which it almost reaches 0.08 in 2020 and 0.17 in 2050. Applying the retrofitting strategies to the roof panels decreases the chance of failure at a scattering scale. After “do something” in 2020, all strategies manifest the effectiveness. Particularly it can be clearly observed that strategies 3-5 have better reliability, especially

the performances of strategies 4&5 exert superior effectiveness. It also needs to be noted that a lot of researchers have demonstrated that ccSPF, which is used in strategies 4&5, has great durability and shows very little time-dependent degradation. Due to lacking of evidence and unavailability of data showing the capacity of ccSPF reduces over time, it is assumed that the resistant capacity does not vary with time. Further study needs to be done to quantify the relationship between capacity of ccSPF and time. When such information becomes available, it can be easily incorporated into the proposed evaluation framework to update the analysis. A summary of major assumptions in this chapter is listed below,

1. Nails have no variations in terms of lengths and the resistant capacity of ccSPF is time-independent.
2. Zinc-coating is evenly distributed on the nail surface and does not increase the fastener strength and the order of corrosion for the zinc-coating is symmetrical and simultaneous.
3. Wind speeds change linearly every 10 years for all climate change scenarios.

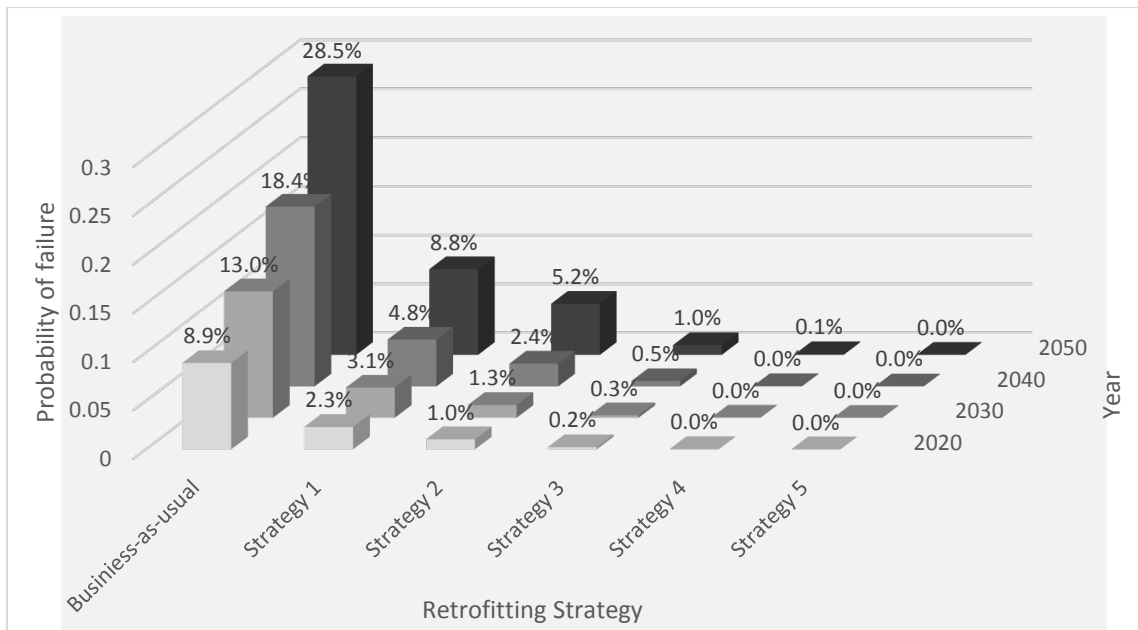


Figure 2.11 Annual probability of failure for roof panel (6d@6/12in.) after applying retrofitting strategies in 2020 under climate change scenario LMA+RCP8.5 (distance between construction and coast greater than 1 km)

2.7 Conclusions

This chapter proposes a framework to assess the combined effects of climate change and embedded corrosion for wood roof panels with zinc-coated fasteners exposed to hurricane events, extending the traditional risk assessment of untreated wood construction to treated wood (CCA). The framework includes time-dependent roof panel withdrawal capacity by embedded corrosion, hurricane wind load considering potential impact of climate change, risk assessment of wood roof panels, and evaluation of various retrofitting strategies.

As shown in the case study, the vulnerability of CCA-treated wood roof panels in hurricane-prone areas increases significantly when climate change and embedded corrosion are considered. The roof panel withdrawal capacity is reduced by 50% in 30 years when embedded corrosion is considered. Subsequently, the annual probability of failure increases by 55% under climate change scenario LMA+RCP8.5 in 50 years.

Various retrofitting strategies are explored and the results show that applying ccSPF is the most effective method to reinforce the roof panels and reduce the damage probability during hurricane events. For example, the probability at wind speed of 54 m/s (120 mph) can be reduced 19% (from 0 to 0.19) if strategy 5 (closed-cell sprayed applied polyurethane foam) is adopted as opposed to strategy 1 (replacing 6d nails with 8d nails).

The proposed framework provides a more comprehensive way to evaluate hurricane damage to wood construction under hurricane events. For the future work, multiple corrosion mechanisms need to be considered including atmospheric corrosion. The combined effects of embedded, atmospheric corrosions and wood decay for untreated wood is another area for further investigation.

3. Hurricanes Risk-Based Assessment of Wood Residential Construction Subjected to Hurricane Events Considering Indirect and Environmental Loss²

3.1 Introduction

Wood residential construction is among structures that are susceptible to natural hazards (e.g., hurricane, earthquake and flooding). Light-frame wood construction is the most widely built structure in the United States (U.S.). 90% of residential buildings are light-frame wood construction (NAHB, 1999). Hurricanes are among the costliest natural hazards to impact residential construction in the coastal area of the US. It is estimated that the damage caused by Atlantic hurricanes in 2004 to 2005 was more than \$150 billion dollars, mainly due to the devastating effects of hurricane Katrina in 2005 (Pielke Jr et al. 2008). The insured coastal property values in Florida also contributed to the rise in insurance claims because they increased by 55% from the year 1988 to 1993, with totals increasing from \$566 billion to \$872 billion (Stewart et al. 2003). Clark (2008) pointed out that Hurricane Katrina caused 1,833 death and countless injuries with an accordingly \$43.6 billion in insurance losses. This indicated that indirect damage accounted for a significant proportion over the overall damage and it needed to be included in the loss analysis. Also, as the populations in hurricane-prone areas continue to increase, it is expected to result in the prospect of even higher damages and losses in the future (Bjarnadottir et al. 2011).

Potentially the future hurricane damage to wood structures could be more severe than that of the past observed losses. For one reason, it is predicted that the effects of climate change will be gradually aggravating from 2010 through 2110 (IPCC 2007). Recent studies have shown that the effects of climate change will likely change hurricane patterns (e.g., intensity and frequency) which could cause more intense hurricane events and

² A version of this chapter was previously published in *Journal of Sustainable and Resilient Infrastructure* and is re-used herein with permission from Taylor & Francis. The permission is presented in Appendix B.

subsequently render greater load on structures (IPCC 2013; Wang et al. 2012). For the other reason, structural resistance could be reduced by atmospheric and embedded corrosion (e.g., metal fastener) (Dong and Li 2015).

Studies were performed to assess environmental impact of buildings under earthquake events. The monetary losses due to environmental issues under natural hazards have been drawing attentions (Alduse et al. 2015). Hurricanes may cause environmental losses because each time a damaged structure is rehabilitated after a hurricane event, new materials are consumed and greenhouse gases emissions produced (Arroyo et al. 2015). Feese et al. (2014) examined the cost and environmental impacts of buildings by using a cradle-to-grave analysis subjected to seismic events. Arroyo et al. (2015) proposed a probabilistic framework to evaluate the environmental losses of a five-story framed building under seismic event. It is worth mentioning that this study is among the first to quantify the environmental losses for wood construction subjected to hurricane events.

The proposed study is to establish a framework to evaluate the loss of the wood residential construction subjected to hurricane winds including direct, indirect loss and environmental impact. Hurricane simulation model is used to predict the future wind speed accounting for the key parameters of climate change such as intensity and frequency. Four structural damage modes and the effect of corrosion are considered in the structural fragility analysis.

3.2 Hurricane Simulation

3.2.1 Stationary Hurricane Simulation

It has been recognized that hurricane simulation is the most widely means of hurricane risk analysis (Vickery et al. 2000). Hurricane simulation models involve using key hurricane parameters (e.g., hurricane spatial variations) and Monte Carlo simulation for assessing hurricane hazard level. Hurricane simulation is also used to account for the potential effects

of climate change in that it allows variables such as frequency and intensity to be considered in the simulation model.

The number of hurricanes for any given year can be simulated according to a Poisson distribution (Xu and Brown 2008). The Poisson distribution is modelled as:

$$f(x) = \frac{\lambda^x}{x!} e^{-\lambda}; \quad x = 0,1,2, \dots \quad (3.1)$$

where x is the number of hurricanes per year, λ is the average number of hurricanes in a given year computed from historical records, and $f(x)$ is the probability of x hurricanes in a given year.

The landing position of a simulated hurricane is usually expressed in latitude and longitude. The landing position is assigned based on the distribution of historical hurricanes landing in a specific area by dividing the coastline into bins as suggested by Xu and Brown (2008) and Huang et al. (2001). The approach angle shows the direction a hurricane heads to after making landfall. The approach angle is measured with North as 0 degree. Based on historical data, the approach angle is modeled with a bi-normal distribution (Kaplan and DeMaria 1995; Xu and Brown 2008):

$$f(\theta) = \frac{a_1}{\sqrt{2\pi}\sigma_1} \exp\left[-\frac{1}{2}\left(\frac{\theta - \mu_1}{\sigma_1}\right)^2\right] + \frac{(1 - a_1)}{\sqrt{2\pi}\sigma_2} \exp\left[-\frac{1}{2}\left(\frac{\theta - \mu_2}{\sigma_2}\right)^2\right] \quad (3.2)$$

where μ_1 and μ_2 are the means, σ_1 and σ_2 are the standard deviations, and a_1 is the weighting factor. The landing position and approach angle determines the path of a hurricane after landfall. Xu and Brown (2008) demonstrated that it is reasonable to assume hurricanes travel along a straight path in Florida due to the narrow shape of the state.

Translation velocity is the forward speed of the hurricane. It can be modeled as a lognormal distribution as (Brown 2009; Georgiou et al. 1983; Huang et al. 2001; Vickery and Twisdale 1995):

$$f(c) = \frac{1}{\sqrt{2\pi c\zeta}} \exp\left[-\frac{1}{2}\left(\frac{\ln c - \lambda}{\zeta}\right)^2\right] \quad (3.3)$$

where c is the translation velocity, λ is the logarithmic mean, and ζ is the logarithmic standard deviation. The translation velocity is assumed to be constant after landfall (Xu and Brown 2008).

The central pressure difference is modeled from historical data using the Weibull distribution (Georgiou et al. 1983; Huang et al. 2001; Vickery and Twisdale 1995; Xu and Brown 2008) as:

$$f_v(v) = \frac{\alpha}{u} \left(\frac{\Delta p}{u}\right)^{\alpha-1} \exp\left[-\left(\frac{\Delta p}{u}\right)^\alpha\right] \quad (3.4)$$

where Δp is the central pressure difference, and u and α are the parameters of the Weibull distribution determined from historical data.

The rise in central pressure (which results in weakening of intensity) of the hurricane after landfall is modeled as (Huang et al. 2001; Vickery and Twisdale 1995; Xu and Brown 2008):

$$\Delta p(t) = \Delta p_o \exp(-at) \quad (3.5)$$

where $\Delta p(t)$ is the central pressure difference at time t , Δp_o is the central pressure difference at landfall, a is a decay constant. For Florida, a is given by (Vickery and Twisdale 1995):

$$a = 0.006 + 0.00046 \cdot \Delta p_o + \varepsilon \quad (3.6)$$

where ε is an error term that is normally distributed with a mean of zero and standard deviation of 0.025.

Hurricane wind speed decays after landfall due to friction by land mass and reduction in storm's moisture. The most widely used speed decay model is known as KD95 developed by Kaplan and DeMaria (1995). The model is based on the assumption that hurricane wind speeds decay at a rate proportional to their landfall intensity and decay exponentially over land. The wind speed at any given time is given by (DeMaria et al. 2006; Kaplan and DeMaria 1995):

$$V(t) = V_b + (RV_0 - V_b)e^{-\alpha t} \quad (3.7)$$

where R is a sea-land wind speed reduction factor with a value of 0.9, $V_b = 13.75$ m/s and is a constant "background" intensity, V_0 is the maximum sustained 1-min wind speed at landfall, and $\alpha = 0.095 \text{ h}^{-1}$ which is a decay constant.

For any given hurricane, the gradient wind speed ($V_G(t)$) at any location at every time instant is given by (Holland 1980; Vickery et al. 2009):

$$V_G(t) = \left[\left(\frac{R_{max}}{r} \right)^B \left(\frac{B(t)\Delta p \exp \left[- \left(\frac{R_{max}}{r} \right)^B \right]}{\rho} \right) + \frac{r^2 f^2}{4} \right]^{1/2} - \frac{rf}{2} \quad (3.8)$$

where R_{max} is the radius to maximum wind speed, r is the distance from hurricane eye to point of interest, B is the Holland parameter, Δp is the central pressure difference, ρ is air density, and f is the Coriolis parameter. The radius to maximum wind is given by (MRI 2003):

$$\ln R_{max} = 2.556 - 0.000050255\Delta p^2 + 0.042243032\psi \quad (3.9)$$

where ψ is the storm latitude and Δp is the central pressure difference.

The Holland parameter B is given by (Powell et al. 2005):

$$B(t) = \frac{\rho e(V(t))^2}{\Delta p} \quad (3.10)$$

in which V_0 is the maximum wind speed, e is the base of natural logarithm, Δp is the central pressure difference, ρ is air density.

The gradient wind speed ($V_G(t)$) needs to be converted to surface wind speed by a surface wind speed factor (SF) in order to assess the performance. The conversion factor ranges from 0.8 to 0.86 based on the intensity of storms (Vickery et al. 2000). However, the wind speed in ASCE7 Eq. (3.10) is 3-sec wind speed at the height of 10 m. Hence, the surface wind speed needs to be further converted to 3-sec gust wind speed by a gust wind speed factor (GS). Xu and Brown (2008) conducted a 1000-year simulation to estimate the 3-sec gust factor using the ESDU model and found that the distribution of the calculated values of the factor is highly concentrated around 1.287 with a standard deviation of 0.002. This value has been adopted for use in this research. Given any hurricane wind speed from above, the velocity pressure on a building is calculated as (ASCE 2010)

$$q_h(t) = 0.613K_hK_{zt}K_d(V_{G2}(t))^2 \text{ (N/m}^2\text{)} \quad (3.11)$$

where V_{G2} = 3s wind speed at the height of 10 m in an open-country exposure at t year. ($V_{G2} = V_G * SF * GS$), K_h =exposure factor, K_{zt} =topographic factor (taken equal to unity in this chapter), K_d =directional factor.

The wind pressure $W(t)$ acting on structure is determined by (ASCE 2010):

$$W(t) = q_h(t)[GC_p - GC_{pi}] \quad (3.12)$$

in which $q_h(t)$ = velocity pressure evaluated at mean roof height at t year, G = gust factor, C_p = external pressure coefficient, C_{pi} = internal pressure coefficient. This is the basis for the winds pressures in *ASCE Standard 7* (ASCE 2010). Table 3.1 summarizes the wind load statistics for a typical low-rise residential structure. The dimensions are 8.5m by 12.2 m (28 ft by 40 ft), and the mean roof height is 3.8m (12.5 ft). The external pressure coefficients (GC_p) are dependent on various gable roof slopes. The hurricane simulation and wind pressure calculation are shown in Figure 3.1.

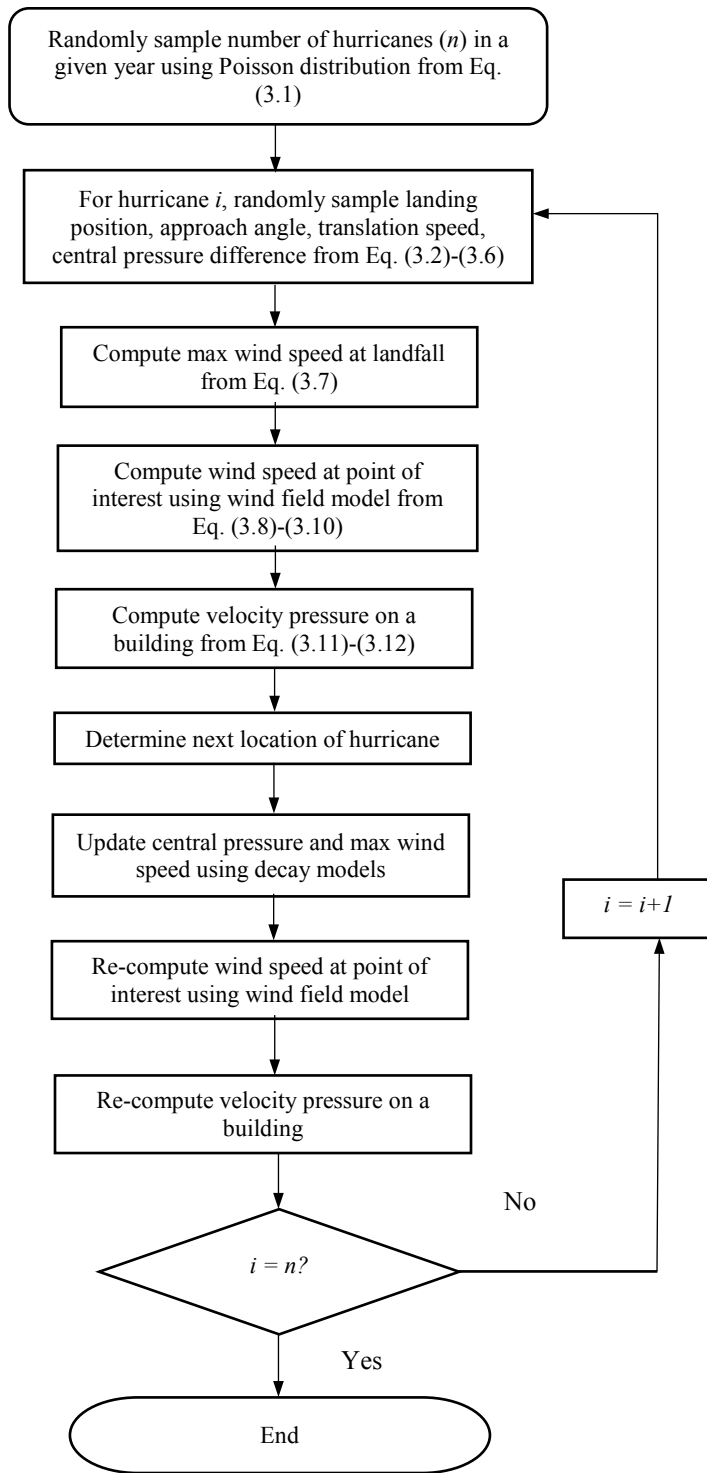


Figure 3.1 Hurricane simulation model flowchart

Table 3.1 Wind load statistics

Variable	Mean	COV	CDF	Source
K_h (Exposure B)	0.57	0.12	Normal	
GC_p (C&C) Zone 3 (slope 1:12, $\theta < 7^\circ$)	2.02	0.22	Normal	(Li and Ellingwood 2006)
GC_p (C&C) Zone 3 (slope 6:12, $7^\circ < \theta \leq 27^\circ$)	2.32	0.22	Normal	
GC_p (C&C) Zone 3 (slope 12:12, $27^\circ < \theta \leq 45^\circ$)	1.12	0.22	Normal	
GC_{pi} (Enclosed)	0.15	0.05	Normal	
GC_{pi} (Partial enclosed)	0.45	0.09	Normal	
K_d	0.89	0.14	Normal	

C&C: Component and cladding

The output of the model aforementioned is the annual maximum wind speed for a simulation of 300,000 years (number of Monte Carlo simulation iterations) at a particular location (27.3°N, 80.3°W) in Port St Lucie, FL, which is the assumed location of interest to be discussed later. The maximum annual hurricane wind speed had been modeled by the extreme value (EV) distributions, namely, Gumbel (Type-1), Frechet (Type-2), and Weibull (Type-3). All the three types of EV distributions were fitted to the data as illustrated in Figure 2. From the figure, Weibull and Frechet distributions are more likely to fit the data than Gumbel distribution. Hence the latter is not considered for the future analysis. Furthermore, Weibull distribution was identified as the best candidate for modeling hurricane wind speed in coastal areas (Li and Ellingwood 2006). The scale and shape parameters of the Weibull distribution determined using maximum likelihood method are 26.5 and 1.78 respectively. The shape, scale, and location parameters of the Frechet distribution are 0.22, 8.56, and 16.33 respectively.

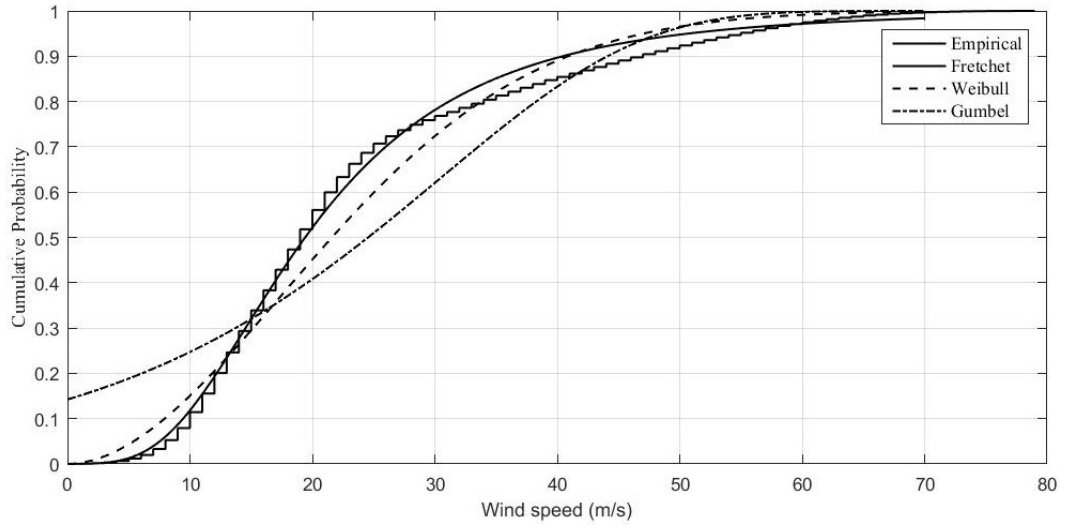


Figure 3.2 Validation of Hurricane Simulation

To validate the hurricane simulation model, wind speeds corresponding to different mean recurrence intervals (MRI) for the chosen location are calculated and compared to values in ASCE (2010). From Table 4.2 it can be seen that Weibull distribution is the closest one to those obtained from ASCE (2010). Note that the ASCE (2010) wind speeds corresponding to different MRI were extracted from ATC (2015). The Frechet distribution presents an unrealistically high wind speeds for larger MRIs, and this results are in accord with the study conducted by Yeo et al. (2013). Hence, Weibull distribution is selected for modeling the hurricane wind speeds in this chapter.

Table 3.2 Comparison of wind speeds corresponding to different return periods

MRI (years)	ASCE (2010) values (m/s)	Values predicted by Weibull distribution (m/s)	Values predicted by Fréchet distribution (m/s)
10	39	42	41
25	48	51	56
50	54	57	69
100	59	62	84
300	66	70	114
700	72	76	142
1700	77	82	177

3.2.2 Non-Stationary Hurricane Simulation Considering a Changing Climate

In recent decades, it has been indicated that the effects of climate change could alter patterns of hurricane hazard which can aggravate the degree of damage to coastal buildings (Banholzer et al. 2014). Many researchers have reported increasing hurricane activities over the last 30 years (Emanuel 2005; IPCC 2007; Mudd et al. 2014). It was estimated that the effects of climate change will increase hurricane-induced losses in the U.S. by up to 75% by 2080 (Donat et al. 2011).

The most recent climate change scenarios proposed by Intergovernmental Panel On Climate Change (IPCC (2013)) are based on greenhouse gas concentration pathways (CPs) which are determined by their radiative forcing at the end of the 21st century. Four Representative Concentration Pathways (RCPs) were produced by IPCC (2013) that correspond to radiative forcing levels of 8.5, 6.0, 4.5, and 2.6 watts/m² and are termed RCP 8.5, RCP 6.0, RCP 4.5, and RCP 2.6, respectively.

The key parameters of hurricane simulation model considering climate change are frequency and intensity of hurricanes. Wang et al. (2013) suggested that ± 10 m/s changes in extreme wind gust speeds in a 500-year return period are likely to happen when subjected

to $\pm 20\%$ intensity change and $\pm 50\%$ occurrence frequency change of hurricanes. Knutson et al. (2010) concluded that the global frequency of tropical cyclones will either decrease or remain unchanged with the authors predicting a decrease between -6 to -34%. Bender et al. (2010) modeled the effect of one of the SRES climate change scenarios on the frequency of Atlantic hurricanes and concluded that the frequency of the most intense hurricanes (category 3-5) is expected to increase through the year 2100.

The existing study showed the change of the hurricane intensity will range from -20% to +40% (Staid et al. 2014). Landsea et al. (2010) on the other hand reported the range of future hurricane frequency to be between -30% to +35%. Based on the information above, the following climate change scenarios from the year of 2020 to 2050 are assumed in Table 3.3.

Table 3.3 Climate change scenarios

Scenario	1	2	3	4	5	6	7
Change in intensity	0	10%	0	10%	10%	20%	-20%
Change in frequency	0	0	10%	-10%	10%	15%	15%

The hazard curves for the chosen location (27.3°N, 80.3°W) in Port St Lucie are plotted in Figure 3.3 for the baseline scenario (no change) and the six climate change scenarios above. For frequency variation, the parameter of the Poisson distribution, λ , is altered. For intensity variation, the randomly sampled central pressure difference at landfall is altered. The change in frequency and intensity from the present time to the end of the 21st century is assumed to be linear as suggested by Stewart et al. 2013. It can be noted from the figure that changes in intensity has higher effect on wind speeds than changes in frequency. For example, scenario 2 (+10% change in intensity, no change in frequency) results in higher wind speeds at all return periods than scenario 3 (+10% change in frequency, no change in intensity). The same conclusion can be drawn by comparing scenario 3 and scenario 4. Among the seven scenarios, only scenario 7 (+15% change in frequency, -20% change in

intensity) resulted in decrease in wind speed at all return periods despite 15% increase in frequency.

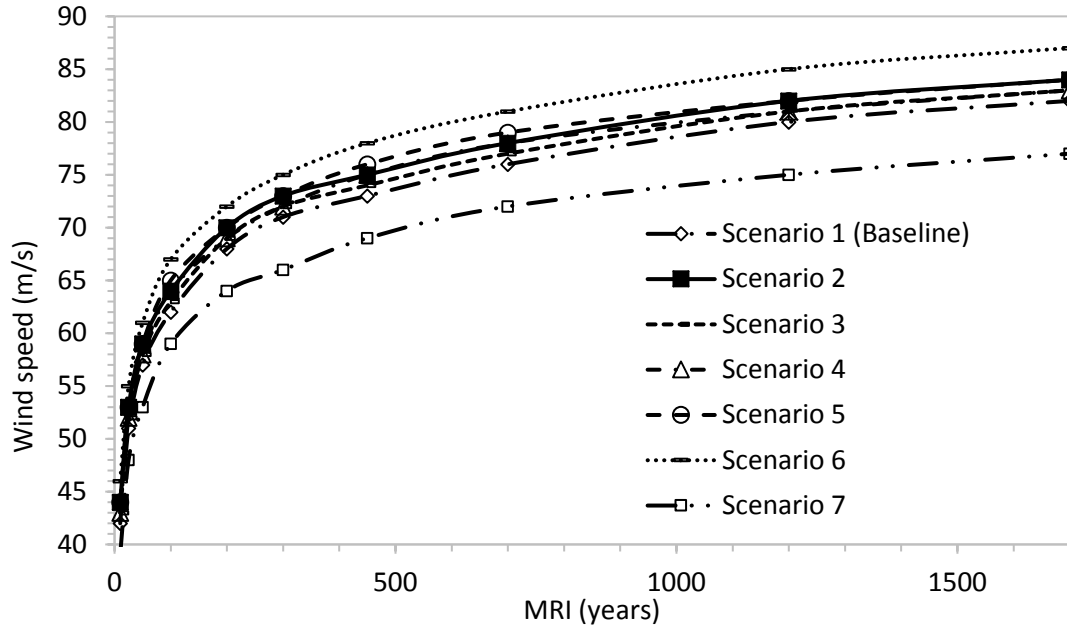


Figure 3.3 Hurricane wind speed at 27.3°N, 80.3°W for various climate scenarios

3.3 Basic Failure Modes and Limit State Function

A typical one-story light-frame wood residential house is considered for this chapter. Gable roof without roof overhang is selected with a slope of 6:12 for illustration purpose. The roof coverings are clay tiles with adhesive-set. The roof panel is 1.2 m by 2.4 m with two nailing patterns: nominal nail diameters are 2.9 mm and 3.3 mm for “6d” and “8d” nails, respectively. The building codes suggest that the steel fasteners are hot-dip galvanized to ASTM A153, Class D. The coating thickness regarding to density required to equal 1 oz of zinc per square foot of surface is $43\mu\text{m}$. American Galvanizers Association (AGA) stipulated that the coating thickness for all shapes and sizes of nail ranges from 35.6 to 99.1 μm AGA (2012). Based on above information, the zinc coating thickness is set to be $43\mu\text{m}$ in the chapter.

Panels are nailed at a spacing of 150 mm at the edges of the perimeter and 300 mm in the panel interior and the sheathing thickness 15.9 mm (Li and Ellingwood 2006). The framing members, such as trusses or rafters, consist of 50.8 mm by 101.6 mm Spruce-Pine-Fir (SPF) lumbers and are spaced 0.6 m on center with a specific gravity of 0.36.

It has been identified in the past literature that there are four failure modes for wood residential construction, which are: (1) breakage of openings; (2) loss of roof covering (e.g., tiles and shingles); (3) loss of roof or gable sheathing; (4) roof to wall connection (Pinelli et al. 2004). For a specific wind speed, the building will either not experience damage, or experience several of these five failure modes. Some damage modes are independent of each other (e.g., loss of shingles and breakage of openings); others are not (e.g., given that the building has experienced window breakage, the probability of its losing sheathing increases). The four failure modes will be discussed in detail in the later section.

3.3.1 Roof Covering Resistance

There are numerous roof coverings in the market such as asphalt shingles and tiles. Gurley et al. (2006) indicated that tile covering homes are more likely to experience damage compared to homes in shingle covering; furthermore, tiles are a major concern for window vulnerability when wind speeds are high enough to cause significant loss of roof cover. Here for illustration purpose, tiles are selected to explore the performance under hurricane events (Dixon et al. 2014). Barrel tiles are a preferred architectural choice for pitched roofs even though their wind resistance in high-velocity hurricane zones (HVHZ) has become a concern in the last few years (Shdid et al. 2010). Paruthyvalappil Alduse et al. (2015) performed fragility analysis for roof covering considering time-dependent roof shingle capacity based on sensor measurement and employed Bayesian approach to overcome the uncertainties related to the measurement.

Shdid et al. (2010) conducted experiments to explore various the performance of various tile settings subjected to wind loading. There are four specimens which are: 1) clay tiles

with adhesive-set; 2) concrete tiles with adhesive-set; 3) Clay tiles with mortar set; 4) concrete tiles with mortar-set. Shdid et al. (2010) show the statistical data for uplift resistance of single concrete and clay with adhesive-set and mortar-set with an assumption of Gaussian distribution. In this chapter, roof covering refers to tile instead of shingles and it needs to be noted roof shingles can be easily incorporated in the framework proposed. The limit states for roof covering is defined as

$$R - W(t) = 0 \quad (3.13)$$

where R = resistance of the roof covering, and $W(t)$ = time-dependent wind load.

3.3.2 Time-dependent roof sheathing capacity

The roof sheathing capacity can be determined based on the intended fastener and rafter framing spacing. Sutt (2000) demonstrated that tributary area method is appropriate for determining panel withdraw capacity from single fastener capacity. The fasteners with the largest tributary areas in the interior areas of the panes are of the most concern to the designer as these large areas have more negative pressure. In order to computer the design panel withdrawal capacity for negative pressure, the fastener withdrawal resistance should be divided by the largest tributary area. Sutt (2008) considered the panel effect and the underperformance of the nails in single fastener withdrawal based on test data and proposed the maximum panel withdraw capacity as:

$$P(t) = \left[\frac{R(t)*CF}{TA} \right] / SF \quad (3.14)$$

in which $P(t)$ is the design panel withdrawal capacity at t year; CF is 1.7, which is correction factor of panel effect and delta between actual nail withdrawal and design for smooth shank nail; TA is tributary area; SF is a factor of safety of 2. $R(t)$ is resistant force at t year.

Embedded corrosion is generated by corrosive agents that are within the surrounding wood, including wood acidity and timber moisture content (Nguyen et al. 2011). Parts inside the wood, such as the shank of nails, screws are affected.

The mean embedded corrosion depth, over the period t years is calculated by a power-law function (Nguyen et al. 2008),

$$C_{emb}(t) = C_0 t^n \quad (3.15)$$

where $C_0(\mu m)$ is the embedded corrosion depth for the first year; for metal embedded in untreated wood $n = 0.5$ for zinc and $n = 0.6$ for steel; for metal embedded in copper chrome arsenate (CCA)-treated wood $n = 0.6$ for zinc and $n = 1.0$ for steel.

The roof sheathing limit state is defined as the breach of the first roof panel, and specifically the component limit state is roof panel uplift due to fastener failure (Li and Ellingwood 2006). The governing limit state for roof performance is expressed as,

$$R(t) - (W(t) - D) = 0 \quad (3.16)$$

in which $R(t)$ = time-dependent structural resistance to wind uplift, and D and $W(t)$ are respectively, the dead and wind load effects, all terms expressed in dimensionally consistent units.

The limit state for the roof sheathing is modeled as the failure of the first panel because of the strong correlation between panel removal and subsequent contents damage noted previously. Panels at the roof corner are subjected to the highest wind uplift forces according to ASCE (2010). Once failure of a single fastener occurred, the load is distributed to the surrounding fasteners causing failure to propagate throughout the panel. The reliability of roof sheathing is defined as the first panel failure. The roof panel withdrawal capacity with 6d nails with 152.4/304.8 mm is demonstrated in Figure 4.4.

Three exposure conditions of nails are given, which are sheltered, vertically surface exposed, and horizontal surface exposed (Dong and Li 2015). The overall trend of time-dependent capacity is presented as negligently decreasing in the first stage, then dropping down significantly afterwards. The first stage means the zinc-coating still exists on the fastener surface, and afterwards is the point of all zinc-coating being exhausted. For roof panels under all conditions, before taking sharp downturns, roof panel withdrawal capacities decrease less than 5%. It can be observed that the performance of the roof panels could remain excellent and the capacities only reduce slightly under all circumstances before the zinc coatings are fully corroded (Dong and Li 2015).

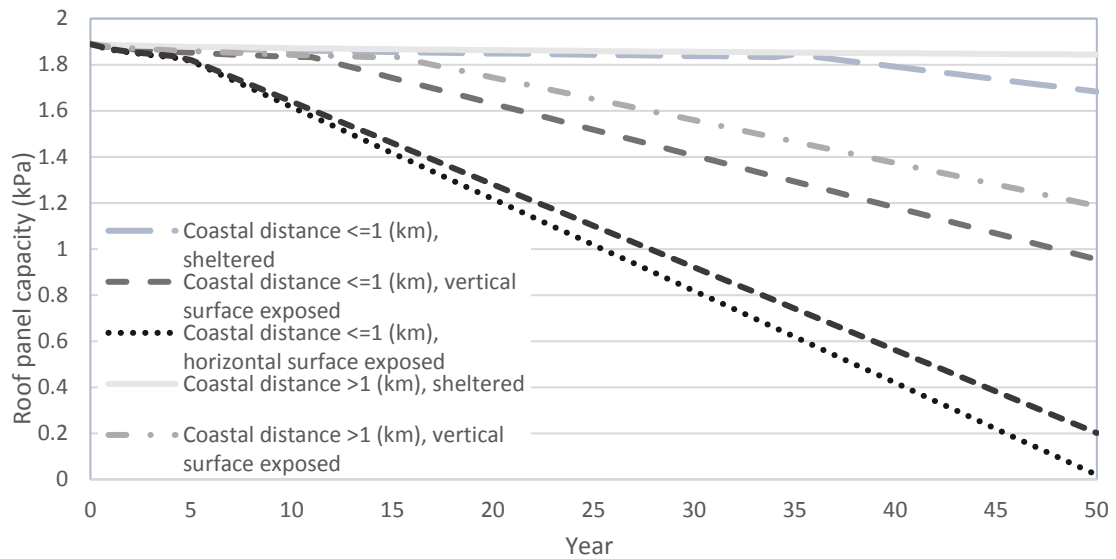


Figure 3.4 Roof panel capacity for CCA-treated roof panels (6d nails with 152.4/304.8 mm)

3.3.3 Roof-to-Wall Connection Resistance to Wind Uplift

Li and Ellingwood (2006) summarizes the statistics of uplift capacity of two common types of roof-to-wall connections: a connection in which the rafter is connected to the upper sill by three “8d” toenails and a connection in which the rafter is connected to the wall using

an H2.5 hurricane clip, installed as per manufacturer specifications. The first set is from laboratory tests of 15 specimens conducted at Clemson University. The second set was obtained from tests of 16 specimens conducted at the University of Missouri (Li and Ellingwood 2006). Pinelli et al. (2004) mentioned that the walls will become extreme vulnerable to wind loading when the roof-to-wall connection is compromised.

For roof-to-wall connection, the second connection from the end zone of a gable roof is most critical because the tributary area of that connection lies on the critical edge of the end zones of the roof, where the pressures are amplified by the characteristics of the wind flow over and around the roof. The limit states for roof-to-wall connection is defined as

$$R - W(t) = 0 \quad (3.17)$$

where R = resistance of the roof-to-wall connection and $W(t)$ = time-dependent wind load.

3.3.4 Window and door resistance to wind pressure

The American Society of Testing and Materials (ASTM) Standard E-1300 (2003) specifies the strength of annealed glass as the strength under uniform wind pressure with a 60-sec load duration with a probability of failure of 0.008. The 60-sec resistance value of annealed glass can be converted to a 3-sec strength that is consistent with the 3-sec gust wind used in ASCE Standard 7 by multiplying by a factor of 1.2. A Weibull cumulative distribution is a common model for defining the probability of failure of brittle materials such as glass, and it is used to model strength of glass to uniform wind load (Vallabhan et al. 1985). Vallabhan et al. (1985) found that the coefficient of variation of glass strength is in the range of 0.22 to 0.27.

Li and Ellingwood (2006) summarized the statistics of glass capacity due to wind pressure. The limit states for glass and door is defined as

$$R - W(t) = 0 \quad (3.18)$$

where R = resistance of the glass and door to wind pressure, and $W(t)$ = time-dependent wind load.

3.4 Fragility Analysis

Fragility analysis presents the probability of exceeding a damage limit state for a given structural type subjected to natural or man-made hazards (e.g., earthquake, hurricane) (Li and Ellingwood 2006). Figure 3.5 illustrates the time-dependent fragility analysis of CCA-treated roof panels under the case (6d nails with 152.4/304.8 mm) with coastal distance less than 1 km. The analysis includes time periods from 2020 through 2050 respectively for demonstrating the time-dependent embedded corrosion by assuming the wood construction was built in 2000. For a given wind speed of 35.8 m/s (80 mph), the probability of failure is less than 0.1 from 2020 through 2030, but it increases to approximately 0.45 in 2040 and 0.75 in 2050. Similarly, when wind speed is 44.7 m/s (100 mph), the chance of failure is around 0.35 before 2020; however, it increases to 0.54 in 2030 and doubles in 2040. It can be observed that after the zinc coatings being exhausted, the embedded corrosion has increasingly impact on the reliability of roof panels with higher wind speeds.

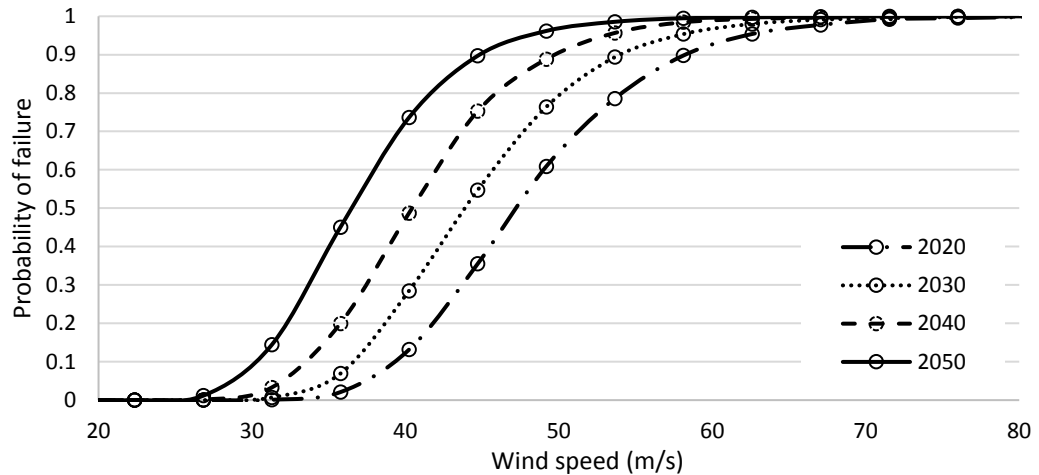


Figure 3.5 Fragility analysis of time-dependent CCA-treated roof panels (6d nails with 152.4/304.8 mm).

Fragility of damage modes mentioned above are shown in Figure 3.6. As it can be seen in the graph, roof covering is the most vulnerable component, while roof-to-wall connection is the most reliable component compared others. For example, the probability of failure is 0.8 when the wind speed is roughly 40 m/s for roof covering. For roof-to-wall connection, the probability is 0.8 when the wind speed is approximately 70 m/s.

This chapter is among the first to perform the fragility analysis of roof covering (clay tiles) and hence there is no existing fragility curve that can be used to compare with. However, the input of the fragility curves were verified by both finite element analysis and experiments by Shdid et al. (2010). The fragility curves for sheathing with 6d nails with 152.4/304.8 mm, glass (3.175 mm in 3.72 sq. m window) and clip (Exposure B) are calibrated with previous studies (e.g., Li and Ellingwood (2006)) The probabilities of failure for glass (3.175 mm in 3.72 sq. m window) and clip (Exposure B) are 0.53 at 54 m/s and 0.5 at 98 m/s respectively (Li and Ellingwood 2006). In comparison, the probabilities of failure for glass (3.175 mm in 3.72 sq. m window) and clip (Exposure B) are 0.82 at 54 m/s and 0.63 at 98 m/s here respectively. The reasons for the difference in

terms of sheathing, windows and doors include the different external pressure coefficient and component capacity (Dong and Li 2015).

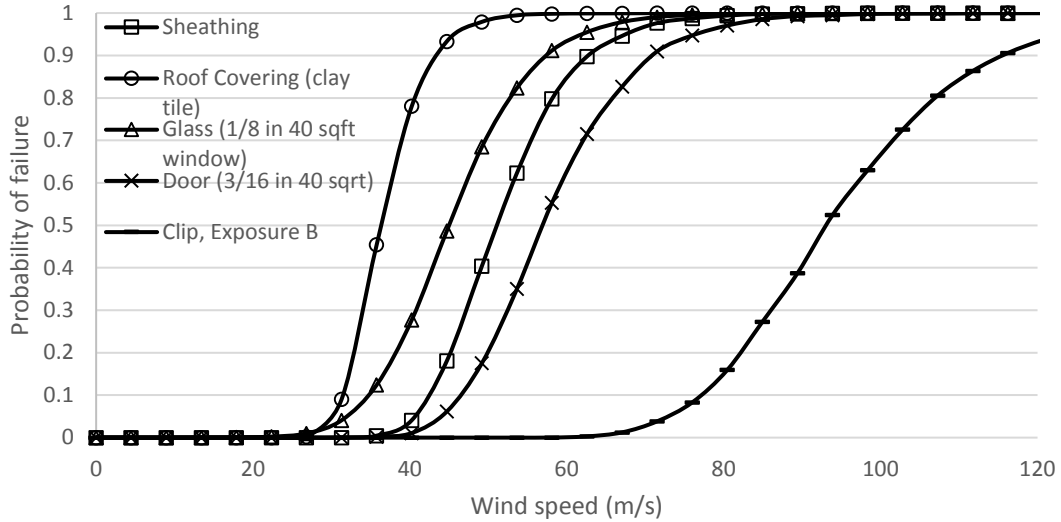


Figure 3.6 Fragility of four damage modes in wind

Li et al. (2011) defined three building damage states to failures of building components: minor damage—one roof panel; moderate damage—more than one window panel or multiple roof panels; and severe damage—roof-to-wall connections. In this chapter, roof covering damage is added into the damage states, and hence the authors defined four damage states here as shown in Table 3.4.

Table 3.4 Damage state definition

Damage state	Definition
Slight	First roof covering damage
Minor	First roof sheathing damage
Moderate	More than one window/door breakage
Severe	roof-to-wall connection damage

Figure 3.7 demonstrates the fragility of damage states in wind. For slight damage state, the probability of failure is 0.5 when the wind speed is around 30 m/s. For severe damage state, the probability of failure is 0.5 when the wind speed is around 70 m/s.

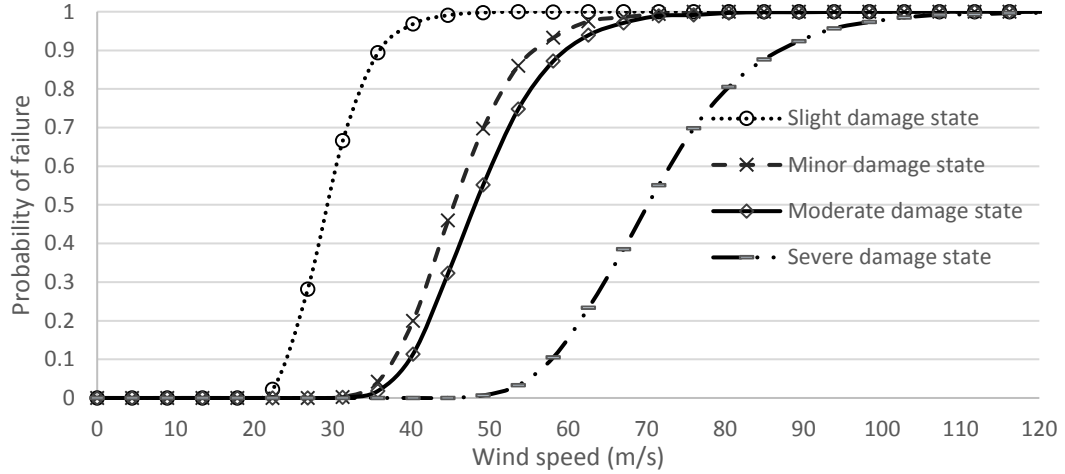


Figure 3.7 Fragility of damage states in wind

3.5 Risk-Based Loss Estimation

3.5.1 Hurricane Risk Analysis

Risk can be defined here as the annual probability of failure of the structural system and is (Li and Ellingwood 2006):

$$P_f = \int_0^{\infty} F_R(v, t) f_v(v, t) dv \quad (3.19)$$

where $F_R(v, t)$ is the time-dependent cumulative distribution function (CDF) of the structural fragility, and $f_v(v, t)$ is the time-dependent probability density function (PDF) of the annual maximum hurricane wind speed. $f_v(v, t)$ is modeled using the Weibull

distribution as discussed earlier while $F_R(v, t)$ can be modeled using Lognormal distribution (Bjarnadottir et al. 2013).

Figure 3.8 demonstrates the annual probability of failure for four damage modes under climate change scenario 5 (+10% change in intensity, +10% change in frequency). It can be seen that the probabilities of failure for all damage modes are increased to a certain extent. Notably the greatest increase is for roof sheathing from 0.06 at 2020 to 0.35 at 2050. The reason is that the vulnerability of the roof sheathing is affected by both the effects of climate change and material corrosion. In this chapter, the effects of corrosion for other damage modes are not considered. It needs to be addressed in the future research.

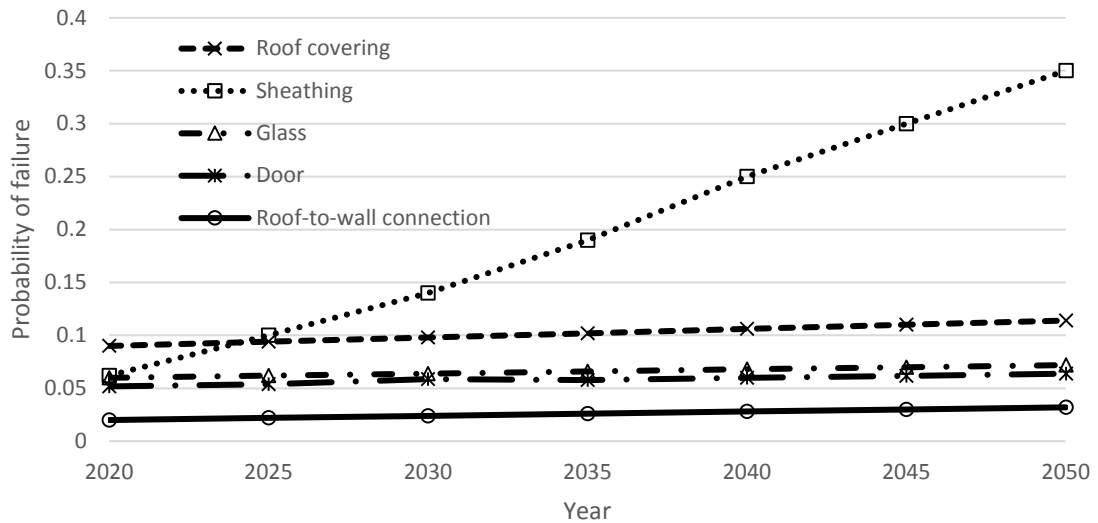


Figure 3.8 Annual probability of failure for four damage modes under climate change scenario 5 (+10% change in intensity, +10% change in frequency)

Figure 3.9 illustrates the annual probability of failure for a specific damage mode (window) under all climate change scenarios. It can be seen that the probability of failure decreased at the scenario 7 (-20% change in intensity, +15% change in frequency). Scenario 6 (+20% change in intensity, +15% change in frequency) has the greatest increase. From the comparison, it can be seen that the change in intensity has the major effect on the vulnerability of the structures.

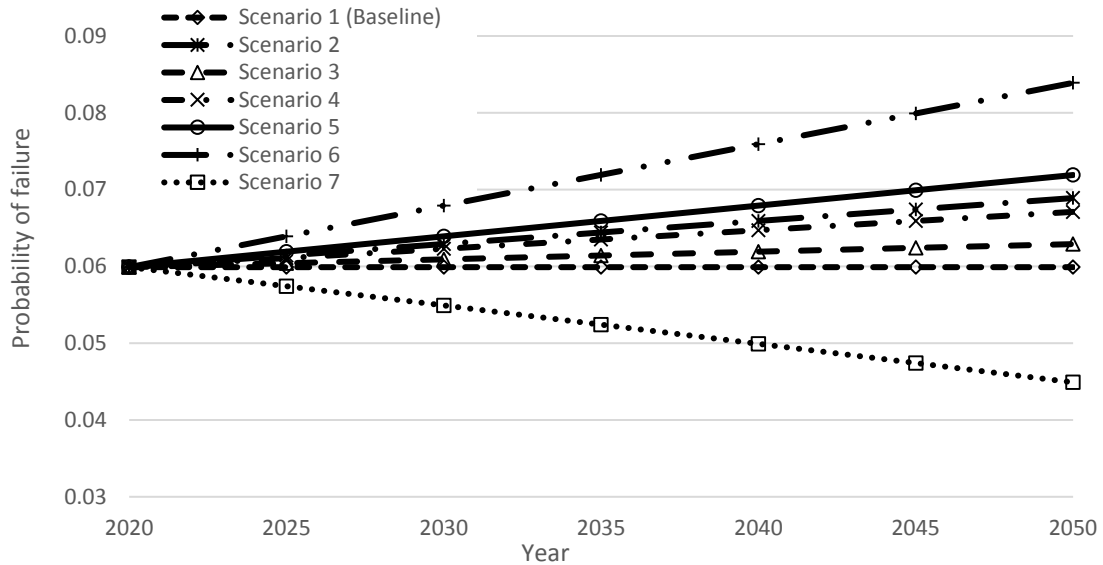


Figure 3.9 Annual probability of failure for window under climate change scenarios

Economic losses of low-rise structures under hurricane events has been evaluated using life-cycle assessment (Arroyo et al. 2015; Li et al. 2011). Life-cycle analysis allows buildings and infrastructures to be assessed, designed or retrofitted in an optimal manner considering its entire lifespan. Most decision-makers could benefit from the knowledge of cumulative monetary losses over a certain period or a lifetime. The life cycle loss can be obtained by evaluating annual losses. Life cycle loss of buildings under hurricane events have been modeled as Poisson process (Katz 2002; Li and Ellingwood 2009; Wen and Kang 2001).

3.5.2 Direct Loss Analysis

Direct loss analysis had been recognized a mature method to evaluate structural losses under extreme event. For example, the direct loss from the hurricane wind and the resulting rainwater intrusion is computed using the method of (Dao and van de Lindt 2011; van de Lindt and Dao 2011). Loss is computed as financial loss and then adjusted to be a percent of the building replacement value. In this chapter, the direct loss refers to structural and non-structural losses. Here for illustrative purpose, consider the value of the house is

\$200,000 in 2020. The value of potential losses from hurricanes, over a period of T, can be determined as (Li et al. 2011)

$$L(T) = \sum_{t=1}^T \sum_{i=1}^4 \frac{\lambda_i e^{-\lambda_i t} D_i}{(1+d)^{t-1}} \quad (3.20)$$

in which i is damage state (slight, minor, moderate, and severe); T is remaining service life (e.g., 50 years) of the building; D_i is losses attributable to hurricane in terms of percentage of total value as the consequence of i th limit state; d is annual discount rate that is assumed to be constant; λ_i is mean annual damage ratio attributable to hurricanes, which can be determined by Eq. (3.19), but double calculation needs to be avoided in the process. For example, probability of slight damage includes probability of minor damage, and then the slight damage level should subtract the moderate damage. The damage ratios of 2, 5, 20 and 50% are used for slight, minor, moderate, severe damage states for hurricane (Li et al. 2011). The annual probabilities of damage for difference damage states from year 2020 to 2050 are shown in Figure 3.10. For slight damage state, the probability of failure increases from 11.2% to 13.0%; while for severe damage state, the probability increases from 1.1% to 1.8% under climate change scenario 5 (+10% change in intensity, +10% change in frequency).

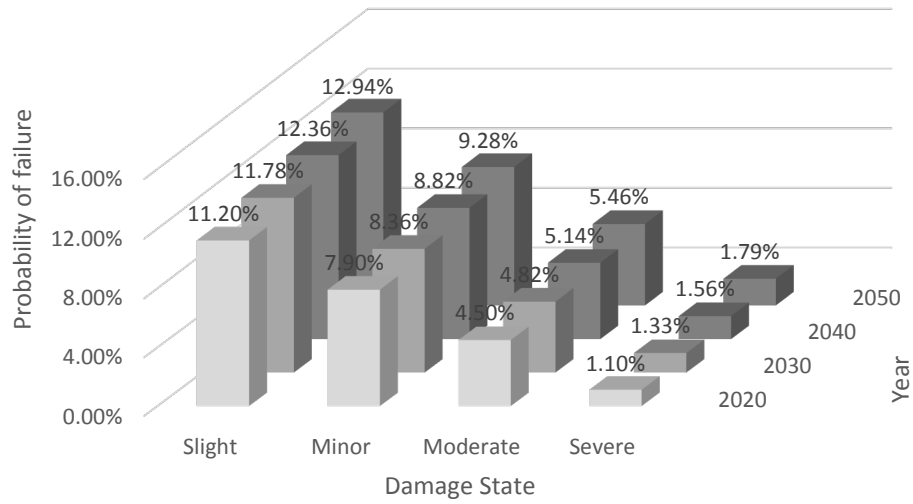


Figure 3.10 Annual probability of failure for various damage states subjected to climate change scenario 5 (+10% change in intensity, +10% change in frequency)

Figure 3.11 demonstrates the life-time direct loss under various damage states subjected to climate change scenario 5 (+10% change in intensity, +10% change in frequency). The cumulative damage for slight damage state is around \$1,300, and for severe damage state is around \$15,000. The costs of slight and minor damage states are much less than moderate and severe damage state, and the ratio of them is around 20%. The total direct loss is \$33,872.

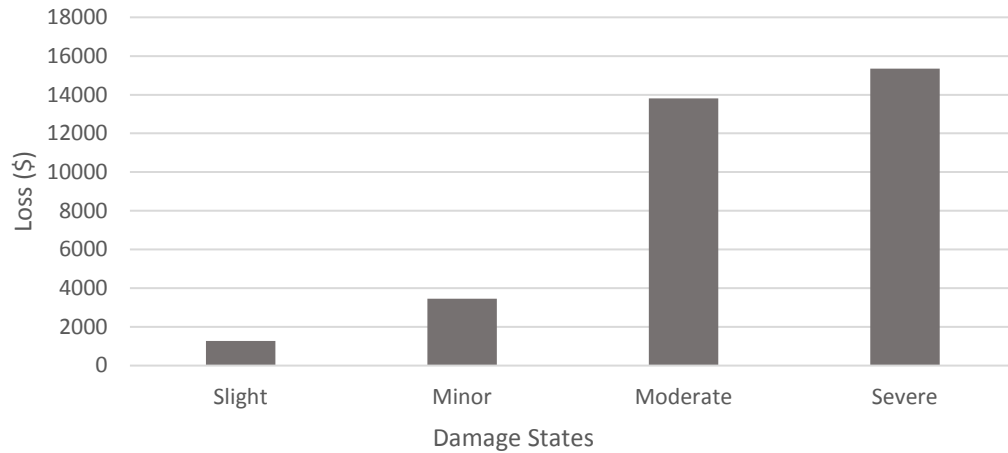


Figure 3.11 Life-time direct loss under various damage states subjected to climate change scenario 5 (+10% change in intensity, +10% change in frequency)

3.5.3 Indirect Loss Analysis

Many empirical studies have been conducted to estimate the economic impacts of hurricane in general (Elliott et al. 2015; Fischer et al. 2015; Li et al. 2011). However, only few of them have focused to measure the indirect loss due to hurricane. Modeling approaches for this purpose are mainly based on mathematical methodology and economic theories broadly divided into three categories: I-O models, regression analysis based on past hurricane damage data, and computable general equilibrium (CGE) models.

The I-O model is the most widely used tool for regional economic impact analysis, and its use for natural loss estimations dates from the 1970s (Rose 2004). The disadvantages of an I-O model include its linearity, lack of explicit resource constraints, limitation in spatial representation and lack of input and import substitution possibilities (Rose 2004). Hallegatte (2008) displayed the indirect losses as function of direct losses for Hurricane Katrina. Based on the results, Stewart et al. (2013) proposed an indirect cost ratio (ICR), defined as the ratio of direct-to-indirect costs, and built a mathematical relation between ICR and hazard vulnerability by conducting regression analysis based on the data from

Hurricane Katrina, Rita and cyclone Tracy. CGE models have gained popularity to estimate losses of hazards because of the inherent limitations of I-O models. Applying the CGE model, Rose and Liao (2005) studied the economic impact of the Portland, Oregon region for disruptions in water systems due to an earthquake. However, without further refinement, CGE models, as well as many other economic models are based on historical data.

In this chapter, the indirect cost is defined as the injuries and death since the scope of the study only includes residential construction. The estimated cost of injury and fatality in earthquake risk analysis was mentioned in Ellingwood and Wen (2005). However, very few studies has been done with regarding to cost estimation of injury and fatality subjected to hurricane events (Dixon et al. 2014). Ellingwood and Wen (2005) proposed four performance levels, which are immediate occupancy (IO), life safety (LS), collapse prevention (CP), and incipient collapse (IC) respectively and illustrated the related injury and fatality index as shown in Table 3.5. The four damage states in this chapter (slight, minor, moderate, severe) shares the similar concept and definition of the four performance levels proposed by Ellingwood and Wen (2005).

Table 3.5 Damage state/ injury/ fatality relationship.

Damage State	Slight	Minor	Moderate	Severe	Source
Injury rate	0	0.05	0.1	0.2	(Ellingwood and Wen 2005)
Death rate	0	0.005	0.01	0.02	
Damage ratio	0.05	0.2	0.4	0.9	

The injury and fatality costs are estimated \$7500/person and value of life is assumed to be \$2 million/ person (Ellingwood and Wen 2005). An occupancy rate of 2 persons/93 m^2 (1000 ft^2) is used. To estimate the life-cycle cost, a discount rate $\lambda = 5\%$ per year and

a future period of 30 years are assumed (from year 2020 to 2050). The expected life-time indirect loss can be expressed as

$$E[C_{indirect}(t)] = \sum_{t=1}^T \left(\frac{1}{dt} (1 - e^{-dt}) \sum_{i=1}^4 -C_i [\ln(1 - P_i) - \ln(1 - P_{i+1})] \right) \quad (3.21)$$

where P_i is t-year probability of i th damage state being exceeded. C_i is the injury/fatality cost.

Table 3.6 lists the life-time indirect loss considering various climate change scenarios. It can be seen that the indirect loss varies based on different scenarios. The least loss is for scenario 7 (-20% change in intensity, +15% change in frequency), \$14,668 in total; while the greatest loss is for scenario 6, \$19,089 totally. Compare with the direct loss under scenario 5 (+10% change in intensity, +10% change in frequency), which is \$33,872, the indirect loss account for 36% of the direct and indirect losses combined.

Table 3.6 Life-time indirect loss considering various climate change scenarios

Damage State	Scenario 1	Scenario 2	Scenario 3	Scenario 4	Scenario 5	Scenario 6	Scenario 7
Slight	\$459	\$478	\$466	\$472	\$501	\$607	\$399
Minor	\$1274	\$1,485	\$1,318	\$1,395	\$1,642	\$2,102	\$866
Moderate	\$3,759	\$4,345	\$3,842	\$4,092	\$4,906	\$6,142	\$3,426
Severe	\$9,549	\$12,217	\$10,537	\$11,478	\$13,022	\$16,788	\$8,668
Total	\$15,041	\$18,525	\$16,163	\$17,437	\$20,071	\$25,639	\$13,359

3.5.4 Environmental Impact

The construction of buildings has a considerable impact on the environment, and the construction industry is one of the greatest consumers of resources and raw materials (Dimoudi and Tompa 2008). According to data from the Worldwatch Institute, the

construction of buildings consumes 40% of the stone, sand and gravel, 25% if the timber and 16% of the water used annually in the world (Arena and De Rosa 2003). In Europe, the building sector accounts for approximately 50% of the total energy consumption (Bribián et al. 2009). In the U.S., 54% of energy consumption is directly or indirectly related to buildings and their construction.

Hurricanes may cause environmental losses because each time a damaged facility is rehabilitated after a hurricane event, new materials are consumed and greenhouse gases emitted (Arroyo et al. 2015). Thus, considering environmental losses is needed in the framework of hurricane risk analysis. The damage cost of structures involves the consideration of their initial cost and the potential future losses caused by hurricanes.

In order to quantify greenhouse emissions for a given process, those corresponding to the different gases are transformed into an equivalent carbon dioxide emission (i.e. $CO_2 - e$). Normally, the estimation of $CO_2 - e$ emissions related to a certain process is made through life cycle analysis (LCA) (EPA/600 2006). The $CO_2 - e$ emissions for concrete ranges from 11 to 179 $Kg CO_2 - e/ton$, glass from 257 to 2,100 $Kg CO_2 - e/ton$, steel from 35 to 3,809 $Kg CO_2 - e/ton$, wood from 14 to 400 $Kg CO_2 - e/ton$ (Arroyo et al. 2015). Carbon-tax approach will be used to place a value on the societal cost of greenhouse gas emissions. It needs to be noted that the values of carbon tax usually span 3 orders of magnitude and the large scatter is in part a consequence of various approach used in the estimation of the value of the carbon tax (Watkiss and Downing 2008). The present value of the environmental losses for a hurricane event occurring at time t can be computed as:

$$L_e(T) = \sum_{t=1}^T \sum_{i=1}^4 \sum_{j=1}^4 \frac{\lambda_i e^{-d_e t} H_i \eta_j}{(1 + d_e)^{t-1}} \quad (3.22)$$

in which H_i is the total insured value of a building; η_j is the ratio of the environmental cost and the total insured value of the buildings under j th emission scenarios; $j=1 \dots 4$, where 1 is the slightest scenario and 4 is severest scenario; $H_i \eta_j$ is the cost of greenhouse gas

emissions produced under j th emission scenarios during their construction; d_e is environmental associated discount rate.

Three emission scenarios and five carbon tax values are proposed in Table 3.7 accounting for the sensitivity of those variables. For simplicity, each emission scenario will take the average values. For slight scenario, $\eta_1 = 0.00188$; for minor scenario, $\eta_2 = 0.00362$; for moderate scenario, $\eta_3 = 0.01806$; for severe scenario, $\eta_4 = 0.037$. For parameter d_e , it has been recognized that d_e should be negative because the damage related to $CO_2 - e$ emissions is a function of the cumulated stock (Arroyo et al. 2015). A value of d_e equal to -0.008 was selected in the context of a linear regression analysis by fitting an exponential curve by Arroyo et al. (2015).

Table 3.7 η_j values related to the cost of $CO_2 - e$ emissions for wood buildings

Emission scenarios	$CO_2 - e$ (ton)	Carbon tax values				
		US\$10	US\$20	US\$50	US\$70	US\$220
1	5	0.0003	0.0005	0.0013	0.0018	0.0055
2	10	0.0001	0.001	0.0025	0.0035	0.011
3	50	0.0003	0.005	0.0125	0.0175	0.055
4	100	0.005	0.01	0.025	0.035	0.11

Figure 3.12 demonstrates the percentage of direct/indirect/environmental losses under scenario 1 (baseline), 5 (+10% change in intensity, +10% change in frequency), 6 (+20% change in intensity, +15% change in frequency) and 7 (-20% change in intensity, +15% change in frequency) from year 2020 to 2050. The life-cycle losses including direct, indirect and environment are \$56,778, \$63,113, \$73,636 and \$54,398, respectively. It can be seen from the charts that direct loss shares the largest percentage and the least is environmental loss. Indirect losses are increasing significantly when the climate scenarios aggravate. It needs to be noted that in this chapter, environmental loss is assumed to be insensitive to

changing climate, hence the monetary loss is \$12,100 for all climate scenarios. For the future study, the effects of climate change will be considered.

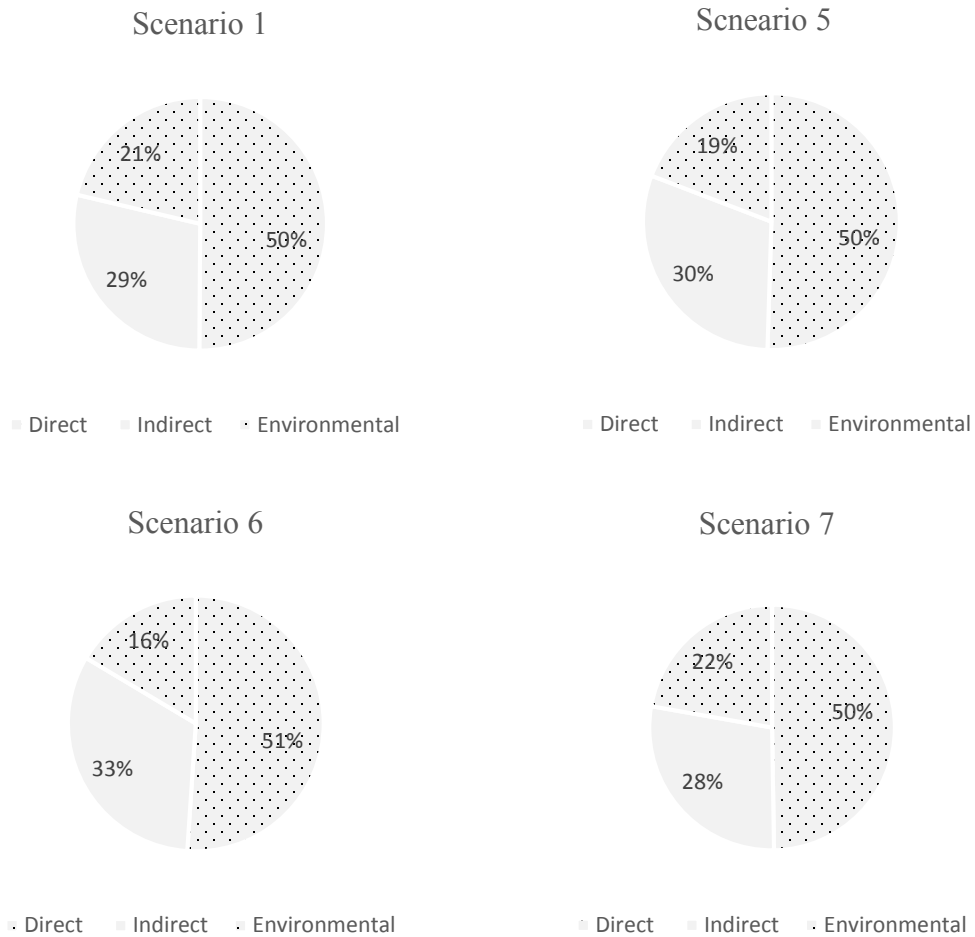


Figure 3.12 Direct/indirect/environmental losses comparison under scenario 1 (baseline), 5 (+10% change in intensity, +10% change in frequency), 6 (+20% change in intensity, +15% change in frequency) and 7 (-20% change in intensity, +15% change in frequency)

Figure 3.13-3.14 demonstrate the percentage increase in monetary loss of residential buildings subjected to hurricane events for the six different climate change scenarios compared to baseline case (No climate change, no corrosion) for year 2020 and 2050. It can be seen that when considering changing climate, the losses are time-dependent and dependent on the climate change scenarios. The rate of change for indirect losses are very

time-sensitive and vary widely by different climate scenarios. For instance, the percentage increase for climate scenario 6 (+20% change in intensity, +15% change in frequency) is 33% in 2020; while the value for climate scenario 6 is 136% in 2050. Scenario 7 (-20% change in intensity, +15% change in frequency) is the only scenario that both the direct and indirect share the negative increase.

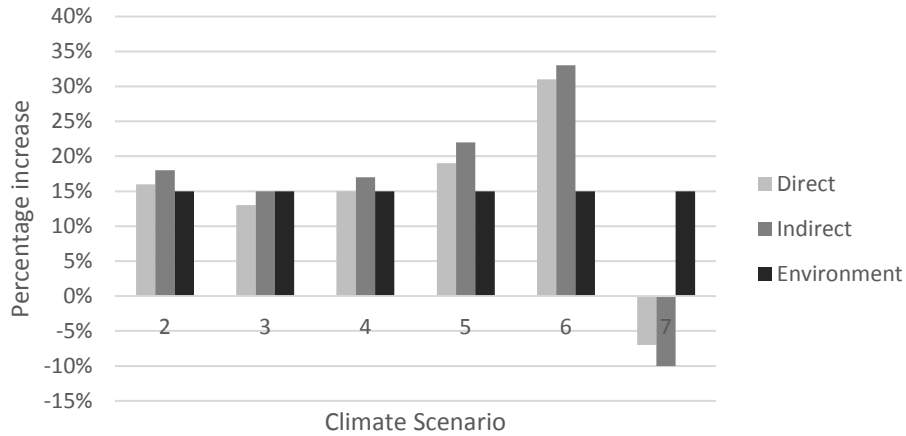


Figure 3.13 The percentage increase in monetary loss of residential buildings compared to scenario 1 (baseline) subjected to hurricane events for different climate change scenarios for year 2020

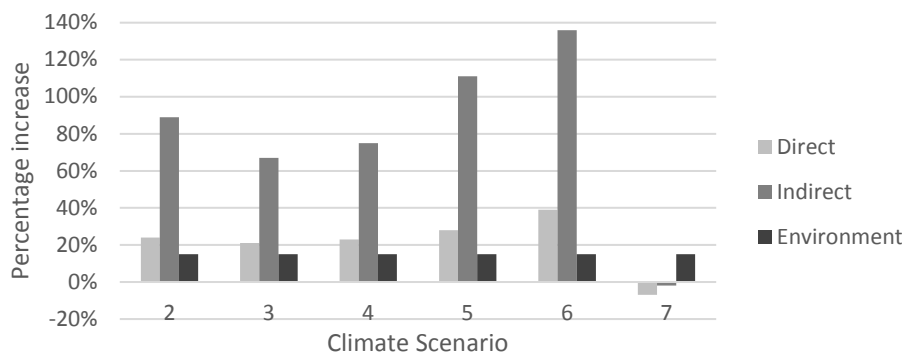


Figure 3.14 The percentage increase in monetary loss of residential buildings compared to scenario 1 (baseline) subjected to hurricane events for different climate change scenarios for year 2050

The results show that indirect and environmental losses play a very important role in the total loss estimation. This finding show that with the potential effects of climate change, the indirect and environmental losses to wood frame construction caused by hurricanes are severe and should not be ignored by decision makers. Further research is needed to evaluate environmental losses subjected to hurricanes considering a changing climate.

3.6 Conclusions

This chapter proposed a framework to evaluate direct, indirect, and environmental losses of wood residential construction subjected to hurricane events considering a changing climate. The framework contains four damage modes (i.e., roof covering, roof sheathing, roof-to-wall connection, and buildings openings), hurricane simulations including stationary and non-stationary scenarios, and loss estimation including the environmental losses of wood residential construction subjected to hurricane events.

Most climate change scenarios (e.g., climate change scenario 6 (+20% change in intensity, +15% change in frequency) and climate change scenario 7 (-20% change in intensity, +15% change in frequency)) may result in -5% to +5% increase in annual loss. Indirect loss and environmental loss can be accounted for 40% to 55% of the total loss, which should not be ignored by decision makers.

The proposed framework provides a more comprehensive way to evaluate hurricane damage risk to wood construction under hurricane events considering a changing climate. This framework can also be used to evaluate the damage risk associated with hurricane mitigation strategies. For future work, a more comprehensive model for environmental loss estimation needs to be studied; multiple hazards (e.g., combined hurricane wind and hurricane-induced surge) is another area for further investigation (e.g., flooding and earthquake).

4. A Framework for Hurricane Resilience of Residential Community³

4.1 Introduction

Community resilience refers to the ability of communities to withstand the impacts of natural or man-made hazards and to recover from such disasters in effective and efficient manners (Pimm 1984). The framework of resilience often is thought of as including four attributes: *robustness* - the ability to withstand an extreme event and deliver a certain level of service even after the occurrence of that event; *rapidity* - to recover the desired functionality as fast as possible; *redundancy* - the extent to which elements and components of a system can be substituted for one another; and *resourcefulness* - the capacity to identify problems, establish priorities, and mobilize personnel and financial resources after an extreme event. In this chapter, the individual building resilience is quantified by a mathematical formation including all four attributes mentioned above. In the formulation of the individual resilience, fragility function accounts for the robust attribute, while recovery function accounts for rapidity. For redundancy, it is assumed that the recovery can be restored at a maximum level of 90% of its states before hurricane events. For resourcefulness, it is assumed that after the hurricane event, the retrofit and rescue efforts can be carried out immediately and continuously. The uncertainty here involves the definition of maximum level of recovery and when the retrofit and rescue efforts can take place. For example, high maximum level of recovery usually takes more time and money. With different levels of recovery, the recovery time model could be significant different. Also the start of retrofit and rescue effects in poor areas seems to be later than that of the rich areas.

Several methods have been proposed for quantification of hazard resilience (Chang and Shinozuka 2004; Cutter et al. 2010; Miles and Chang 2006; Omer et al. 2009; Tokgoz and Gheorghe 2013; Twigg 2009). Bruneau et al. (2003) and Bruneau and Reinhorn (2007)

³ A version of this chapter has been submitted to *ASCE-ASME Journal of Risk and Uncertainty in Engineering Systems, Part A: Civil Engineering*.

established framework to conceptualize, define, and enhance seismic resilience of communities using engineering perspectives. They emphasized that a clear definition and identification of its dimensions are necessary in order to quantify resilience. Cimellaro et al. (2010) developed a framework for a resilience equation based on the conditional and total probability theorems. Bruneau and Reinhorn (2007) quantified seismic resilience of acute care facilities. Though the framework was for seismic resilience, their goal was to develop general concepts and formulations for other hazards. Reed et al. (2009) proposed a methodology to evaluate resilience of subsystems of network infrastructures by combining fragilities and quality characteristics of the infrastructure with an input-output model for a natural disaster. Tokgoz and Gheorghe (2013) attempted to quantify resilience for residential buildings for a hurricane event.

There is existing literature that attempted to link the individual facility resilience to community resilience. Mieler et al. (2014) employed concepts and procedures from the framework used to design and regulate commercial nuclear power plants to outline a conceptual framework for linking community resilience goals to design targets for individual facilities. Mieler et al. (2014) assumed that the performance of each facility is mutually statistical independent of all others. This assumption leads to individual buildings performance requirement that is conservative with respect those needed to collectively ensure the broader community resilience goal and public welfare, as shown in Wang and Ellingwood (2015). They demonstrated that the feasibility of disaggregating broader community resilience goals to obtain performance objective of individual facilities considering the correlations for the performance of each individual facility. For example, it showed that if the probability of failure for an individual building is 0.012, then probability of failure for the community could be 0.05, while the probability of failure of the community could be 0.012 if buildings are assumed statistically independent.

With the knowledge of quantification of community resilience, pre-retrofitting strategies and accordingly the monetary cost can be evaluated. Kanda and Ellingwood (1991) proposed the concept of pre-disaster inventory retrofit cost (IRC) and developed a linear

function between the building target performance and the individual building retrofit cost. Wang and Ellingwood (2015) defined expected inventory recovery time (IRT) and modeled the relationship between the restoration time for an individual building and the damage level of the building following hazard events. Mahsuli and Haukaas (2013) modeled the inventory as a series of development areas or “zones” that are related to the structural characteristics of the dominant buildings found in each zone. Wang and Ellingwood (2015) developed direct financial loss model to the housing inventory by introducing a financial index to characterize the overall financial risk to the housing stock based on the “zone” theory from Mahsuli and Haukaas (2013). Li and Ellingwood (2006), Dong and Li (2015) also investigated the retrofitting strategies of residential construction for hurricane events.

Though the method for quantifying individual building resilience had been proposed (Tokgoz and Gheorghe 2013), the loss function in the formulation of the individual resilience is limited to direct loss which lowers the accuracy and overestimate the individual building resilience. Wang and Ellingwood (2015) proposed the de-aggregating process to break down community resilience goal to individual facility resilience goal; however, the chapter did not address the quantification of individual facility resilience.

This chapter proposed a framework to evaluate if a residential community could achieve its resilience goal by de-aggregating the community resilience goal to individual building resilience goal and quantifying the individual building resilience. The de-aggregating of community resilience for hurricanes will be investigated. The presented results also can be used for decision makers to achieve the goals of community resilience through initial design and hurricane mitigation. For illustration purposes, the study location for the framework is set in Florida. The flowchart regarding the procedures of the proposed framework is shown in Figure 4.1.

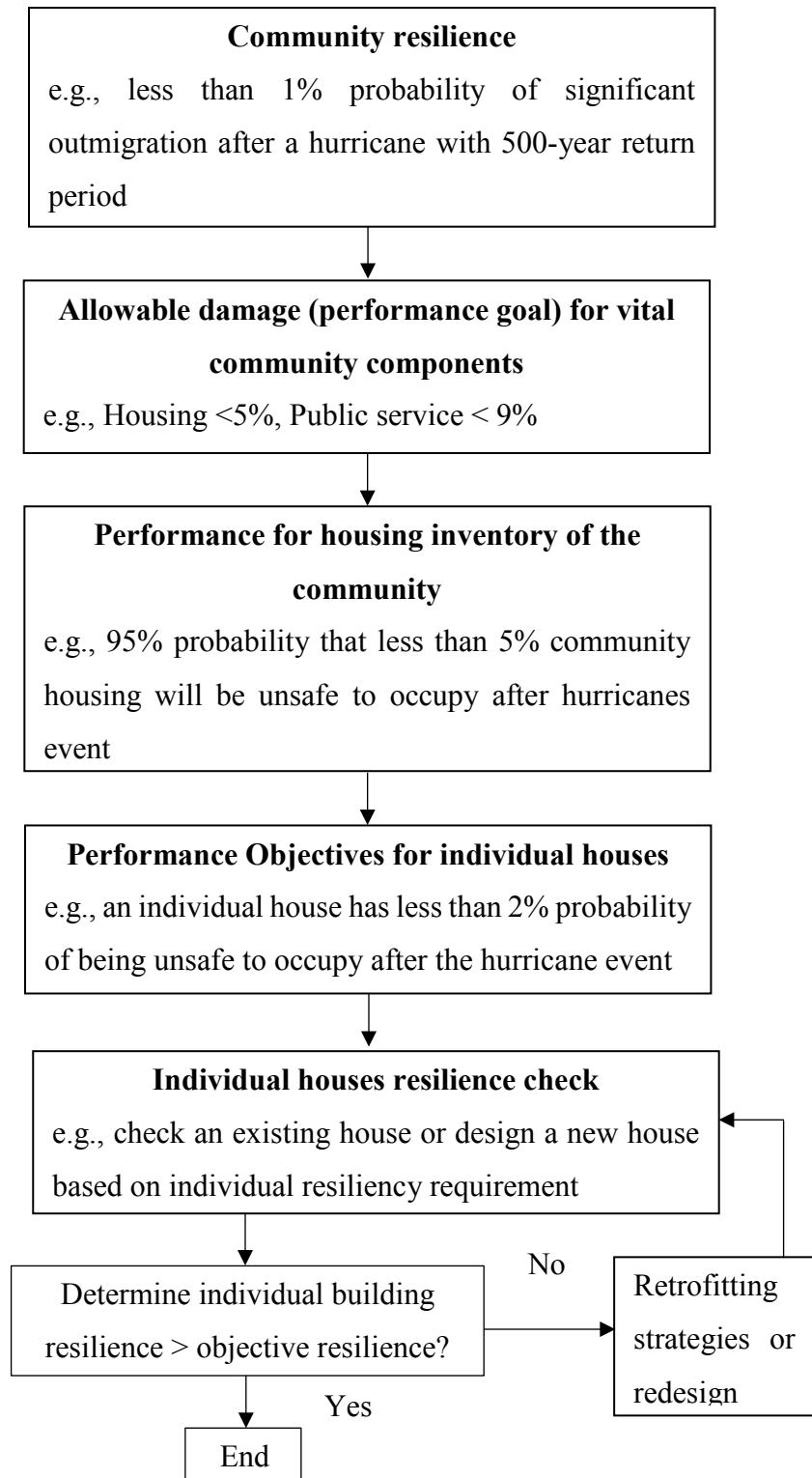


Figure 4.1 Flowchart of the framework

4.2 Community Resilience and De-aggregation

It is worth mentioning that 90% of residential buildings in the United States (U.S.) are light-frame wood construction (Li and Ellingwood 2007). In this chapter, community resilience refers to the resilience of wood residential buildings in the community. Usually there are three levels of performance in assessing resilience, including performance of a community, of a group of buildings, and of individual buildings. In this chapter, the performance of a residential community is directly linked with the performance of building stocks, which is determined by the performance of the individual buildings in the

The performance goals for community resilience are closely linked with its functional requirements such as physical, social, and economic needs. For example, after a significant hurricane event, a community may require that less than 5% of buildings become unsafe to occupy, less than 15% of residences cannot provide shelter, less than 25% of commercial buildings unable to open for business, and less than 35% of industrial buildings cannot sustain manufacturing, etc.

Though the performance goals are easy to set and obtain, it is not practical to evaluate community resilience without de-aggregating the community goals into individual performance objectives (Wang and Ellingwood 2015). To illustrate the de-aggregation process, an allowable damage level mentioned above needs to be determined. For example, one of the community objectives can be “less than 10% of buildings within the community are unsafe for occupancy following a category 4 hurricane”.

At the individual building level, usually there are four damage levels x_j for buildings (i.e., slight, minor, moderate, and severe) (FEMA/NIBS. 2003). Following the occurrence of a scenario hazard event, the building inventory damage state can be defined as a state vector $X = (X_1, X_2 \dots X_n)$ where n is total number of buildings. $S(X)$ is defined as the joint probability distribution of the inventory damage states. The building damage levels within an inventory are correlated (Wang and Ellingwood 2015). Demands on buildings within a

community from hurricane events would be positively correlated, and the neglect of these positive correlations leads to an overestimation of system reliability and underestimation of losses (Adachi and Ellingwood 2008; Wang and Takada 2005). The correlation in performance between buildings resulting from the common hazard (e.g., hurricane) and common design and engineering practices was described by an exponential function (Wang and Takada 2005),

$$\rho_h = \exp\left(\frac{-|h|}{L_c}\right) \quad (4.1)$$

in which $|h|$ is the separation distance between buildings; L_c is the correlation length which represents the strength of the spatial correlation. A function state variable Y_i is further defined for building i representing the building functional status,

$$Y_i = \begin{cases} 0, & X_i = 1,2 (SO) \\ 1, & X_i = 3,4 (UO) \end{cases} \quad (4.2)$$

UO represents unsafe to occupy, while SO is safe to occupy. The marginal probability mass function of the function state Y_i can be defined as (Wang and Takada 2005),

$$P_{Y_i} = \begin{cases} P_{SO_{1i}} + P_{SO_{2i}} \\ P_{UO_{3i}} + P_{SO_{4i}} \end{cases} \quad (4.3)$$

The system resilience, R_{sys} defined as the probability that less than N buildings in the community become UO after a hurricane event is (Wang and Takada 2005),

$$R_{sys} = P(\sum_{i=1}^n Y_i \leq N) = \sum_X S(X)[\sum_{i=1}^n Y_i \leq N] \quad (4.4)$$

The de-aggregation approach requires the determination of the threshold probability that an individual building is unsafe to occupy (P_{UO}^T), given that a desired prescribed target

inventory system reliability (R_{sys}^T) is achieved, to satisfy the overall community resilience goal. This is the inverse if the problem in which the inventory reliability is computed. Computation of the system reliability considering correlated building performance requires Monte Carlo Simulation (MCS) (Wang and Ellingwood 2015). The advantage of MCS is that its convergence does not depend on the number of random variables in the system, which makes it a practical approach for solving high-dimensional problems (Cutter et al. 2010). In the current analysis, the MCS requires that building functional state deviates, Y_i , be simulated from a multivariate distribution in which the marginal random variable are defined by a Bernoulli distribution as in Eq. (4.3) and the correlation matrix in Eq. (4.1).

For the purposes of illustration, it is assumed that a certain community has 100 residential buildings that are the same type and were built in the same time. The assumption here indicates that the housing stocks are also homogeneous. In this chapter, buildings located in different community or built according to different building codes and engineering practices are not considered; however, this assumption can be easily relaxed when a real world community is considered. It also needs to be noted that the correlation in an inhomogeneous building stock is weaker and hard to quantify, despite the correlation due to the common hazard demand still exists unless the buildings are widely separated. The system reliability as a function of the failure of probability of failure for an individual building are determined from Eqs. (4.1)-(4.4) as shown in Figure 4.2. The results are calibrated with previous studies (e.g., Wang and Ellingwood (2015)). The failure probability of individual residential buildings are approximately 0.012 when the system reliability is set to be 0.95 (Wang and Ellingwood 2015). In comparison, the failure probability of individual residential buildings is approximately 0.013 when the system reliability is set to be 0.95 in this chapter. The curve titled as uncorrelated means the correlation in performance between buildings is zero; while the curve titled as correlated shows the damage between buildings are correlated. As shown in Figure 4.2, when the system reliability of the community is required to be above approximately 85%, the uncorrelated curve significantly underestimates the probability of failure of individual

building required to achieve the accordingly system reliability of the community. In practice, the building performances are positively correlated.

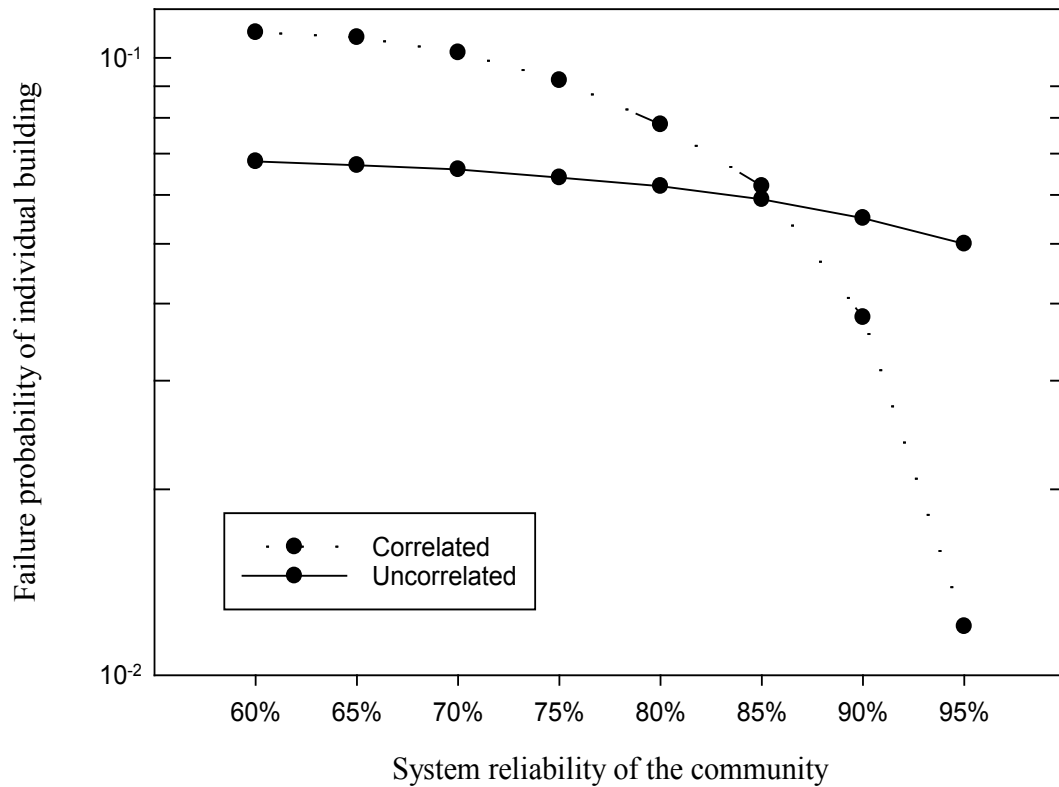


Figure 4.2 Probability of failure for individual building versus system reliability of the housing stock

From Figure 4.2, it shows high community resilience requires low probability of failure for individual building. For example, it can be seen that in order to achieve a system reliability of 0.93, the probability of failure for individual building should be less than approximately 0.023; a system reliability of 0.85 requires the probability of failure for individual building less than approximately 0.06. If all the buildings are considered as uncorrelated, the system reliability will be 95% as long as the probability of failure for each buildings is below approximately 5%. This de-aggregating process provides the criteria for designers and decision makers when the community resilience is considered in the planning stage of

community construction. It also provides a measure index for hurricane damages as well as the evaluation of different mitigation strategies.

4.3 Formulation of resilience for individual residential buildings

Several methods have been proposed for quantification of resilience (Bruneau et al. 2003; Cutter et al. 2010). The adoption of a metric can help improve resilience strategies and aid alternative prioritization for hurricane mitigation. In this chapter, a methodology for quantification of resilience against hurricane events is presented by adopting functionality, and loss and recovery functions from the previous research on earthquake hazard (Cimellaro et al. 2010). Such an adoption is reasonable, because both hazards have different damage levels causing different levels of loss and damage with certain probabilities. Recoveries from both disasters depend on preparedness, mitigation, response, and recovery efforts. The methodology presented in this article can also be modified and extended to make it applicable to other types of hazards, after defining the functionality for the according hazard (Tokgoz and Gheorghe 2013).

The adopted formulation is being used to compute for individual residential buildings as shown in Eq. (4.5). Fragility analysis, wind speed probability distribution, recovery functions, and loss of use function are incorporated into the formulation.

$$R = 100 \int_{v_1}^{v_2} \frac{1}{T_e(v)} \left[\int_0^{T_e(v)} Q(t, v) dt \right] g(v) dv / \int_{v_1}^{v_2} g(v) dv \quad (4.5)$$

$$Q(t, v) = 1 - \sum_{j=1}^X L_j(v) f_{rec}^{(j)}[t, T_a(v)] \quad (4.6)$$

where R is resilience of a building (%), v is wind speed, v_1 is the minimum wind speed considered, v_2 is the maximum wind speed considered, T_e is expected recovery time, Q is functionality, t is time, g is distribution for probability of having winds with a speed of v ,

X is damaged states, L_j is direct and indirect losses for damage state j , $f_{rec}^{(j)}$ is recovery function for damage state j , and T_a is actual recovery time. The following assumptions were made: (1) Environmental losses are not considered in this chapter; (2) Complex terrain effects are not taken into consideration; (3) Recovery actions will take into place immediately after hurricane events; (4) Recovery process is continuous and recovery can be restored until 90% of its original states. The key components of the formulation is demonstrated in Figure 4.3.

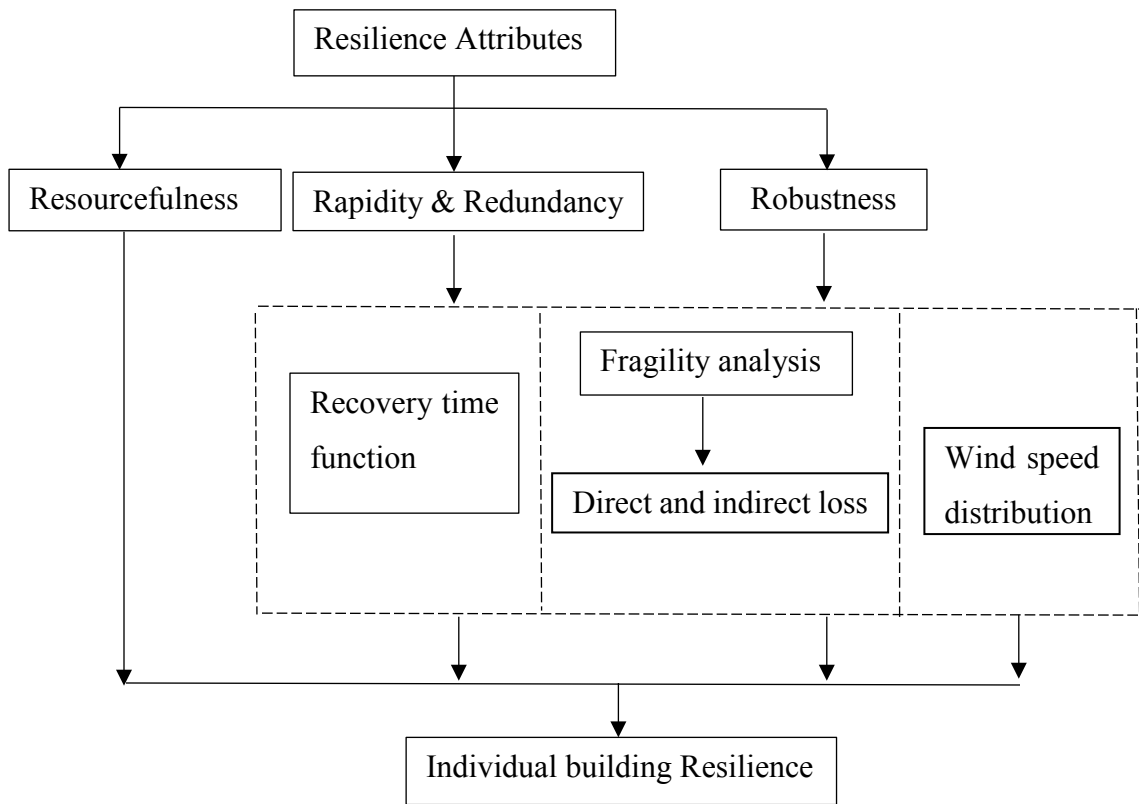


Figure 4.3 Flowchart of formulation for individual building resilience

4.3.1 Hurricane Wind speed

Previous studies have estimated wind speeds (Mudd et al. 2014; Russell and Schueller 1974; Twisdale et al. 1983; Vickery et al. 2000; Vickery et al. 2006). Vickery et al. (2000)

performed hurricane simulations and proposed that the Weibull distribution is an appropriate model for hurricane wind speed prediction in the U.S. The two-parameter Weibull distribution probability distribution function (PDF) is given below,

$$g(v) = \alpha \left(\frac{v}{u}\right)^{\alpha-1} \exp\left[-\left(\frac{v}{u}\right)^\alpha\right] \quad (4.7)$$

where v is the wind speed, u and α are site-specific parameters. The wind speed v , is related to the return period (T) of the hurricane by

$$v = u \left[-\ln\left(\frac{1}{T}\right)\right]^{\frac{1}{\alpha}} \quad (4.8)$$

The wind speed maps developed from Vickery et al. (2000) indicate that the 50, 100, and 1000-year return period 3-sec gust wind speeds at Miami-Dade County, Florida are 59, 67 and 81 m/s (132, 150 and 182 mph) respectively. The corresponding Weibull distribution parameters are $u = 27.58$, $\alpha = 1.79$ (Li and Ellingwood 2006).

4.3.2 Fragility curves

Fragility analysis presents the probability of exceeding a damage limit state for a given structural type subjected to natural or man-made hazards (e.g., earthquake, hurricane) (Dong and Li 2015; Li and Ellingwood 2006). Fragility analysis of residential construction has been studied by Dong and Li (2015); Ellingwood and Wen (2005). The structural system fragility has been modeled by a lognormal cumulative distribution function (CDF) (Li and Ellingwood 2006). The lognormal fragility model is given by,

$$F_R(y) = \Phi\left[\frac{\ln\left(\frac{y}{m_R}\right)}{\xi_R}\right] \quad (4.9)$$

where $\Phi(\cdot)$ is standard normal probability integral; m_R is median capacity; ξ_R is logarithmic standard deviation, which is the inherent variability in the capacity, approximately equal to the coefficient of variation (COV) when its value is less than 0.3. By using the lognormal distribution, the entire fragility curve and its uncertainty can be expressed by only two parameters. The validity of the lognormal assumption had been established for wood construction (Li and Ellingwood 2006). Usually first-order (FO) reliability analysis and Monte Carlo simulation are the common tools to develop the fragility curves (Li and Ellingwood 2006). In this chapter, Monte Carlo simulation is adopted in developing fragility curves. Table 4.1 lists the random variables used in the analysis. The wind load statistics in the table include five variables, where K_h is exposure factor, K_d is directional factor, G is gust factor, C_p is external pressure coefficient, and C_{pi} is internal pressure coefficient. The structural resistance statistics shown in the table contain five components including resistance of roof sheathing, roof covering, roof-to-wall connections, glass door, and window glasses.

Table 4.1 Random variables

Type	Variable	Mean	COV	CDF	Source
Load	K_h (Exposure B)	0.57	0.12	Normal	(Dong and Li 2015; Li and Ellingwood 2007)
	GC_p (C&C)	2.32	0.22	Normal	
	GC_{pi} (Fully)	0.15	0.05	Normal	
	GC_{pi} (Partially)	0.45	0.09	Normal	
	K_d	0.89	0.14	Normal	
Resistance	Roof sheathing	1.89(Kpa)	0.1	Normal	
	Roof covering	1.77(KN)	0.23	Normal	
	Roof-to-wall Connections	5.84(KN)	0.1	Normal	
	Glass Door	2.45(Kpa)	0.25	Weibull	
	Window glasses	2.61(Kpa)	0.25	Weibull	

C&C = component and cladding; CDF = cumulative distribution function;
Full = fully enclosed; Partially = Partially enclosed

Li et al. (2011) defined three building damage states to failures of building components: minor damage—one roof panel; moderate damage—more than one window panel or multiple roof panels; and severe damage—roof-to-wall connections. In this chapter, roof covering damage is also considered as a damage state. The four defined damage states are shown in Table 4.2.

Table 4.2 Damage state definition.

Damage state	Definition
Slight	First roof covering damage
Minor	First roof sheathing damage
Moderate	More than one window/door breakage
Severe	roof-to-wall connection damage

Figure 4.4 demonstrates the hurricane fragility of damage states for a typical residential building. The probability of slight damage is 0.5 when the wind speed is around 30 m/s. In comparison, when the wind speed is around 70 m/s. the probability of severe damage is 0.5.

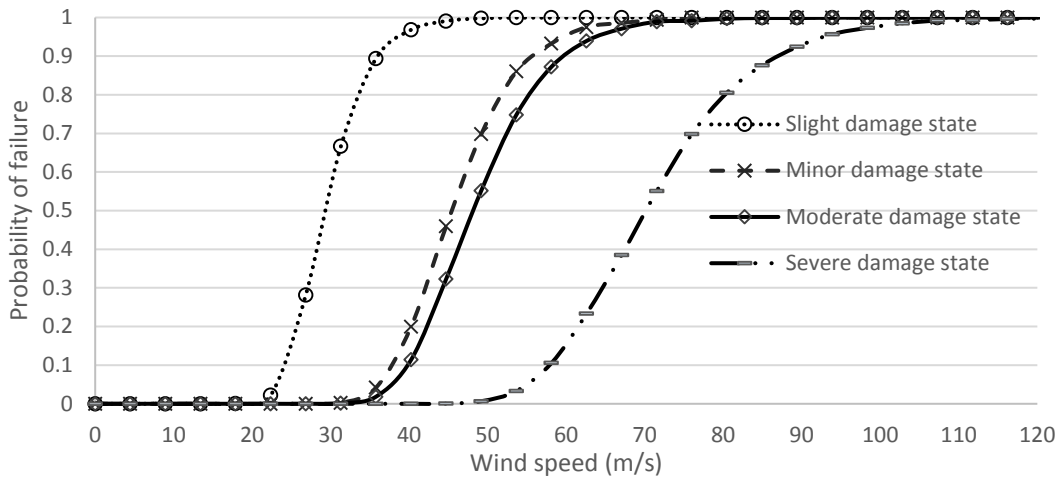


Figure 4.4 Hurricane fragility with four different damage states

4.3.3 Direct and indirect loss estimation

Direct loss analysis has typically been used to evaluate structural losses under extreme event. For example, the direct loss from the hurricane wind and the resulting rainwater intrusion is computed using such a method by Dao and van de Lindt (2010). Loss is computed as financial loss and then adjusted to be a percent of the building replacement value. In this chapter, the direct loss refers to structural and non-structural losses. The direct economic loss function can be determined as (Li et al. 2011).

$$L_{j,Direct}(v) = \sum_{j=1}^4 P_j(v) D_j I \quad (4.10)$$

in which I is the total replacement cost for an individual construction; j is damage state (slight, minor, moderate, and severe); D_j is losses attributable to hurricane in terms of percentage of total value as the consequence of j th limit state; $P_j(v)$ is probability to be in damage state j at a given wind speed v , but double calculation needs to be avoided in the process. For example, probability of slight damage includes probability of minor damage, and then the slight damage level should subtract the moderate damage. The damage ratios of 2, 5, 20 and 50% are used for slight, minor, moderate, severe damage states for hurricane (Li et al. 2011).

Many empirical studies have been conducted to estimate the economic impacts of hurricane in general (Elliott et al. 2015; Fischer et al. 2015; Li et al. 2011). In this chapter, the indirect cost is defined as the cost associated with injuries and death. The injury and fatality costs are estimated \$7500/person and value of life is assumed to be \$2 million/person (Ellingwood and Wen 2005). The injury rate, fatality rate, and damage ratio are shown in Table 4.3, in this chapter, the slight injury rate and death rate are assumed to be 0.01 and 0.001, respectively.

Table 4.3 Damage state/ injury/ fatality relationship

Damage State	Slight	Minor	Moderate	Severe	Source
Injury rate	0.01	0.05	0.1	0.2	(Ellingwood and Wen 2005)
Death rate	0.001	0.005	0.01	0.02	
Damage ratio	0.05	0.2	0.4	0.9	

The indirect loss can be expressed as,

$$L_{j,inDirect}(v) = \sum_{j=1}^4 -C_j [\ln(1 - P_j(v)) - \ln(1 - P_{j+1}(v))] \quad (4.11)$$

where C_j is the injury/fatality cost, and $P_j(v)$ is probability to be in damage state j at a given wind speed v .

The total structural loss can be presented as

$$L_j(v) = L_{j,Direct}(v) + L_{j,inDirect}(v) \quad (4.12)$$

It is assumed that the insured value of a typical residential house is \$200,000 and all residential buildings in the community have identical values. Figure 4.5 illustrates the momentary losses including direct loss and indirect loss under hurricane events. It can be observed that the losses vary from different damage states. The costliest damage is associated with severe damage state, from which the total damage could reach approximately \$140,000 when the wind speed is around 100 m/s.

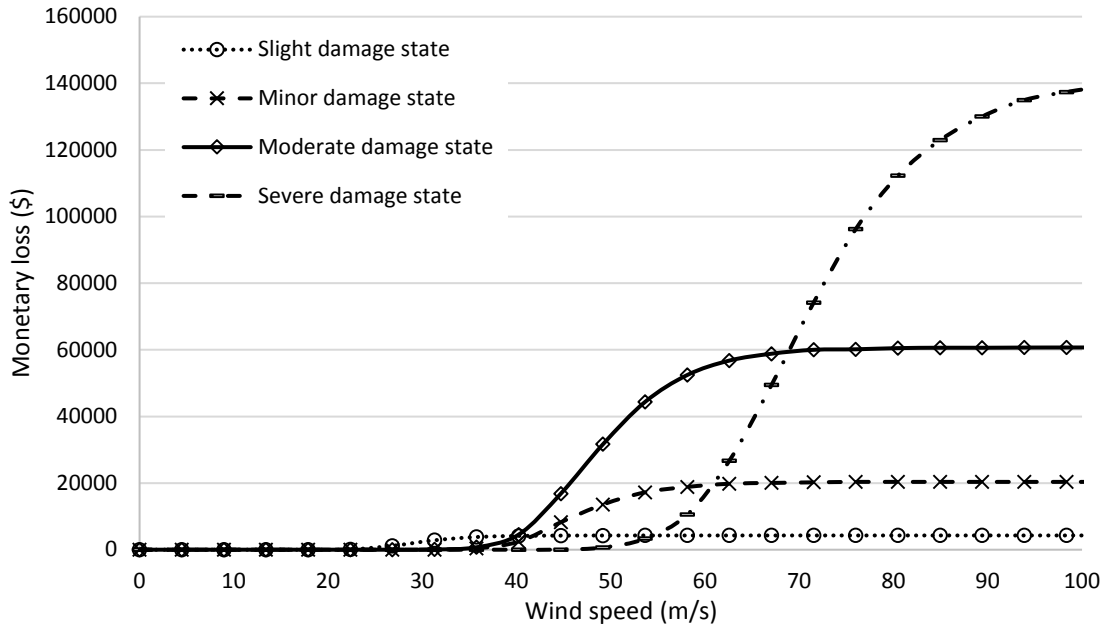


Figure 4.5 Monetary losses including direct and indirect losses

Figure 4.6 demonstrates the sensitivity analysis for monetary loss including direct and indirect losses. 10th, 30th, 50th, 70th, and 90th percentile values account for the uncertainty involved in the estimation. For example, the values are around \$59,100 (10th), \$54,820(30th), \$50,200 (50th), \$46,102 (70th), and \$38,550 (90th) when the wind speed is 50 m/s. It can be seen that monetary loss increases dramatically when the wind speed increase from 40 m/s to 60m/s.

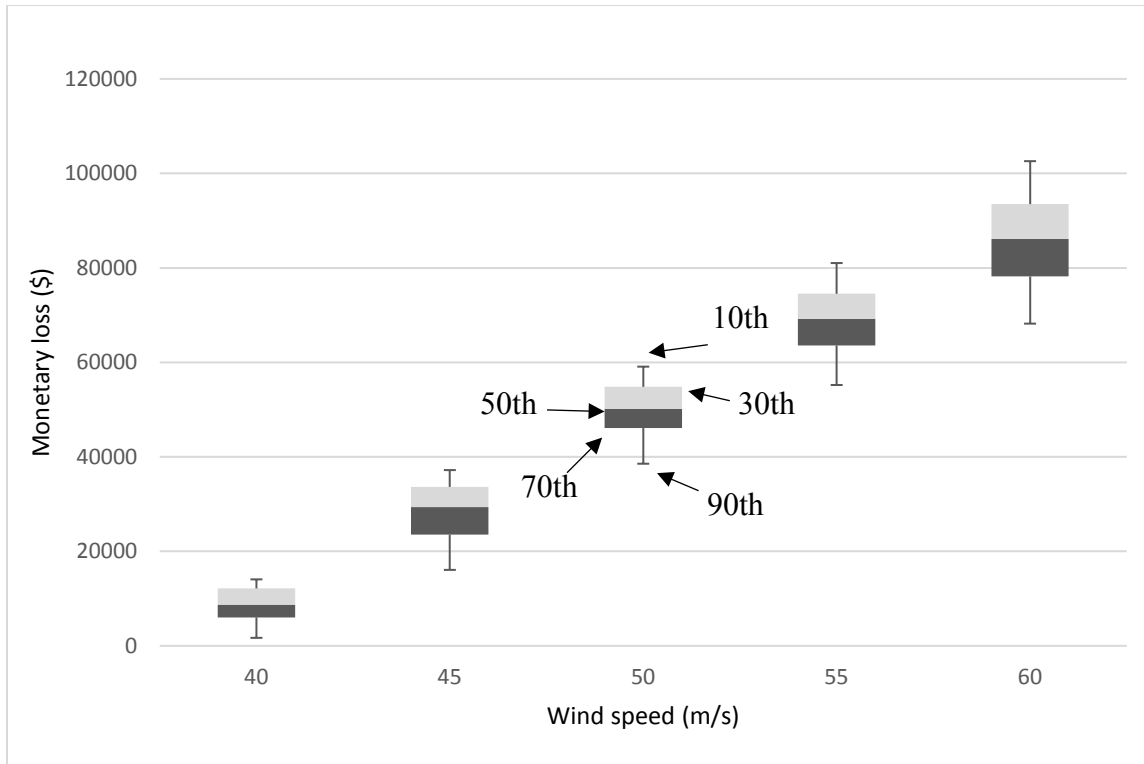


Figure 4.6 Sensitivity analysis for monetary losses direct and indirect losses

4.3.4 Recovery time estimation

There are great uncertainties in defining recovery functions. For instance, recover in poor area from a hurricane event is usually slower than that of a rich area (Tokgoz and Gheorghe 2013). In the literature, there is no consensus reached about the hurricane recovery models (Tokgoz and Gheorghe 2013). A few earthquake models have been proposed. Miles and Chang (2006) performed a comprehensive recovery study for earthquakes and applied to Kobe earthquake. Cimellaro et al. (2010) and (Tokgoz and Gheorghe 2013) proposed some simplified time-dependent recovery functions. In their study, the function selected was based on the response of the affected society. In this study, the exponential, normal, linear, and sinusoidal recovery functions are used, and are assigned to slight damage, minor damage, moderate damage, and severe damage as shown in Eqs. (4.13)-(4.16) (Tokgoz and Gheorghe 2013),

$$f_{rec}^E[t, T_a(v)] = \exp[\log\left(1 - \frac{\lambda}{100}\right) \frac{t}{T_a(v)}] \quad (4.13)$$

$$f_{rec}^N[t, T_a(v)] = \exp[\log\left(1 - \frac{\lambda}{100}\right) \frac{t^2}{T_a(v)^2}] \quad (4.14)$$

$$f_{rec}^L[t, T_a(v)] = \begin{cases} 1 - \frac{\lambda t}{100T_a(v)}, & 0 \leq t \leq \frac{100T_a(v)}{\lambda} \\ 0, & t > \frac{100T_a(v)}{\lambda} \end{cases} \quad (4.15)$$

$$f_{rec}^S[t, T_a(v)] = \begin{cases} \cos[\arccos\left(1 - \frac{\lambda}{100}\right) \frac{t}{T_a(v)}], & 0 \leq t \leq \frac{\pi T_a(v)}{2\arccos\left(1 - \frac{\lambda}{100}\right)} \\ 0, & t > \frac{\pi T_a(v)}{2\arccos\left(1 - \frac{\lambda}{100}\right)} \end{cases} \quad (4.16)$$

Accurate estimation of recovery time is critical to quantify individual building resilience. In order to estimate recovery time, the calculation of Loss of use approach from the hurricane module of HAZUS for residential buildings has been adopted (Tokgoz and Gheorghe 2013). Losses of use for the four damage states are given as 5, 120, 360, and 720 days, respectively (Tokgoz and Gheorghe 2013). A linear interpolation is used in HAZUS to compute expected recovery times for loss ratios different from these four cases.

Both the expected and actually losses of use, in terms of days, are identified as a function of wind speed in order to help with the quantification of reliance. Based on the expected loss of use at different damage states in HAZUS, the expected loss of use can be determined as,

$$T_e(v) = T_e^{(1)}P_1(v) + T_e^{(2)}P_2(v) + T_e^{(3)}P_3(v) + T_e^{(4)}P_4(v) \quad (4.17)$$

where expected recovery time is weighted with the relevant damage state probability for each damage state, and $T_e^{(1)} = 5$, $T_e^{(2)} = 120$, $T_e^{(3)} = 360$, $T_e^{(4)} = 720$ are expected recovery times for slight damage, minor damage, moderate damage, severe damage, respectively. The actual recovery time is defined as,

$$T_a(v) = T_a^{(1)}P_1(v) + T_a^{(2)}P_2(v) + T_a^{(3)}P_3(v) + T_a^{(4)}P_4(v) \quad (4.18)$$

where $T_a^{(1)}$, $T_a^{(2)}$, $T_a^{(3)}$, and $T_a^{(4)}$ are the actual recovery times for slight damage, minor damage, moderate damage, severe damage, respectively. Actual recovery times are also used for damage states. The actual recovery time can be less than, equal to, or greater than the expected recovery time for each damage state. In this chapter, actual recovery time for damage states are assumed to have Rayleigh distribution as $T_a^{(j)} \sim \mathcal{R}(0.8T_e^{(j)})$ (Tokgoz and Gheorghe 2013).

It needs to be noted that the relationship between probability of failure for individual buildings and individual resilience is defined as,

$$R_{individual} = 1 - P_{individual} \quad (4.19)$$

Figure 4.7 demonstrates the relationship between actual recovery time and wind speed. In order to better illustrate how the wind speed affect the actual recovery days, a sensitivity analysis is presented in Figure 4.6. Three levels, 20% percentile, 50% percentile, and 80% percentile, are illustrated. It can be observed that the recovery days in 80% percentile level are significant greater than the recovery days in 50% percentile and 20% percentile. For example, when the wind speed achieves 90 m/s, the actual recovery time is over 1600 days for the 80% percentile; in comparison, the actual recovery time is approximately 600 days for the 20% percentile for the same wind speed.

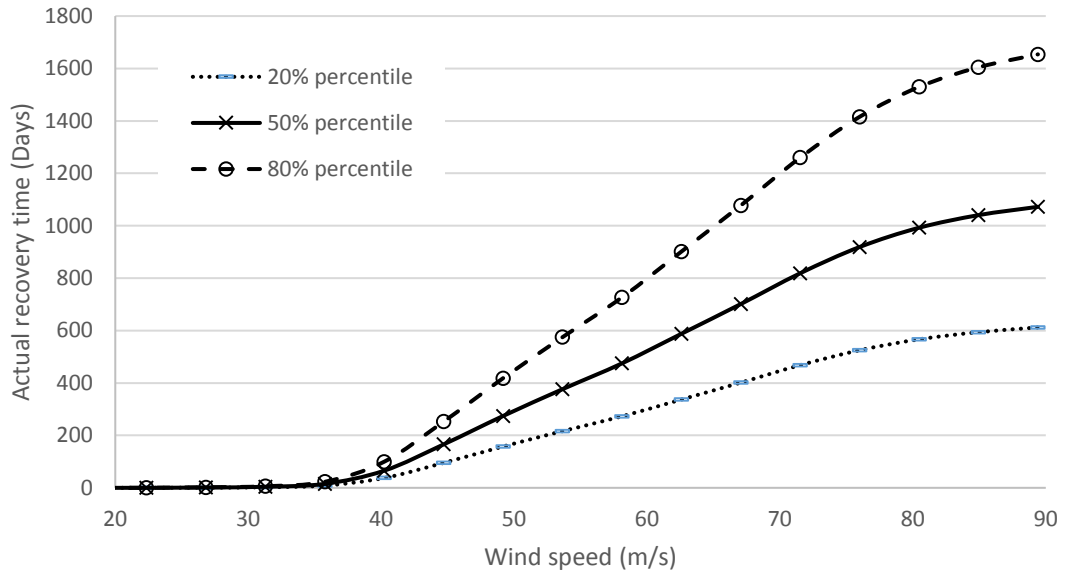


Figure 4.7 Sensitivity analysis of actual recovery time

Figure 4.8 demonstrates the relationship between resilience for individual residential buildings and hurricane wind speeds. Four different recovery functions, which are exponential, normal, linear, and sinusoidal recovery functions, respectively, are considered in the analysis. It can be observed that application of exponential recovery function shares the highest resilience and the application of sinusoidal recovery function shares the lowest resilience. Since there is no consensus about which recovery function should be used in the literature, all four recovery functions are explored (Tokgoz and Gheorghe 2013). When the hurricane wind speed is less than approximately 40 m/s, the building does not lose significant resilience; however, when the wind speed goes over 100 m/s, the resilience under all circumstances goes to zero. This results in the graph are calibrated with those of Tokgoz and Gheorghe (2013).

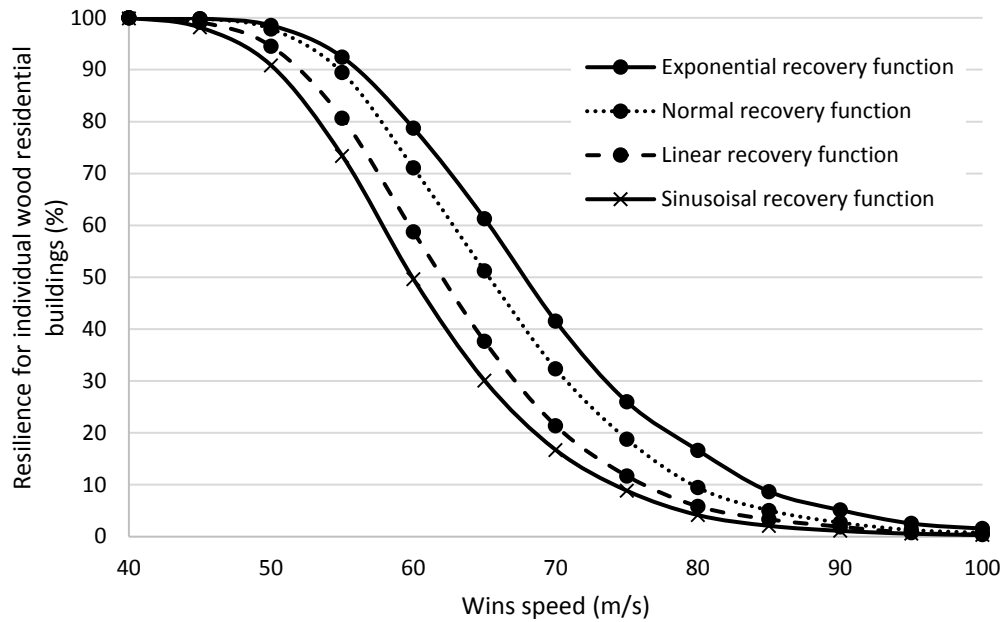


Figure 4.8 Quantification of resilience for individual residential buildings

4.4 Discussions of individual and community resilience

At this point, the gap between individual resilience and community resilience can be bridged. It is worth mentioning that the scope of the community performance objective confines to housing occupiable conditions (e.g., 95% probability that less than 5% community housing will be unsafe to occupy after the hurricane event). For example, a performance target for a community is determined to be “no more than 20% of the community’s housing stock will become unsafe to occupy after a category 3 hurricane event.” The Saffire-Simpson hurricane damage potential scale defines the wind speeds for category 3 hurricane events ranging from 50 m/s to 58 m/s. From the framework, it can be interpreted as “the failure probability of individual residential buildings, which is defined as the collapse of the building, should be less than approximately 7.8%.” It can also be interpreted as “the individual resilience should not be less than approximately 92.2%.” From Fig. 8, it can be seen that when the wind speed reaches 58 m/s, the individual resilience under all circumstances are below 92.2%. Hence, this community resilience goal mentioned above cannot be achieved. In order to achieve the community resilience goal,

retrofit strategy needs to be proposed and evaluated, during which the cost needs to be assessed. Here it is worth to mention that reliability and resilience are not the same concept, and reliability is just a key component in the resilience quantification process.

It needs to be noted that, in the process of de-aggregating community resilience to individual building resilience, the effects of the assumptions of correlation and uncorrelation between buildings in the community would have a significant impact on the output of the analysis. Uncorrelation treatment in the analysis could lead to conservative results, which directly affects the decision making in the initial design and strategies. For example, if all the buildings are considered as uncorrelated, the system reliability will be 95% as long as the probability of failure for each building is below approximately 5%; if considered fully correlated, the probability of failure for each buildings needs to be below approximately 1.2%. Adachi and Ellingwood (2008) mentioned that when a hazard event (e.g., hurricane) affects a complex geographically distributed system like a community, spatial correlations in both demand and capacity must be taken into account. Wang and Ellingwood (2015) emphasized that hazardous events with large footprints introduce spatial and temporal correlations to the demands on the community infrastructure. It is also known that common building practices and code enforcement within a community also introduce positive correlation in structural response above and beyond that introduced by hazards (Tokgoz and Gheorghe 2013). Previously research such as FEMA/NIBS. (2003) considered uncorrelation in evaluating individual building damages and losses. Such correlations depend on the stochastic variability in the demand from hazard events over the affected area at both spatial and temporal scales, the number of structures and their locations, and their susceptibility to damage. These factors must be taken into account for de-aggregating the community resilience into individual building resilience.

4.5 Conclusions

This chapter proposed a framework to evaluate if a residential community could achieve its resilience goal by de-aggregating the community resilience goal to individual resilience goal and quantifying the individual resilience. The individual resilience model contains the hurricane fragility analysis of residential construction, hurricane wind model, direct and indirect loss estimation as well as recovery time estimation. The proposed framework, however, only focuses on residential buildings and does not apply to buildings with difference structures (industrial or commercial buildings) or other infrastructures. Follow-up research will be conducted to consider other types of building structures. In addition, a more complicated correlation model needs to be studied and the more accurate results require further data collection and analysis.

For future work, the retrofit strategies will be evaluated to meet the goals of community resilience. Optimization method can be applied to determine the number of buildings that needs to be retrofitted. Environmental losses will also be incorporated into the loss models. It is also needed to develop a more accurate recovery function to better evaluate the individual building resilience.

5. Evaluation of Hurricane Resilience of Residential Community Considering a Changing Climate, Social Disruption Cost, and Environmental Impact⁴

5.1 Introduction

Hurricane resilience, which has been identified as an effective metric for the risk assessment of residential community, refers to the ability of communities to withstand the impacts of hurricane events and to recover from such disasters in effective and efficient manners. Tokgoz and Gheorghe (2013) quantified hurricane resilience for individual residential building. Other than hurricane, resilience has also been used in assessing risks regarding other natural hazard such as earthquakes (Bonstrom and Corotis 2014; Bruneau et al. 2003; Bruneau and Reinhorn 2007; Cimellaro et al. 2010; Wang and Ellingwood 2015). Some studies managed to link the individual facility resilience to community resilience (Mieler et al. 2014; Wang and Ellingwood 2015). Wang and Ellingwood (2015) attempted to break down community resilience goal to individual facility resilience goal without quantifying individual facility resilience. Yoon et al. (2016) constructed a set of indicators in order to measure community resilience in terms of human, social, economic, environmental, and institutional factors.

The potential effects of a changing climate are considered in this chapter. It has been known that the future hurricane damage to residential community could be aggravated by the potential impact of a changing climate (Bjarnadottir et al. 2014). The effects of a changing climate will be gradually aggravating from 2010 through 2110 (IPCC 2007). Changing climate will likely alter hurricane patterns (e.g., intensity and frequency), subsequently increases the vulnerability of the facilities (IPCC 2013; Wang et al. 2012). Stewart et al. (2011) indicated that the effects of a changing climate is a major cause of reinforcement corrosion in buildings and most infrastructures. Peng and Stewart (2016) stated that a

⁴ A version of this chapter has been submitted to *ASCE Journal of Architectural Engineering*.

changing climate will accelerate the deterioration processes and consequently decline the safety, serviceability and durability of reinforced concrete infrastructures. Dong and Li (2015) demonstrated that wood residential construction will incur severe damage under the combining effects of the changing climate and embedded corrosion.

In recent decades, environmental issues have been drawing great attention. As a result, the public gradually realizes that the environmental costs of residential community subjected to natural hazards such as hurricanes and earthquakes cannot be ignored. The mechanism of hurricane- induced environmental losses is greenhouse gas emission in the process of structural rehabilitation after a hurricane event (Arroyo et al. 2015). Dong and Li (2016) quantified environmental losses of a residential building subjected to hurricane events. Feese et al. (2014) examined the environmental losses of buildings subjected to seismic events. Wei et al. (2015) proposed a lifecycle assessment (LCA) framework to quantify building long-term environmental performance under the impact of natural hazards.

Social disruption cost under natural hazards has been relatively ignored in the many of previous risk assessment due to hurricanes. This chapter considers the social disruption cost during hurricane events and attempt to quantify it in a case study. In this chapter, social disruption is defined as residents in the community having their housing totally or partially damaged by hurricanes, which directly led to the residents moving/repairing houses at work, significant reduction of work productivity as well as their kids missing school, etc. The evaluation of social disruption cost will be categorized into non-environmental cost analysis in later section.

This chapter aims to propose a comprehensive framework to evaluate hurricane resilience of residential community considering the potential effects of a changing climate, social disruption cost, and environmental loss. The hurricane simulations are performed including both stationary and non-stationary scenarios. The de-aggregating of community resilience for hurricanes will be investigated. In the process of quantifying individual resilience, social disruption cost and environmental impact are accounted as a key component in the

formulation. Port St Lucie, Florida is the assumed location of interest for a typical residential community. The framework can be used for facilitate decision makers to achieve the goals of community resilience through initial design or hurricane mitigation.

5.2 Hurricane Simulation

In this chapter, hurricane simulation is employed to account for the potential effects of climate change since it takes hurricane frequency and intensity into consideration in the simulation model. The hurricane frequency can be simulated as a Poisson distribution (Xu and Brown 2008). A bi-normal distribution is used to model the hurricane approach angle (Kaplan and DeMaria 1995; Xu and Brown 2008). After landfall, hurricanes travel along a straight path in Florida due to the narrow shape of the state (Xu and Brown 2008). The central pressure difference is modeled as the Weibull distribution (Georgiou et al. 1983; Huang et al. 2001; Vickery and Twisdale 1995; Xu and Brown 2008). Hurricane wind speed decays after landfall because of friction by land mass and reduction in storm's moisture and the gradient wind speed ($V_G(t)$) at any location at time t is given by (Holland 1980; Vickery et al. 2009):

$$V_G(t) = \left[\left(\frac{R_{max}}{r} \right)^B \left(\frac{B(t)\Delta p \exp \left[- \left(\frac{R_{max}}{r} \right)^B \right]}{\rho} \right) + \frac{r^2 f^2}{4} \right]^{1/2} - \frac{rf}{2} \quad (5.1)$$

where R_{max} is the radius to maximum wind speed, r is the distance from hurricane eye to point of interest, $B(t)$ is the Holland parameter, Δp is the central pressure difference, ρ is air density, and f is the Coriolis parameter.

The 3-sec wind speed at the height of 10 m in an open-country exposure at year t can be calculated as below,

$$V_{G1} = V_G * SF * GS \quad (5.2)$$

where SF is surface wind speed factor ranging from 0.8 to 0.86 based on the intensity of storms (Vickery et al. 2000); GS is gust wind speed factor with a mean value of 1.287 and a standard deviation of 0.002 Xu and Brown (2008). Given any hurricane wind speed from above, the velocity pressure on a building is calculated as (ASCE 2010)

$$q_h(t) = 0.613K_hK_{zt}K_d(V_{G1}(t))^2 \text{ (N/m}^2\text{)} \quad (5.3)$$

where K_h = exposure factor, K_{zt} = topographic factor (taken equal to unity in this chapter), K_d = directional factor.

The wind pressure $W(t)$ acting on structure is determined by (ASCE 2010):

$$W(t) = q_h(t)[GC_p - GC_{pi}] \quad (5.4)$$

in which $q_h(t)$ = velocity pressure evaluated at mean roof height at t year, G = gust factor, C_p = external pressure coefficient, C_{pi} = internal pressure coefficient. This is the basis for the winds pressures in ASCE Standard 7 (ASCE 2010). Table 1 summarizes the wind load statistics for a typical low-rise residential structure. The dimensions are 8.5m by 12.2 m (28 ft by 40 ft), and the mean roof height is 3.8m (12.5 ft). The external pressure coefficients (GC_p) are dependent on various gable roof slopes.

Table 5.1 Wind load statistics

	Mean	COV	CDF	Source
K_h (Exposure B)	0.57	0.12	Normal	
GC_p (C&C) Zone 3 (slope 1:12, $\theta < 7^\circ$)	2.02	0.22	Normal	(Li and Ellingwood 2006)
GC_p (C&C) Zone 3 (slope 6:12, $7^\circ < \theta \leq 27^\circ$)	2.32	0.22	Normal	
GC_p (C&C) Zone 3 (slope 12:12, $27^\circ < \theta \leq 45^\circ$)	1.12	0.22	Normal	
GC_{pi} (Enclosed)	0.15	0.05	Normal	
GC_{pi} (Partial enclosed)	0.45	0.09	Normal	
K_d	0.89	0.14	Normal	

C&C: Component and cladding

An upward trend in hurricane activities has been observed over the last 30 years (Emanuel 2005; IPCC 2007; Mudd et al. 2014). The effects of climate change could alter patterns of hurricane hazard which can aggravate the degree of damage to coastal buildings (Banholzer et al. 2014). Donat et al. (2011) stated that the monetary losses subjected to hurricane due to changing climate could be increased up to 75% by 2080. Hurricane frequency and intensity are the changing variables in the hurricane simulation model due to changing climate. Wang et al. (2013) indicated that ± 10 m/s changes in extreme wind gust speeds with a 500-year return period are likely to happen when subjected to ± 20 % intensity change and ± 50 % occurrence frequency change of hurricanes. Knutson et al. (2010) concluded that the global frequency of tropical cyclones will either decrease or remain unchanged with the authors predicting a decrease between -6 to -34%. Staid et al. (2014) stated the change of the hurricane intensity ranges from -20% to +40%. Landsea et al. (2010) on the other hand reported the range of future hurricane frequency to be between -30% to +35%. Based on the information above, the following seven climate change scenarios from the year 2000 to 2050 are assumed and listed in Table 5.2:

Table 5.2 Climate change scenarios

Scenario	1	2	3	4	5	6	7
Change in intensity	0	10%	0	10%	10%	20%	-20%
Change in Frequency	0	0	10%	-10%	10%	15%	15%

The wind speed for the chosen location (27.3°N, 80.3°W) are listed in Table 5.3 including the baseline scenario (no changing climate) and the six climate change scenarios above. For frequency variation, the parameter of the Poisson distribution is altered. For intensity variation, the randomly sampled central pressure difference at landfall is altered. The change in frequency and intensity from the present time to the end of the 21st century is assumed to be linear as suggested by Stewart et al. (2013).

It can be noted from Table 5.3 that changes in intensity has higher effect on wind speeds than changes in frequency. Among the seven scenarios, only scenario 7 (+15% change in frequency, -20% change in intensity) resulted in decrease in wind speed at all return periods despite 15% increase in frequency. The highest wind speed is 85 m/s in scenario 6 (+20% change in intensity, +15% change in frequency) with a return period of 1200 years. Scenario 7 has the lowest wind speed of 53 m/s with a return period of 50 years.

Table 5.3 Hurricane wind speed (m/s) at 27.3°N, 80.3°W for various climate scenarios

Scenarios	Return Period (years)						
	50	100	200	300	700	1200	1700
1	57	62	68	71	76	80	82
2	59	64	70	73	78	82	84
3	58	63	69	72	77	81	83
4	58	64	69	72	78	81	83
5	59	65	70	73	79	82	84
6	61	72	72	75	81	85	87
7	53	59	64	66	72	75	77

5.3 De-aggregation of Community Resilience

In this chapter, community resilience refers to the resilience of wood residential buildings in a community. The resilience of a residential community is correlated with the performance of the individual buildings in the community. For example, after an intensive hurricane event, a residential community may require that less than 5% of buildings become unsafe to occupy. A community objective can be “less than 3% of buildings within the community are unsafe for occupancy following a category 3 hurricane”.

The building damage levels within an inventory are correlated (Wang and Ellingwood 2015). Under significant hurricane event, building damages within a community would be positively correlated; otherwise it is very likely to overestimate the system reliability and underestimate accordingly losses (Adachi and Ellingwood 2008; Wang and Takada 2005). The correlation in performance between buildings resulting from the common hazard (e.g., hurricane) and common design and engineering practices was described by an exponential function (Wang and Takada 2005). The system resilience, R_{sys} , defined as the probability that less than N buildings in the community become unsafe to occupy after a hurricane event is (Wang and Takada 2005),

$$R_{sys} = \sum_X S(X) [\sum_{i=1}^n Y_i \leq N] \quad (5.5)$$

where X is damage state vector, $S(x)$ the joint probability distribution of the inventory damage states, n the total number of buildings, Y_i is defined for building i representing the building functional status,

$$Y_i = \begin{cases} 0, & X_i = 1,2 \text{ (Safe to occupy)} \\ 1, & X_i = 3,4 \text{ (Unsafe to occupy)} \end{cases} \quad (5.6)$$

5.4 Formulation of Resilience for Individual Residential Buildings

It has been recognized that the appropriate formulation of individual resilience can greatly facilitate quantifying community resilience. Many researchers had attempted to quantify seismic resilience (Bruneau et al. 2003; Cutter et al. 2010). A well-rounded quantification of resilience was proposed by adopting functionality, and loss and recovery functions from the previous research on earthquake hazard (Cimellaro et al. 2010). In this chapter, this formulation is adopted for hurricane hazard because both hazards share similar definitions of damage states and cause loss and damage with certain probabilities (Li and Ellingwood 2009). Recoveries from both disasters will depend on preparedness, mitigation, response, and recovery efforts. The methodology presented in this article can also be modified and extended to make it applicable to other types of hazards, after defining the functionality for the according hazard (Tokgoz and Gheorghe 2013). The formulation is shown in Eq. (5.7).

$$R = 100 \frac{1}{T_e(v)} \left[\int_0^{T_e(v)} (1 - \sum_{j=1}^X L_j(v) f_{rec}^{(j)}[t, T_a(v)]) dt \right] \quad (5.7)$$

where R is resilience of a building (%), v is wind speed, T_e is expected recovery time, t is time, X is damaged states, L_j is direct and indirect losses for damage state j , $f_{rec}^{(j)}$ is recovery function for damage state j , and T_a is actual recovery time. The following assumptions are made: (1) Environmental losses are not considered in this chapter; (2) Complex terrain effects are not taken into consideration; (3) Recovery actions will take into place immediately after hurricane events; (4) Recovery process is continuous and recovery can be restored until 90% of its original states.

5.4.1 Reliability Analysis

A probabilistic assessment provides a method in evaluating uncertainty, performance and reliability of structures subjected to natural hazards such as hurricanes and earthquakes. Before evaluating a probabilistic assessment, structural damage states, or conditions in

which the structural system ceases to perform its intended functions in certain ways must be identified (Li and Ellingwood 2006). Considering this chapter focuses on typical wood residential buildings, the damage state is defined in Table 5.4.

Table 5.4 List of damage state definition

Damage state	Definition
Slight	First roof covering damage
Minor	First roof sheathing damage
Moderate	More than one window/door breakage
Severe	roof-to-wall connection damage

The probability of any damage state of a structure is defined in Eq. (5.8) as the probability of exceeding a damage limit state for a given structural type subjected to natural or man-made hazards (Li and Ellingwood 2009).

$$P(DS) = \sum P(DS|D = y)P(D = y) \quad (5.8)$$

where $P(D=Y)$ is the probability that the demand equals a specific level y , and $P(DS|D=y)$ is the conditional system limit state probability. The summation emphasizes the role of the theorem of total probability in risk assessment. The conditional probability of failure of the system for a given loading condition is defined as the system fragility. The fragility is central to the probabilistic analysis to assess the capacity of a system to withstand a specific demand (e.g., a 100-yr return period hurricane event). The structural system fragility has been modeled by a lognormal cumulative distribution function (CDF) (Li and Ellingwood 2006). The lognormal fragility model is given by,

$$F_R(y) = \Phi\left[\frac{\ln\left(\frac{y}{m_R}\right)}{\xi_R}\right] \quad (5.9)$$

where $\Phi(\cdot)$ is standard normal probability integral; m_R is median capacity; ξ_R is logarithmic standard deviation, which is the inherent variability in the capacity,

approximately equal to the coefficient of variation (COV) when its value is less than 0.3. By using the lognormal distribution, the entire fragility curve and its uncertainty can be expressed by only two parameters. The validity of the lognormal assumption had been established for wood construction (Li and Ellingwood 2006).

5.4.2 Non-Environmental Loss estimation considering social disruptions

In this chapter, non-environmental loss refers to direct, indirect, and social disruption costs. Direct loss usually is defined as structural loss under extreme event. For example, Li (2012) performed direct loss analysis by using assembly-based method under hurricane event. In this chapter, the direct loss refers to structural losses (e.g., roof panel, truss) and non-structural losses (e.g., assets inside the house including computer, TV, etc.). The direct economic loss function is shown as (Li et al. 2011),

$$L_{j,Direct}(v) = \sum_{j=1}^4 P_j(v) D_j I \quad (5.10)$$

in which I is the total replacement cost for an individual construction; j is damage state (slight, minor, moderate, and severe); D_j is losses attributable to hurricane in terms of percentage of total value as the consequence of j th limit state; $P_j(v)$ is probability to be in damage state j at a given wind speed v , but double calculation needs to be avoided in the process (Li 2012). The damage ratios of 2, 5, 20 and 50% are used for slight, minor, moderate, severe damage states for hurricanes (Li et al. 2011).

The indirect cost refers to the injuries, death of human being. The injury and fatality costs are estimated \$7500/person and value of life is assumed to be \$2 million/ person (Ellingwood and Wen 2005). Social disruption has yet been considered in probability-based cost analysis in the past. However, the reality shows the social disruption is a main contributor for the indirect loss (Galea et al. 2008; Harvey 2016). It needs to be noted that

since there is no available data with regards to social disruptions, for illustration purpose, this chapter will make assumption on damage state for social disruptions. The social disruption costs are estimated \$50,000/household. The injury rate, fatality rate, and damage ratio are shown in Table 5.5,

Table 5.5 Damage state/ injury/ fatality/social disruptions relationship

Damage State	Slight	Minor	Moderate	Severe	Source
Injury rate	0.01	0.05	0.1	0.2	(Ellingwood and Wen 2005; Li 2010)
Death rate	0.001	0.005	0.01	0.02	
Social disruption rate	0.1	0.2	0.3	0.4	
Damage ratio	0.05	0.2	0.4	0.9	

The indirect loss can be expressed as,

$$L_{j,inDirect}(v) = \sum_{j=1}^4 -C_j [\ln(1 - P_j(v)) - \ln(1 - P_{j+1}(v))] \quad (5.11)$$

where C_j is the injury/fatality cost, and $P_j(v)$ is probability to be in damage state j at a given wind speed v . The non-environmental loss can be expressed as

$$L_j(v) = L_{j,Direct}(v) + L_{j,inDirect}(v) \quad (5.12)$$

5.4.3 Environmental impact from hurricanes

Over decades, it has been well recognized that global warming and its potential effects are a result of greenhouse gases (e.g., Carbon dioxide, Carbon monoxide, Sulfur dioxide, Nitrous oxide, etc.) (Arroyo et al. 2015). Carbon dioxide (CO_2) emissions are considered as the most hurricane activity related greenhouse gas as the byproduct of manmade product (such as cement, asphalt etc.) and the use of fossil fuels. However, recently more studies have been showing that the natural hazards could cause significant greenhouse gas

emissions. For example, hurricanes may cause environmental losses because each time a damaged facility is rehabilitated after a hurricane event, greenhouse gases (e.g., CO_2) will be emitted because of the repair and replacement of the damaged materials (Arroyo et al. 2015). Therefore, considering environmental losses is needed in the framework of hurricane risk analysis. The damage cost of structures involves the consideration of their initial cost and the potential future losses caused by hurricanes. In order to quantify greenhouse emissions for a given process, those corresponding to the different gases are transformed into an equivalent carbon dioxide emission (i.e. $CO_2 - e$). The $CO_2 - e$ emissions for common materials are shown in Fig. 1 (Arroyo et al. 2015). From Figure 5.1, it can be shown that steel and glass share the largest values in upper boundary, while concrete and wood show relatively weaker emissions. However, it needs to be noted that the lower boundary of glass is much higher than the rest of the materials.

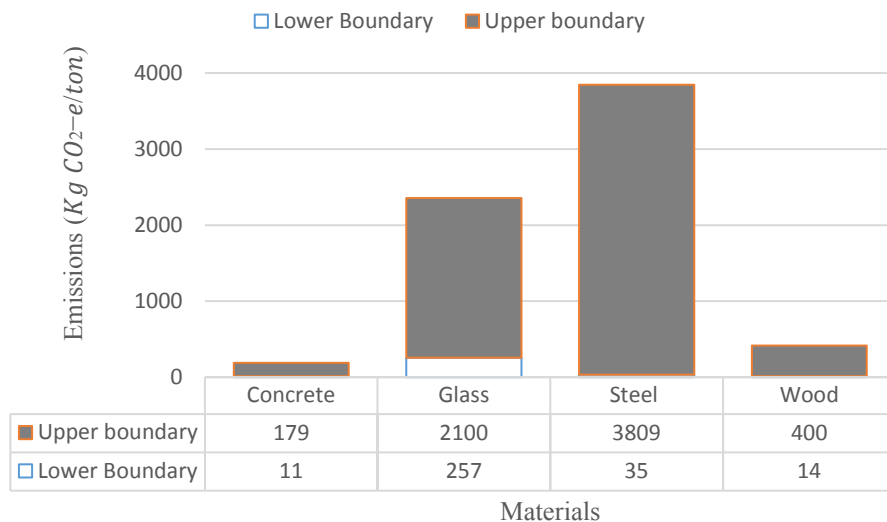


Figure 5.1 Emissions for common materials

Carbon-tax approach will be used to place a value on the societal cost of greenhouse gas emissions. It needs to be noted that the values of carbon tax usually span 3 orders of magnitude and the large scatter is in part a consequence of various approach used in the

estimation of the value of the carbon tax (Watkiss and Downing 2008). The present value of the environmental losses for a hurricane event occurring at time t can be computed as:

$$L_e = \sum_{i=1}^4 \sum_{j=1}^4 \lambda_i e^{-d_e H_i \eta_j} \quad (5.13)$$

in which H_i is the total insured value of a building; η_j is the ratio of the environmental cost and the total insured value of the buildings under j th emission scenarios; $j=1 \dots 4$, where 1 is the slightest scenario and 4 is severest scenario; $H_j \eta_j$ is the cost of greenhouse gas emissions produced under j th emission scenarios during their construction; d_e is environmental associated discount rate; λ_i is mean annual damage ratio attributable to hurricanes, which are 2, 5, 20 and 50% for slight, minor, moderate, severe damage states for hurricanes (Dong and Li 2016).

Three emission scenarios and five carbon tax values are proposed in Table 6 accounting for the sensitivity of those variables. For simplicity, each emission scenario will take the average values. For slight scenario, $\eta_1 = 0.00188$; for minor scenario, $\eta_2 = 0.00362$; for moderate scenario, $\eta_3 = 0.01806$; for severe scenario, $\eta_4 = 0.037$. For parameter d_e , it has been recognized that d_e should be negative because the damage related to $CO_2 - e$ emissions is a function of the cumulated stock (Arroyo et al. 2015). A value of d_e equal to -0.008 was selected in the context of a linear regression analysis by fitting an exponential curve by (Arroyo et al. 2015).

Table 5.6 η_j values related to the cost of $CO_2 - e$ emissions for wood buildings

Emission scenarios	$CO_2 - e$ (ton)	Carbon tax values				
		US\$10	US\$20	US\$50	US\$70	US\$220
1	5	0.0003	0.0005	0.0013	0.0018	0.0055
2	10	0.0001	0.001	0.0025	0.0035	0.011
3	50	0.0003	0.005	0.0125	0.0175	0.055
4	100	0.005	0.01	0.025	0.035	0.11

5.4.4 Recovery time estimation

Existing literatures have demonstrated great immaturity in determining post-disaster housing recovery (Nejat and Ghosh 2016). The complex nature of recovery process makes hard for scholars to quantifying recovery time. There are many internal and external factors affecting this process. For example, recover in poor area from a hurricane event is usually slower than that of a rich area (Tokgoz and Gheorghe 2013). Other factors include: (1) availability of insurance; (2) tenure or place attachment; and (3) availability of funding from external resources such as federal, state, local, and charities (Nejat and Ghosh 2016).

Tokgoz and Gheorghe (2013) adopted Loss of use approach from the hurricane module of HAZUS for residential buildings in consideration of these factors (Tokgoz and Gheorghe 2013). Losses of use for the four damage states are given as 5, 120, 360, and 720 days, respectively (Tokgoz and Gheorghe 2013). A linear interpolation is used in HAZUS to compute expected recovery times for loss ratios different from these four cases. In this chapter, this method is adopted in order to estimate the recovery time from hurricane event in the framework. The exponential, normal, linear, and sinusoidal recovery functions are used, and are assigned to slight damage, minor damage, moderate damage, and severe damage (Tokgoz and Gheorghe 2013). The expected loss of use at different damage states can be determined as,

$$T_e(v) = T_e^{(1)}P_1(v) + T_e^{(2)}P_2(v) + T_e^{(3)}P_3(v) + T_e^{(4)}P_4(v) \quad (5.14)$$

where expected recovery time is weighted with the relevant damage state probability for each damage state, and $T_e^{(1)} = 5$, $T_e^{(2)} = 120$, $T_e^{(3)} = 360$, $T_e^{(4)} = 720$ are expected recovery times for slight damage, minor damage, moderate damage, severe damage, respectively. The actual recovery time can be less than, equal to, or greater than the expected recovery time for each damage state. In this chapter, actual recovery time for damage states are assumed to have Rayleigh distribution as $T_a^{(j)} \sim \mathcal{R}(0.8T_e^{(j)})$ (Tokgoz and Gheorghe 2013).

5.5 Illustrative Case Study

For the purposes of illustration, it is assumed that a residential community with 100 residential buildings that are the same type and built in the same time located at a particular location (27.3°N, 80.3°W) in Port St Lucie, FL. A performance target for this community is set to be “no more than 20% of the community’s housing stock will become unsafe to occupy after a 100-yr return period hurricane event.

Monte Carlo Simulation (MCS) is employed to construct the relationship between community resilience considering correlated building performance and individual building resilience (Wang and Ellingwood 2015). From the de-aggregating process, the community performance target can be interpreted as “the failure probability of individual residential buildings, which is defined as the collapse of the building, should be less than approximately 7.8%.” In other word, the individual resilience should not be less than approximately 92.2%.” The results are calibrated with previous studies (e.g., Wang and Ellingwood (2015)).

The assumed community is identified with typical light-frame residential buildings with the dimensions of 8.5 m by 12.2m (28 ft by 40 ft), one story, mean roof height of 3.8 m

(12.5 ft), and 6:12 slope gable roof without overhang. Panels are nailed at a spacing of 150 mm at the edges of the perimeter and 300 mm in the panel interior and the sheathing thickness 15.9 mm. The roof covering is adhesive-set clay tiles. The roof panels is 1.2m by 2.4m with nominal nail diameter of 2.9 mm (6d). The steel fasteners are hot-dip galvanized to ASTM A153, Class D. The zinc coating thickness is set to be 43 μm in the chapter (Dong and Li 2016). The framing members, such as trusses or rafters, consist of 50.8 mm by 101.6 mm Spruce-Pine-Fir (SPF) lumbers and are spaced 0.6 m on center with a specific gravity of 0.36. A common type of roof-to-wall connections is used which the rafter is connected to the wall using an H2.5 hurricane clip, installed as per manufacturer specifications.

The dead loads include the weights of roof covering, sheathing, which increase the structural resistance. The mean value of the dead load is 77 Pa (1.6 psf) with a coefficient of variation (COV) of 0.1 (Li and Ellingwood 2006). The resistant statistics of five components including resistance of roof sheathing, roof covering, roof-to-wall connections, glass door, and window glasses are considered in Table 5.7.

Table 5.7 Resistance statistics

Type	Variable	Mean	COV	CDF	Source
Resistance	Roof sheathing	1.89 (Kpa)	0.1	Normal	(Dong and Li 2016)
	Roof covering	1.77 (KN)	0.23	Normal	
	Roof-to-wall Connections	5.84 (KN)	0.1	Normal	
	Glass Door	2.45 (Kpa)	0.25	Weibull	
	Window glasses	2.61 (Kpa)	0.25	Weibull	

Hurricane fragility analysis presents the probability of exceeding a damage limit state for a given structural type subjected to hurricane. Figure 5.2 demonstrates the hurricane fragility of damage states for a typical residential building mentioned above. It can be observed that probability of failure for different damage states differs significant, especially for between slight damage state and severe damage state. For example, when the wind speed reaches to

approximately 30 m/s, the probability of failure for slight damage states is 0.5; however, it takes a wind speed of 70 m/s to get to 50% probability of failure. The difference between minor damage state and moderate damage state is smaller, for instant, both damage states share 50% probability of failure when their wind speeds are in the range of 42 m/s and 48 m/s.

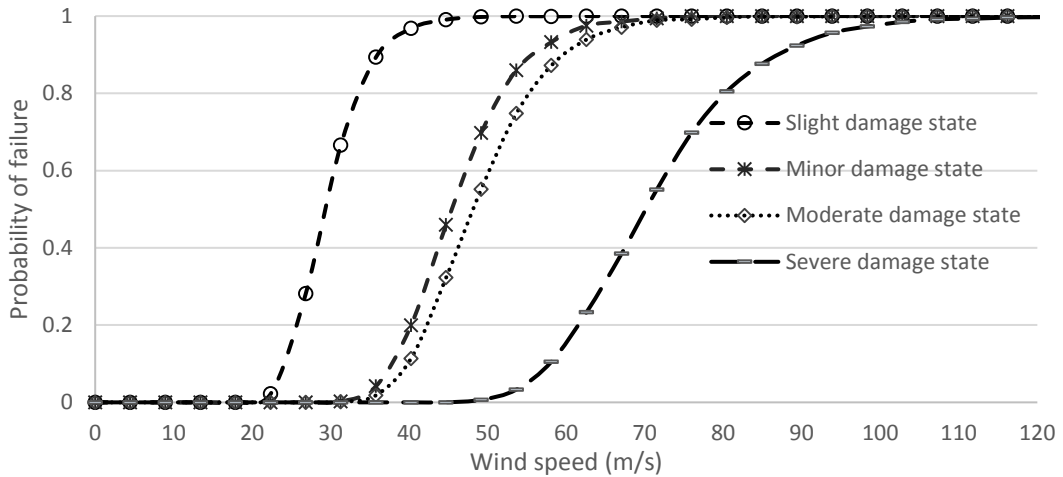


Figure 5.2 Hurricane fragility with four different damage states

Figure 5.3 shows the overall monetary losses including environmental and non-environmental losses for different damage states. The potential maximum losses occur at severe damage state, which is approximately \$165,100. In this chapter, for each damage state, the environmental cost is insensitive to wind speed due to lack of considering input variable for wind speed. For future chapter, a more comprehensive environmental loss model needs to be studied for the accuracy of the loss model. For a 100-yr hurricane event, the monetary losses combining all damage states together for proposed climate change scenarios are \$145,233, \$158,733, \$151,298, \$158,733, \$165,061, \$204,054, \$112,408. It can be observed that for in climate change scenario 6 (+20% chance in intensity, +15% change in frequency), the monetary losses for the 100-yr hurricane event exceed the house insured value, which is \$200,000.

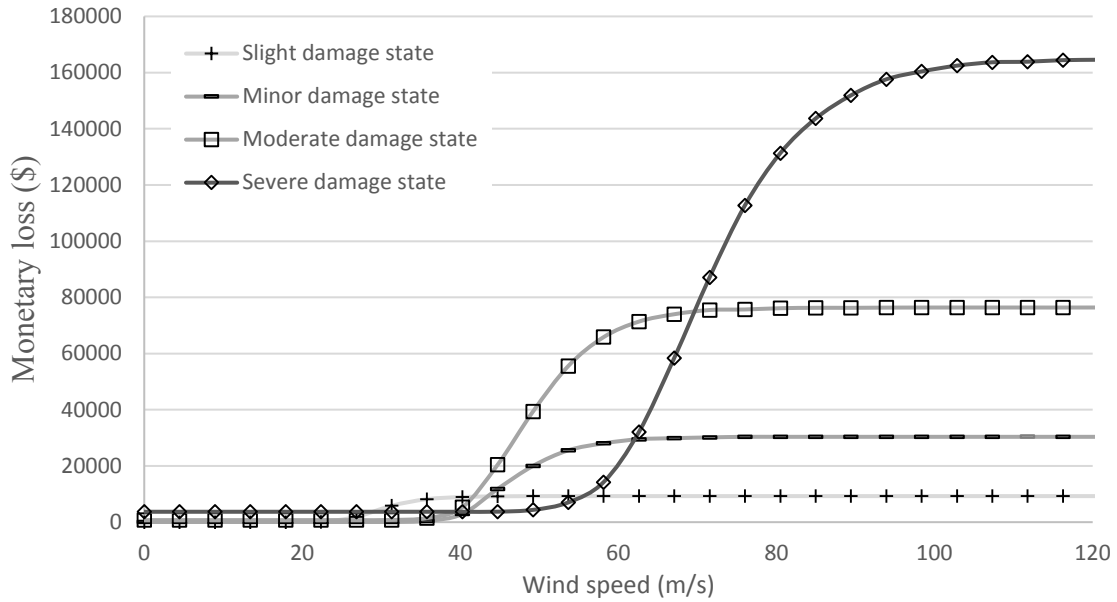


Figure 5.3 Monetary losses including environmental and non-environmental losses

Figure 5.4 illustrates the loss comparisons between different types of losses under climate change scenario 6 (+20% chance in intensity, +15% change in frequency), which is the most intensive climate change scenario proposed in this chapter under the 100-yr return period hurricane event. In the past, the inputs such as social disruption cost and environmental loss have been ignored for hurricane risk assessment. From Fig. 5, it can be seen that social disruption cost and environmental loss account for over 14%, especially social disruption cost share over 10%. In general, direct loss shares the largest ratio, which is approximately 63% and the accordingly monetary loss is \$87,516. Despite the environmental loss only account for 4% in the evaluation, it should be noted that the current environmental loss evaluation model is still premature and needs to be developed in the future chapter. In evaluating environmental loss, the carbon tax values scatter three magnitudes and many other uncertainties are involved in the model. The accuracy in evaluating environmental loss and social disruption cost can be greatly improved once there are enough real world data available in the future. Hence, it is likely that the evaluation of environmental loss and social disruption costs could be underestimated. The results clearly show that such loss inputs (i.e., social disruption cost and environmental

loss) cannot be ignored and the effects of losses incurred by these two parameters need to be highlighted.

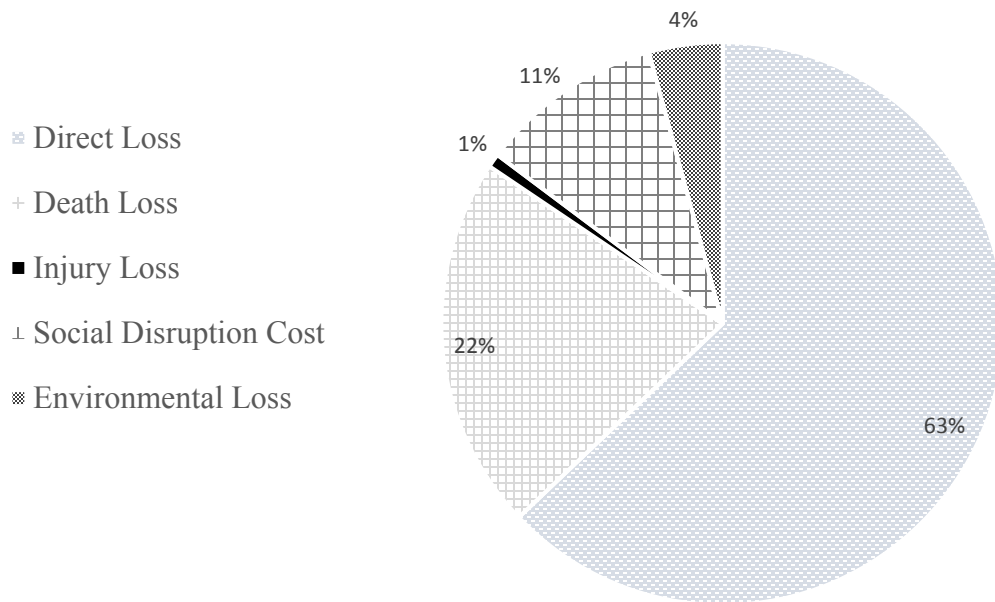


Figure 5.4 Loss Comparison under climate change scenario 6 (+20% chance in intensity, +15% change in frequency) under 100-yr return period hurricane event

The relationship between individual resilience and proposed climate change scenarios under 100-yr return period hurricane event is shown in Figure 5.5. Four damage states, which are slight, minor, moderate, and severe are considered. It can be see that for each climate change scenarios, severe damage state accounts for the lowest resilience, and contrarily slight damage state shares the highest resilience. In sum, climate change scenario 7 (+15% change in frequency, -20% change in intensity) holds the highest resilience, which is approximately 80% for slight damage state. In comparison, climate change scenario 6 (+20% chance in intensity, +15% change in frequency) becomes the lowest resilience, which accounts for only nearly 10% for severe damage state.

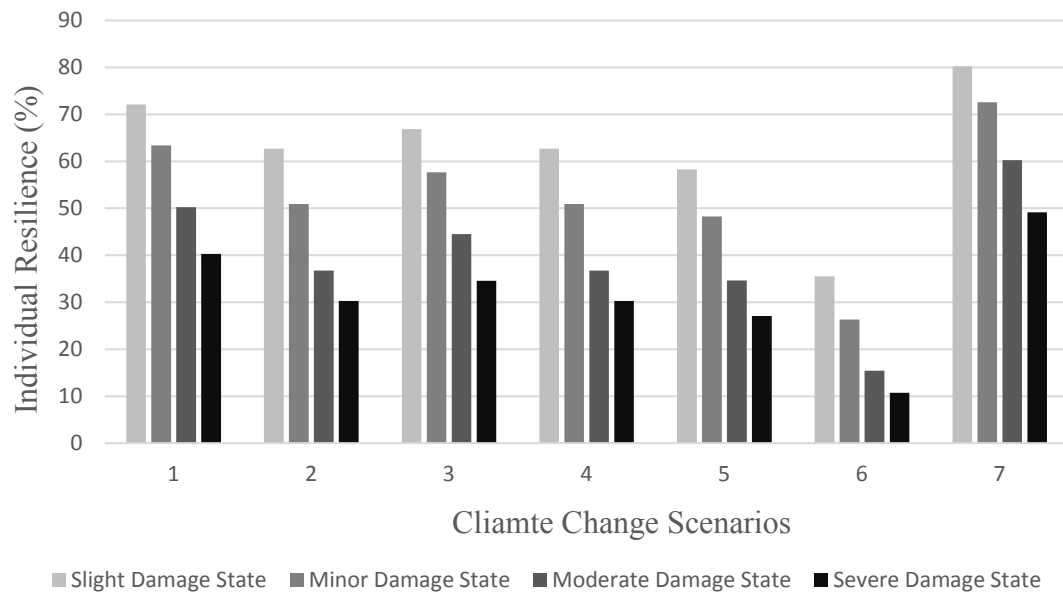


Figure 5.5 Individual resilience for climate change scenarios under 100-yr return period hurricane event

Since the highest resilience value in Figure 5.5 is approximately 80%, it indicates that this kind of structural configurations cannot meet the target objective in which the individual resilience should not be less than approximately 92.2% in the case study. The results shown above give designer and decision makers a clear pathway and criteria to make a resilience oriented objective. An iteration process can be used in order to make the structure configurations fit the community resilience goal.

5.6 Conclusions

This chapter proposes a framework to evaluate hurricane community resilience by including key elements such as various scenarios of changing climate, hurricane fragility, direct hurricane damage loss, environmental and non-environmental losses considering social disruption events. In the case study of Port St Lucie in FL shows that the indirect damage loss, environmental damage, and social disruption cost accounts for 22%, 4%.

11%, respectively, for a 100-yr return period hurricane event, which shows that the social disruption cost and environmental impact play an important role in probability-based cost analysis. A de-aggregating process made the transition between community and individual resilience feasible. By applying this framework, the existing community can be evaluated for its hurricane resilience and the community-to-be can achieve the specific community resilience goal.

To improve the framework, a more comprehensive environmental loss evaluation model need to be studied in the future study; more real world data are in demand in order to develop a social disruption loss evaluation model. This framework can also be applied to other natural hazards such as earthquake and flooding. The community resilience under multiple hazards such as hurricane and flooding combination is another area that needs to be explored in the future.

6. Summary, Conclusions, and Future Work

6.1 Summary and Conclusions

This dissertation proposed a comprehensive framework to assess and quantify hurricane resilience of residential community. In small scale, the framework can be used to evaluate structural reliability in residential construction; in large scale, it can be employed to assess hurricane resilience in a community level. In summary, this dissertation

1. Evaluated the reliability of wood roof panels with zinc-coated fasteners subjected to hurricane events considering the combining effects of changing climate and embedded corrosion.
2. Extended the traditional risk assessment of untreated wood construction to treated wood construction.
3. Proposed and evaluated various retrofitting strategies to reduce the hurricane damage to the roofing structure.
4. Assessed hurricane damage to wood residential construction in monetary losses including direct, indirect, social disruption, and environmental impact. Four major damage modes (i.e., roof covering, roof sheathing, roof-to-wall connection, and buildings openings) are included in the structural analysis.
5. Conducted hurricane simulations including both stationary and non-stationary scenarios in the process of risk analysis.
6. Proposed a probability-based comprehensive framework to assess hurricane resilience of residential community by integrate hurricane fragility analysis,

hurricane simulations, direct, indirect, social disruptions, and environmental costs as well as post-event recovery time estimation.

Major findings are summarized as follows:

1. The performance of the roof panels only reduce slightly under all circumstances before the zinc coatings are fully corroded. Afterwards, the roof panel reliability will lose over half in 30 years with the combined effects of changing climate and embedded corrosion are considered
2. Applying closed-cell sprayed applied polyurethane foam (ccSPF) is the most effective method to reinforce the roof panels during hurricane events. The deterioration pattern of ccSPF is still unknown. The corresponding studies need to be performed and once the information is available, the time-dependent ccSPF performance can be evaluated and the effectiveness of such strategy can be re-assessed.
3. It should be noted that there are considerable uncertainties exist in hurricane simulation with various climate change scenarios. It is recommended to analyze all possible climate change scenarios and find out the worst scenario. The uncertainty here includes if the worst scenario can be identified, otherwise the results of risk analysis could be unconservative.
4. Social disruption cost is estimated to account for bigger percentage in the total loss than environmental and injury losses. However, there exists great uncertainty in quantifying social disruption cost as well as the damage state. More real world data needs to be collected in order to account for social disruption cost.
5. Indirect and environmental losses can be accounted for 40% to 55% of the total loss with hurricane intensity ranging from -20% to 40% and hurricane frequency

ranging from -30% to 35%. In particular, indirect loss increases significantly when certain climate change scenario aggravates the situation.

6. In the process of de-aggregating community resilience to individual building resilience, the effects of the assumptions of correlation and uncorrelation between buildings in the community would have a moderate impact on the output of the analysis. Uncorrelation treatment in the analysis can lead to conservative results, which directly affects the decision making in the initial design and mitigation strategies. For example, if all the buildings are considered as uncorrelated, the system probability will be 95% as long as the probability of failure for each building is below approximately 5%; while the buildings are considered fully correlated, the probability of failure for each building needs to be below approximately 1.2%.

The limitations of the conclusions:

1. The accuracy of the calculated structural resistance is limited due to the great uncertainty in roof panel ultimate capacity prediction and corrosion propagation path, and the ignorance of roof covering load.
2. The assumptions made in hurricane simulation affect the hurricane speed and direction predictions. For example, the hurricane simulation model assumes hurricane travel along a straight path in Florida due to the narrow shape of the state. The translation velocity is assumed to be constant after landfall.
3. There are great uncertainties in loss evaluation models including environmental and social disruption costs. However, the accuracy of the loss evaluations can be improved by developing more comprehensive mathematical models for both.

4. The uncertainty in quantifying recovery time limited the accuracy of resilience evaluation. In the process, assumptions need to be made such as the determination of recovery level, when the recovery can take place and other unpredictable factors.

6.2 Future Work

The future investigations are suggested to further improve the accuracy of the proposed framework as well as related mathematical models.

1. Multiple corrosion mechanisms need to be considered including atmospheric corrosion. The combined effects of embedded, atmospheric corrosions and wood decay for untreated wood is another area for further investigation.
2. A more accurate mathematical model for ultimate capacity prediction for roof panel needs to be developed.
3. More comprehensive mathematical models for environmental and social disruption loss estimation need to be studied; multiple hazards (e.g., combined hurricane wind and hurricane-induced surge) is needed for further investigation (e.g., flooding and earthquake).
4. The retrofit strategies need to be evaluated to meet the goals of community resilience. Optimization method can be applied to determine the number of buildings that needs to be retrofitted. It is also needed to develop a more accurate recovery function to better evaluate the individual building resilience.
5. More data are in demand in order to develop a social disruption loss evaluation model. The community resilience under multiple hazards such as hurricane and flooding combination needs to be explored in the future.

7. References

- Adachi, T., and Ellingwood, B. R. (2008). "Serviceability of earthquake-damaged water systems: Effects of electrical power availability and power backup systems on system vulnerability." *Reliability engineering & system safety*, 93(1), 78-88.
- AFPA (2005). *National design specification for wood construction (NDS)*, American Forest and Paper Association, Washington, DC.
- AGA (2012). "Hot-dip Galvanizing for Corrosion Protection, A specifier's guide." American Galvanizers Association, Centennial, CO.
- Alduse, B. P., Jung, S., and Vanli, O. A. (2015). "Condition-based updating of the fragility for roof covers under high winds." *Journal of Building Engineering*, 2, 36-43.
- Ang, A. H.-S., and Tang, W. H. (2007). *Probability concepts in engineering: emphasis on applications in civil & environmental engineering*, Wiley New York.
- APA (2000). "Retrofitting a Roof for High Wind Uplift." APA-The Engineered Wood Association.
- Arena, A., and De Rosa, C. (2003). "Life cycle assessment of energy and environmental implications of the implementation of conservation technologies in school buildings in Mendoza—Argentina." *Building and Environment*, 38(2), 359-368.
- Arroyo, D., Ordaz, M., and Teran-Gilmore, A. (2015). "Seismic Loss Estimation and Environmental Issues." *Earthquake Spectra*, 31(3), 1285-1308.
- ASCE (2010). *Minimum Design Loads for Buildings and Other Structures: ASCE Standard 7-10*, ASCE Publications, New York, USA.
- ATC (2015). "Windspeed by Location." <<http://windspeed.atcouncil.org/>>. (6/25, 2015).
- AWC (2013). "Wood Structural Panel Awareness Guild." American Wood Council, Leesburg, VA.
- Banholzer, S., Kossin, J., and Donner, S. (2014). "The Impact of Climate Change on Natural Disasters." *Reducing Disaster: Early Warning Systems For Climate Change*, Springer, 21-49.
- Barbato, M., Petrini, F., Unnikrishnan, V. U., and Ciampoli, M. (2013). "Performance-based hurricane engineering (PBHE) framework." *Structural Safety*, 45, 24-35.
- Baskaran, A., and Dutt, O. (1997). "Performance of roof fasteners under simulated loading conditions." *Journal of Wind Engineering and Industrial Aerodynamics*, 72(0), 389-400.

- Bender, M. A., Knutson, T. R., Tuleya, R. E., Sirutis, J. J., Vecchi, G. A., Garner, S. T., and Held, I. M. (2010). "Modeled impact of anthropogenic warming on the frequency of intense Atlantic hurricanes." *Science*, 327(5964), 454-458.
- Bergman, R. (2010). *Drying and control of moisture content and dimensional changes*, USDA Forest Service, Madison, WI.
- Bjarnadottir, S., Li, Y., and Stewart, M. (2013). "Hurricane Risk Assessment of Power Distribution Poles Considering Impacts of a Changing Climate." *Journal of Infrastructure Systems*, 19(1), 12-24.
- Bjarnadottir, S., Li, Y., and Stewart, M. G. (2011). "A probabilistic-based framework for impact and adaptation assessment of climate change on hurricane damage risks and costs." *Structural Safety*, 33(3), 173-185.
- Bjarnadottir, S., Li, Y., and Stewart, M. G. (2014). "Regional loss estimation due to hurricane wind and hurricane-induced surge considering climate variability." *Structure and Infrastructure Engineering*, 10(11), 1369-1384.
- Bonstrom, H., and Corotis, R. (2014). "First-Order Reliability Approach to Quantify and Improve Building Portfolio Resilience." *Journal of Structural Engineering*, C4014001.
- Bribián, I. Z., Uson, A. A., and Scarpellini, S. (2009). "Life cycle assessment in buildings: State-of-the-art and simplified LCA methodology as a complement for building certification." *Building and Environment*, 44(12), 2510-2520.
- Brown, R. E. (2009). "Cost-benefit analysis of the deployment of utility infrastructure upgrades and storm hardening programs." Quanta Technology, Raleigh.
- Bruneau, M., Chang, S. E., Eguchi, R. T., Lee, G. C., O'Rourke, T. D., Reinhorn, A. M., Shinozuka, M., Tierney, K., Wallace, W. A., and von Winterfeldt, D. (2003). "A framework to quantitatively assess and enhance the seismic resilience of communities." *Earthquake spectra*, 19(4), 733-752.
- Bruneau, M., and Reinhorn, A. (2007). "Exploring the concept of seismic resilience for acute care facilities." *Earthquake Spectra*, 23(1), 41-62.
- Carter, T. (2007). "Membrane Roofing for Flat Roofs." <<http://www.askthebuilder.com/membrane-roofing-for-flat-roofs/>>.
- Chang, S. E., and Shinozuka, M. (2004). "Measuring Improvements in the Disaster Resilience of Communities." *Earthquake Spectra*, 20(3), 739-755.
- Cimellaro, G. P., Reinhorn, A. M., and Bruneau, M. (2010). "Seismic resilience of a hospital system." *Structure and Infrastructure Engineering*, 6(1-2), 127-144.

- Clark, G. E. (2008). "Climate Policy's Quiet Giants." *Environment: Science and Policy for Sustainable Development*, 50(4), 6-7.
- Cooper, P., Ung, T., and MacVicar, R. (1997). "Effect of water repellents on leaching of CCA from treated fence and deck units: an update." *Document-the International Research Group on Wood Preservation (Sweden)*.
- CSIRO (2014). "Climate change in Australia: Technical Report 2014." CSIRO, Melbourne.
- Cutter, S. L., Burton, C. G., and Emrich, C. T. (2010). "Disaster resilience indicators for benchmarking baseline conditions." *Journal of Homeland Security and Emergency Management*, 7(1).
- Dao, T. N., and van de Lindt, J. W. (2011). "Loss analysis for wood frame buildings during hurricanes. I: Structure and hazard modeling." *Journal of Performance of Constructed Facilities*, 26(6), 729-738.
- Datin, P. L., Prevatt, D. O., and Pang, W. (2011). "Wind-Uplift Capacity of Residential Wood Roof-Sheathing Panels Retrofitted with Insulating Foam Adhesive." *Journal of Architectural Engineering*, 17(4), 144-154.
- DeMaria, M., Knaff, J. A., and Kaplan, J. (2006). "On the decay of tropical cyclone winds crossing narrow landmasses." *Journal of applied meteorology and climatology*, 45(3), 491-499.
- Dimoudi, A., and Tompa, C. (2008). "Energy and environmental indicators related to construction of office buildings." *Resources, Conservation and Recycling*, 53(1), 86-95.
- Dixon, C., Masters, F., Prevatt, D., and Gurley, K. (2014). "Wind Uplift Resistance of Artificially and Naturally Aged Asphalt Shingles." *Journal of Architectural Engineering*, 20(4), B4014003.
- Donat, M. G., Leckebusch, G. C., Wild, S., and Ulbrich, U. (2011). "Future changes in European winter storm losses and extreme wind speeds inferred from GCM and RCM multi-model simulations." *Nat. Hazards Earth Syst. Sci.*, 11(5), 1351-1370.
- Dong, Y., and Li, Y. (2015). "Reliability of Roof Panels in Coastal Areas Considering Effects of Climate Change and Embedded Corrosion of Metal Fasteners." *ASCE-ASME Journal of Risk and Uncertainty in Engineering Systems, Part A: Civil Engineering*, 2(1), 04015016.
- Dong, Y., and Li, Y. (2016). "Risk-based assessment of wood residential construction subjected to hurricane events considering indirect and environmental loss." *Sustainable and Resilient Infrastructure*, 1-17.

- Ellingwood, B., Rosowsky, D., Li, Y., and Kim, J. (2004). "Fragility Assessment of Light-Frame Wood Construction Subjected to Wind and Earthquake Hazards." *Journal of Structural Engineering*, 130(12), 1921-1930.
- Ellingwood, B. R., and Wen, Y. K. (2005). "Risk-benefit-based design decisions for low-probability/high consequence earthquake events in Mid-America." *Progress in Structural Engineering and Materials*, 7(2), 56-70.
- Elliott, R. J. R., Strobl, E., and Sun, P. (2015). "The local impact of typhoons on economic activity in China: A view from outer space." *Journal of Urban Economics*, 88, 50-66.
- Elsner, J. B., Kossin, J. P., and Jagger, T. H. (2008). "The increasing intensity of the strongest tropical cyclones." *Nature*, 455(7209), 92-95.
- Emanuel, K. (2005). "Increasing destructiveness of tropical cyclones over the past 30[thinsp]years." *Nature*, 436(7051), 686-688.
- EPA/600, U. (2006). *Life-cycle assessment: principles and practice*, National Risk Management Research Laboratory, Office of Research and Development, US Environmental Protection Agency.
- Feese, C., Li, Y., and Bulleit, W. (2014). "Assessment of Seismic Damage of Buildings and Related Environmental Impacts." *Journal of Performance of Constructed Facilities*, 29(4), 04014106.
- FEMA/NIBS. (2003). "Multi-Hazard Loss Estimation Methodology: Earthquake Model." *Department of Homeland Security, FEMA, Washington, DC*.
- Fischer, T., Su, B., and Wen, S. (2015). "Spatio-Temporal Analysis of Economic Losses from Tropical Cyclones in Affected Provinces of China for the Last 30 Years (1984–2013)." *Natural Hazards Review*, 16(4), 04015010.
- Galea, S., Tracy, M., Norris, F., and Coffey, S. F. (2008). "Financial and social circumstances and the incidence and course of PTSD in Mississippi during the first two years after Hurricane Katrina." *Journal of Traumatic Stress*, 21(4), 357-368.
- Georgiou, P. N., Davenport, A. G., and Vickery, B. (1983). "Design wind speeds in regions dominated by tropical cyclones." *Journal of Wind Engineering and Industrial Aerodynamics*, 13(1), 139-152.
- Goldenberg, S. B., Landsea, C. W., Mestas-Nuñez, A. M., and Gray, W. M. (2001). "The Recent Increase in Atlantic Hurricane Activity: Causes and Implications." *Science*, 293(5529), 474-479.
- Grayson, J. (2014). "Building Envelope Failure Assessment of Residential Developments Subjected to Hurricane Wind Hazards."

- Gurley, K., Davis, J. R., Ferrera, S., Burton, J., Masters, F., Reinhold, T., and Abdullah, M. (2006). "Post 2004 Hurricane Field Survey -- An Evaluation of the Relative Performance of the Standard Building Code and the Florida Building Code." *Structures Congress 2006*, American Society of Civil Engineers, 1-10.
- Hallegatte, S. (2008). "An adaptive regional input-output model and its application to the assessment of the economic cost of Katrina." *Risk Analysis*, 28(3), 779-799.
- Harvey, D. C. (2016). "The Discourse of the Ecological Precariat: Making Sense of Social Disruption in the Lower Ninth Ward in the Long-Term Aftermath of Hurricane Katrina." *Sociological Forum*, n/a-n/a.
- He, W. X., and Hong, H. P. (2012). "Probabilistic characterization of roof panel uplift capacity under wind loading." *Canadian Journal of Civil Engineering*, 39(12), 1285-1296.
- Holland, G. J. (1980). "An analytic model of the wind and pressure profiles in hurricanes." *Monthly weather review*, 108(8), 1212-1218.
- Huang, Z., Rosowsky, D. V., and Sparks, P. R. (2001). "Long-term hurricane risk assessment and expected damage to residential structures." *Reliability Engineering & System Safety*, 74(3), 239-249.
- Hunkeler, F. (2005). *Corrosion in reinforced concrete: processes and mechanisms*, CRC Roca Raton, FL.
- IPCC (2007). "Climate change 2007 – Synthesis Report- An Assessment of the Intergovernmental Panel on Climate Change." IPCC, Geneva, Switzerland, pp 104.
- IPCC (2013). "Summary for Policymakers. In: Climate Change 2013: The Physical Science Basis. Contribution of Working Group I to the Fifth Assessment Report of the Intergovernmental Panel on Climate Change [Stocker, T.F., D. Qin, G.-K. Plattner, M. Tignor, S.K. Allen, J. Boschung, A. Nauels, Y. Xia, V. Bex and P.M. Midgley (eds.)]. "Cambridge University Press, Cambridge, United Kingdom and New York, NY, USA.
- Jones, D. T. (1998). "Retrofit techniques using adhesives to resist wind uplift in wood roof systems." M.S. M.S. thesis, Clemson University, Clemeson, SC.
- Kanda, J., and Ellingwood, B. (1991). "Formulation of load factors based on optimum reliability." *Structural Safety*, 9(3), 197-210.
- Kaplan, J., and DeMaria, M. (1995). "A simple empirical model for predicting the decay of tropical cyclone winds after landfall." *Journal of applied meteorology*, 34(11), 2499-2512.

- Katz, R. W. (2002). "Stochastic modeling of hurricane damage." *Journal of Applied Meteorology*, 41(7), 754-762.
- Keith, E., and Rose, J. (1994). "Hurricane Andrew—Structural Performance of Buildings in South Florida." *Journal of Performance of Constructed Facilities*, 8(3), 178-191.
- Knutson, T. R., McBride, J. L., Chan, J., Emanuel, K., Holland, G., Landsea, C., Held, I., Kossin, J. P., Srivastava, A. K., and Sugi, M. (2010). "Tropical cyclones and climate change." *Nature Geosci*, 3(3), 157-163.
- Landsea, C. W., Vecchi, G. A., Bengtsson, L., and Knutson, T. R. (2010). "Impact of Duration Thresholds on Atlantic Tropical Cyclone Counts*." *Journal of Climate*, 23(10), 2508-2519.
- Lebow, S. T., Tippie, M., Lebow, S., Kartal, S. N., Lebow, S., Lebow, S. T., Evans, J. W., Lebow, H., Brooks, K. M., and Lebow, S. T. (2001). "Guide for minimizing the effect of preservative-treated wood on sensitive environments."
- Lee, K. H., and Rosowsky, D. V. (2005). "Fragility assessment for roof sheathing failure in high wind regions." *Engineering structures*, 27(6), 857-868.
- Leicester, R., Bubb, C., Dorman, C., and Beresford, F. (1979). "An assessment of potential cyclone damage to dwellings in Australia." *Proc., Proc. 5th Int. Conf. on Wind Engineering*, Pergamon, New York, 23-36.
- Leicester, R. H. (2001). "Engineered durability for timber construction." *Progress in Structural Engineering and Materials*, 3(3), 216-227.
- Li, Y. (2012). "Assessment of Damage Risks to Residential Buildings and Cost–Benefit of Mitigation Strategies Considering Hurricane and Earthquake Hazards." *Journal of Performance of Constructed Facilities*, 26(1), 7-16.
- Li, Y., and Ellingwood, B. R. (2005). "Vulnerability of Wood Residential Construction to Hurricane Winds." *Wood Design Focus, Forest Products Society*, 15(1), 11-16.
- Li, Y., and Ellingwood, B. R. (2006). "Hurricane damage to residential construction in the US: Importance of uncertainty modeling in risk assessment." *Engineering structures*, 28(7), 1009-1018.
- Li, Y., and Ellingwood, B. R. (2007). "Reliability of woodframe residential construction subjected to earthquakes." *Structural Safety*, 29(4), 294-307.
- Li, Y., and Ellingwood, B. R. (2009). "Risk-based decision-making for multi-hazard mitigation for wood-frame residential construction." *Australian Journal of Structural Engineering*, 9(1), 17.

- Li, Y., van de Lindt, J., Dao, T., Bjarnadottir, S., and Ahuja, A. (2011). "Loss Analysis for Combined Wind and Surge in Hurricanes." *Natural Hazards Review*, 13(1), 1-10.
- Liu, F., and Pang, W. (2013). "Projection of Future US Design Wind Speeds due to Changes in Hurricane Activity: Storm Frequency and Sea Surface Temperature." *The 12th Americas Conference on Wind Engineering* Seattle, WA, USA.
- Lorenz, E. N. (1967). *The nature and theory of the general circulation of the atmosphere*, World Meteorological Organization Geneva.
- Mahsuli, M., and Haukaas, T. (2013). "Seismic risk analysis with reliability methods, part I: Models." *Structural Safety*, 42, 54-62.
- Mann, M. E., Emanuel, K. A., Holland, G. J., and Webster, P. J. (2007). "Atlantic tropical cyclones revisited." *Eos, Transactions American Geophysical Union*, 88(36), 349-350.
- Manning, B. R., and Nichols, G. G. "Hugo-Lessons Learned. (1991). " *Proc., Hurricane Hugo One Year Later*, ASCE, 186-194.
- Mieler, M., Stojadinovic, B., Budnitz, R., Comerio, M., and Mahin, S. (2014). "A framework for linking community-resilience goals to specific performance targets for the built environment." *Earthquake Spectra*.
- Miles, S. B., and Chang, S. E. (2006). "Modeling community recovery from earthquakes." *Earthquake Spectra*, 22(2), 439-458.
- Mizzell, D. P. (1994). "Wind resistance of sheathing for residential roofs." Clemson University.
- MRI, H.-M. (2003). "Multi-Hazard Loss Estimation Methodology: Earthquake Model." *Department of Homeland Security, FEMA, Washington, DC*.
- Msadek, R., Vecchi, G. A., and Knutson, T. R. (2015). "North Atlantic Hurricane Activity: Past, Present and Future." *Climate Change: Multidecadal and Beyond*, 285.
- Mudd, L., Wang, Y., Letchford, C., and Rosowsky, D. (2014). "Assessing climate change impact on the US East Coast hurricane hazard: temperature, frequency, and track." *Natural Hazards Review*, 15(3), 04014001.
- Mudd, L., Wang, Y., Letchford, C., and Rosowsky, D. (2014). "Hurricane wind hazard assessment for a rapidly warming climate scenario." *Journal of Wind Engineering and Industrial Aerodynamics*, 133(0), 242-249.
- NAHB. (1999). "Reliability of conventional residential construction: An assessment of roof component performance in hurricane Andrew and typical wind regions of the

- United States." National Association of Home Builders, Upper Marlboro, Maryland, USA.
- Nejat, A., and Ghosh, S. (2016). "LASSO Model of Postdisaster Housing Recovery: Case Study of Hurricane Sandy." *Natural Hazards Review*, 04016007.
- Nguyen, M., Leicester, R., and Wang, C. (2008). "Manual No. 6: Embedded corrosion of fasteners in timber structures." *Forest & Wood Products Australia*.
- Nguyen, M. N., Leicester, R. H., Wang, C.-H., and Foliente, G. C. (2011). "Corrosion effects in the structural design of metal fasteners for timber construction." *Structure and Infrastructure Engineering*, 9(3), 275-284.
- Nguyen, M. N., Wang, X., and Leicester, R. H. (2013). "An assessment of climate change effects on atmospheric corrosion rates of steel structures." *Corrosion Engineering, Science and Technology*, 48(5), 359-369.
- Omer, M., Nilchiani, R., and Mostashari, A. (2009). "Measuring the resilience of the trans-oceanic telecommunication cable system." *Systems Journal, IEEE*, 3(3), 295-303.
- Paruthyalappil Alduse, B., Jung, S., and Arda Vanli, O. (2015). "Condition-based updating of the fragility for roof covers under high winds." *Journal of Building Engineering*, 2, 36-43.
- Peng, L., and Stewart, M. G. (2016). "Climate change and corrosion damage risks for reinforced concrete infrastructure in China." *Structure and Infrastructure Engineering*, 12(4), 499-516.
- Pielke Jr, R. A., Gratz, J., Landsea, C. W., Collins, D., Saunders, M. A., and Musulin, R. (2008). "Normalized hurricane damage in the United States: 1900–2005." *Natural Hazards Review*, 9(1), 29-42.
- Pimm, S. L. (1984). "The complexity and stability of ecosystems." *Nature*, 307(5949), 321-326.
- Pinelli, J., Simiu, E., Gurley, K., Subramanian, C., Zhang, L., Cope, A., Filliben, J., and Hamid, S. (2004). "Hurricane Damage Prediction Model for Residential Structures." *Journal of Structural Engineering*, 130(11), 1685-1691.
- Powell, M., Soukup, G., Cocke, S., Gulati, S., Morisseau-Leroy, N., Hamid, S., Dorst, N., and Axe, L. (2005). "State of Florida hurricane loss projection model: Atmospheric science component." *Journal of Wind Engineering and Industrial Aerodynamics*, 93(8), 651-674.
- Prevatt, D. (2007). "Wind uplift behavior of wood roof sheathing panels retrofitted with spray-applied polyurethane foam." *University of Florida, Gainesville, FL*.


- Prevatt, D. O., McBride, K., Roueche, D. B., and Masters, F. J. (2014). "Wind Uplift Capacity of Foam-Retrofitted Roof Sheathing Subjected to Water Leaks." *Bridges*, 10, 9780784412626.9780784412027.
- Reed, D., Kapur, K. C., and Christie, R. D. (2009). "Methodology for assessing the resilience of networked infrastructure." *Systems Journal, IEEE*, 3(2), 174-180.
- Rose, A. (2004). "Economic Principles, Issues, and Research Priorities in Hazard Loss Estimation." *Modeling Spatial and Economic Impacts of Disasters*, Y. Okuyama, and S. Chang, eds., Springer Berlin Heidelberg, 13-36.
- Rose, A., and Liao, S.-Y. (2005). "Modeling Regional Economic Resilience to Disasters: A Computable General Equilibrium Analysis of Water Service Disruptions*." *Journal of Regional Science*, 45(1), 75-112.
- Rowell, R. M. (2012). *Handbook of wood chemistry and wood composites*, CRC press.
- Russell, L. R., and Schueller, G. I. (1974). "Probabilistic models for Texas Gulf Coast hurricane occurrences." *Journal of Petroleum Technology*, 26(03), 279-288.
- Salman, A. M., and Li, Y. (2016). "Assessing Climate Change Impact on System Reliability of Power Distribution Systems Subjected to Hurricanes." *Journal of Infrastructure Systems*.
- Schmid, K. F. (2013). *Concise Encyclopedia of Construction Terms and Phrases*, Momentum Press.
- Shdid, C., Mirmiran, A., Wang, T., Jimenez, D., and Huang, P. (2010). "Uplift Capacity and Impact Resistance of Roof Tiles." *Practice Periodical on Structural Design and Construction*, 16(3), 121-129.
- Shibata, T., Solo-Gabriele, H. M., Fleming, L. E., Cai, Y., and Townsend, T. G. (2007). "A mass balance approach for evaluating leachable arsenic and chromium from an in-service CCA-treated wood structure." *Science of the total environment*, 372(2), 624-635.
- Simpson, W. T. (1999). "Drying and control of moisture content and dimensional changes" *Wood handbook : wood as an engineering material*, USDA Forest Service, Forest Products Laboratory, Madison, WI, Pages 12.11-12.20.
- Sparks, P. R. "Damages and lessons learned from Hurricane Hugo." *Proc., The 23 rd Joint Meeting of the US-Japan Cooperative Program in Natural Resources Panel on Wind and Seismic Effects, Tsukuba, Jpn, 05/14-17/91*, 435-450.
- Staid, A., Guikema, S. D., Nateghi, R., Quiring, S. M., and Gao, M. Z. (2014). "Simulation of tropical cyclone impacts to the U.S. power system under climate change scenarios." *Climatic Change*, 127(3), 535-546.


- Stainforth, D. A., Aina, T., Christensen, C., Collins, M., Faull, N., Frame, D. J., Kettleborough, J. A., Knight, S., Martin, A., and Murphy, J. (2005). "Uncertainty in predictions of the climate response to rising levels of greenhouse gases." *Nature*, 433(7024), 403-406.
- Stewart, M., Wang, X., and Willgoose, G. (2013). "Direct and Indirect Cost-and-Benefit Assessment of Climate Adaptation Strategies for Housing for Extreme Wind Events in Queensland." *Natural Hazards Review*, 15(4), 04014008.
- Stewart, M. G., and Deng, X. (2015). "Climate Impact Risks and Climate Adaptation Engineering for Built Infrastructure." *ASCE-ASME Journal of Risk and Uncertainty in Engineering Systems, Part A: Civil Engineering*, 1(1), 04014001.
- Stewart, M. G., Rosowsky, D. V., and Huang, Z. (2003). "Hurricane risks and economic viability of strengthened construction." *Natural hazards review*, 4(1), 12-19.
- Stewart, M. G., Wang, X., and Nguyen, M. N. (2011). "Climate change impact and risks of concrete infrastructure deterioration." *Engineering Structures*, 33(4), 1326-1337.
- Stewart, M. G., Wang, X., and Nguyen, M. N. (2012). "Climate change adaptation for corrosion control of concrete infrastructure." *Structural Safety*, 35, 29-39.
- Stocker, T., Qin, D., Plattner, G., Tignor, M., Allen, S., Boschung, J., Nauels, A., Xia, Y., Bex, B., and Midgley, B. (2013). "IPCC, 2013: climate change 2013: the physical science basis. Contribution of working group I to the fifth assessment report of the intergovernmental panel on climate change."
- Stubbs, N., and Perry, D. "A damage simulation model for buildings and contents in a hurricane environment." *Proc., Building an international community of structural engineers*, ASCE, 989-996.
- Sutt, E., Leichti, R. J., and Reinhold, T. (2008). "Design methodology for fastener schedules on sheathing panels subject to negative pressure." *10th World Conf. on Timber Engineering*, Engineered Wood Products Association (EWPA), Madison, WI.
- Sutt, E. G. (2000). "The Effect of Combined Shear and Uplift Forces on Roof Sheathing Panels." PhD thesis, Clemson University, Clemson, S. C.
- Tokgoz, B. E., and Gheorghe, A. V. (2013). "Resilience quantification and its application to a residential building subject to hurricane winds." *International Journal of Disaster Risk Science*, 4(3), 105-114.
- Turner, M., Plaut, R., Dillard, D., Loferski, J., and Caudill, R. (2009). "Tests of Adhesives to Augment Nails in Wind Uplift Resistance of Roofs." *Journal of Structural Engineering*, 135(1), 88-93.

- Twigg, J. (2009). "Characteristics of a disaster-resilient community: a guidance note (version 2)." DFID Disaster Risk Reduction NGO Interagency Group: Teddington, UK.
- Twisdale, L., Dunn, W., and Alexander, B. (1983). "Extreme Wind Risk Analysis of the Indian Point Nuclear Generation Station." *Final Rep. 44T-2491, Addendum to Rep. 44T-2171, Research Triangle Institute, Research Triangle Park, North Carolina.*
- Unnikrishnan, V. U., and Barbato, M. (2016). "Performance-Based Comparison of Different Storm Mitigation Techniques for Residential Buildings." *Journal of Structural Engineering*, 142(6), 04016011.
- Vallabhan, C. V. G., Wang, B. Y. T., Chou, G. D., and Minor, J. E. (1985). "Thin Glass Plates on Elastic Supports." *Journal of Structural Engineering*, 111(11), 2416-2426.
- van de Lindt, J. W., and Dao, T. N. (2011). "Loss analysis for wood frame buildings during hurricanes. II: Loss estimation." *Journal of Performance of Constructed Facilities*, 26(6), 739-747.
- van de Lindt, J. W., Graettinger, A., Gupta, R., Skaggs, T., Pryor, S., and Fridley, K. J. (2007). "Performance of wood-frame structures during Hurricane Katrina." *Journal of Performance of Constructed Facilities*, 21(2), 108-116.
- Vickery, P., and Twisdale, L. (1995). "Prediction of Hurricane Wind Speeds in the United States." *Journal of Structural Engineering*, 121(11), 1691-1699.
- Vickery, P. J., Masters, F. J., Powell, M. D., and Wadhera, D. (2009). "Hurricane hazard modeling: The past, present, and future." *Journal of Wind Engineering and Industrial Aerodynamics*, 97(7), 392-405.
- Vickery, P. J., Skerlj, P., and Twisdale, L. (2000). "Simulation of Hurricane Risk in the U.S. Using Empirical Track Model." *Journal of Structural Engineering*, 126(10), 1222-1237.
- Vickery, P. J., Skerlj, P. F., Lin, J., Twisdale Jr, L. A., Young, M. A., and Lavelle, F. M. (2006). "HAZUS-MH hurricane model methodology. II: Damage and loss estimation." *Natural Hazards Review*, 7(2), 94-103.
- Walsh, K. (2004). "Tropical cyclones and climate change: unresolved issues." *Climate Research*, 27(1), 77-83.
- Wang, C.-H., Wang, X., and Khoo, Y. B. (2013). "Extreme wind gust hazard in Australia and its sensitivity to climate change." *Natural hazards*, 67(2), 549-567.
- Wang, M., and Takada, T. (2005). "Macrosatial correlation model of seismic ground motions." *Earthquake spectra*, 21(4), 1137-1156.

- Wang, N., and Ellingwood, B. R. (2015). "Disaggregating community resilience objectives to achieve building performance goals." *Proceedings of the 12th International Conference on Applications of Statistics and Probability in Civil Engineering (ICASP12)* Vancouver, Canada, .
- Wang, X., Stewart, M. G., and Nguyen, M. (2012). "Impact of climate change on corrosion and damage to concrete infrastructure in Australia." *Climatic Change*, 110(3), 941-957.
- Watkiss, P., and Downing, T. (2008). "The social cost of carbon: Valuation estimates and their use in UK policy." *Integrated Assessment*, 8(1).
- Weart, S. R. (2008). *The discovery of global warming: revised and expanded edition*, Harvard University Press.
- Wei, H., Skibniewski, M., Shohet, I., and Yao, X. (2015). "Lifecycle Environmental Performance of Natural-Hazard Mitigation for Buildings." *Journal of Performance of Constructed Facilities*, 04015042.
- Wen, Y., and Kang, Y. (2001). "Minimum building life-cycle cost design criteria. II: Applications." *Journal of Structural Engineering*, 127(3), 338-346.
- Xu, L., and Brown, R. E. (2008). "Undergrounding assessment Phase 3 Report: Ex Ante Cost and Benefit Modeling." Quanta Technology, Raleigh.
- Yeo, D., Lin, N., and Simiu, E. (2013). "Estimation of Hurricane Wind Speed Probabilities: Application to New York City and Other Coastal Locations." *Journal of Structural Engineering*, 140(6), 04014017.
- Yoon, D. K., Kang, J. E., and Brody, S. D. (2016). "A measurement of community disaster resilience in Korea." *Journal of Environmental Planning and Management*, 59(3), 436-460.

Appendix A: Permission to Publish Chapter 2

 **Copyright Clearance Center**  **RightsLink** [Home](#) [Account Info](#) [Help](#) 

 **ASCE**
AMERICAN SOCIETY OF CIVIL ENGINEERS

Title: Reliability of Roof Panels in Coastal Areas Considering Effects of Climate Change and Embedded Corrosion of Metal Fasteners

Author: Yadong Dong, Yue Li

Publication: ASCE-ASME Journal of Risk Uncertainty and Analysis, Part A: Civil Engineering

Publisher: American Society of Civil Engineers

Date: 03/01/2016

Copyright © 2016, ASCE. All rights reserved.

Logged in as:
Yadong Dong
Account #:
3001069621
[LOGOUT](#)

Permissions Request

As an author of an ASCE journal article, you are permitted to reuse the accepted manuscript version of your article for your thesis or dissertation.

[BACK](#)

[CLOSE WINDOW](#)

Copyright © 2016 [Copyright Clearance Center, Inc.](#) All Rights Reserved. [Privacy statement](#). [Terms and Conditions](#).
Comments? We would like to hear from you. E-mail us at customercare@copyright.com

Appendix B: Permission to Publish Chapter 3



RightsLink®

Home

Account Info

Help



Taylor & Francis
Taylor & Francis Group

Title: Risk-based assessment of wood residential construction subjected to hurricane events considering indirect and environmental loss

Author: Yadong Dong, Yue Li

Publication: Sustainable and Resilient Infrastructures

Publisher: Taylor & Francis

Date: Jun 10, 2016

Copyright © 2016 Taylor & Francis

Logged in as:
Yadong Dong

Account #:
3001069621

LOGOUT

Thesis/Dissertation Reuse Request

Taylor & Francis is pleased to offer reuses of its content for a thesis or dissertation free of charge contingent on resubmission of permission request if work is published.

BACK

CLOSE WINDOW

Copyright © 2016 [Copyright Clearance Center, Inc.](#) All Rights Reserved. [Privacy statement](#). [Terms and Conditions](#).
Comments? We would like to hear from you. E-mail us at customercare@copyright.com